PTNSS

184(1), 2021

COMBUSTION ENGINES

INSTYTUT TECHNICZNY WOJSK LOTNICZYCH

ul. Księcia Bolesława 6, 01-494 Warszawa, skr. poczt. 96
tel.: 261 851 300; faks: 261 851 313
www.itwl.pl e-mail: poczta@itwl.pl

SYSTEM DIAGNOSTYKI TRIBOLOGICZNEJ

Pobieranie próbek oleju z silników, przekładni, skrzynek napędu, instalacji hydraulicznych	**Badania**	**Przekazanie informacji diagnostycznej**	
Użytkownik	Akredytowane laboratorium w ITWL	ITWL	Użytkownik
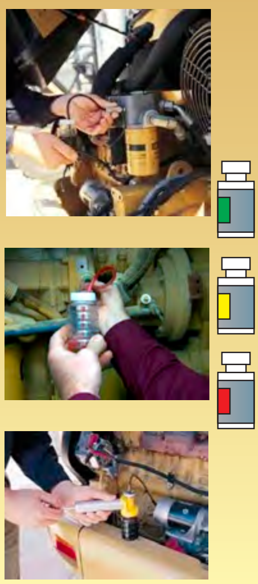		Analiza danych  Baza danych	Diagnoza 

System Diagnostyki Tribologicznej (SDT), opracowany w Instytucie Technicznym Wojsk Lotniczych, przeznaczony jest do wspierania eksploatacji obiektów technicznych.

Na podstawie wyników badań próbek oleju pobranych z układów tribologicznych prowadzi się ocenę i prognozowanie stanu technicznego obiektów technicznych (statki powietrzne, pojazdy mechaniczne, statki wodne, maszyny robocze i inne).

AB 138

9/MON/2017

INSTYTUT TECHNICZNY WOJSK LOTNICZYCH
ZAKŁAD SILNIKÓW LOTNICZYCH
Akredytowane laboratorium:
Laboratorium Diagnostyki Systemów Tribologicznych

PTNSS

COMBUSTION ENGINES

A Scientific Magazine

2021, 184(1)

Year LX

PL ISSN 2300-9896
PL eISSN 2658-1442

Editor:

Polish Scientific Society of Combustion Engines
60-965 Poznan, pl. M. Skłodowskiej-Curie 5, Poland
tel.: +48 61 6475966, fax: +48 61 6652204
E-mail: sekretariat@ptnss.pl
WebSite: http://www.ptnss.pl
Papers available on-line: http://combustion-engines.eu

Contents

Declaration of the original version
The original version of the Combustion Engines journal is the printed version.

Editor
Polish Scientific Society of Combustion Engines
60-965 Poznan, pl. M. Sklodowskiej-Curie 5, Poland
tel.: +48 61 6475966, fax: +48 61 6652204
E-mail: sekretariat@ptnss.pl
WebSite: http://www.ptnss.pl

Subscriptions
Send subscription requests to the Publisher's address.
Cost of a single issue PLN 40.

Preparation for print
ARS NOVA Publishing House
60-782 Poznan, Grunwaldzka 17/10A Street

Circulation: 100 copies

Printing and binding

Zakład Poligraficzny Moś i Łuczak, sp. j.,
Poznan, Piwna 1 Street

The journal is registered in the Polish technical journals content database – **BAZTECH** www.baztech.icm.edu.pl

The journal is listed in the international database **IC Journal Master List – Index Copernicus** www.indexcopernicus.com

Papers published in the
Combustion Engines
quarterly receive 20 points as stated by the Notification of the Minister of Science and Higher Education dated 31 July 2019.

Cover
I – Cummins X15 Engine
(*fot. www.oemoffhighway.com*; background (abstract-cool-orange-texture – *www.123freevectors.com*)
IV – MAN 20V35/44G Otto gas engine
(*fot. vehiclecue.it/*)

Article citation info:
ZHU, D., PRITCHARD, E., DADAM, S.R. et al. Optimization of rule-based energy management strategies for hybrid vehicles using dynamic programming. *Combustion Engines*. 2021, **184**(1), 3-10. https://doi.org/10.19206/CE-131967

Di ZHU
Ewan PRITCHARD
Sumanth Reddy DADAM
Vivek KUMAR
Yang XU

Optimization of rule-based energy management strategies for hybrid vehicles using dynamic programming

Reducing energy consumption is a key focus for hybrid electric vehicle (HEV) development. The popular vehicle dynamic model used in many energy management optimization studies does not capture the vehicle dynamics that the in-vehicle measurement system does. However, feedback from the measurement system is what the vehicle controller actually uses to manage energy consumption. Therefore, the optimization solely using the model does not represent what the vehicle controller sees in the vehicle. This paper reports the utility factor-weighted energy consumption using a rule-based strategy under a real-world representative drive cycle. In addition, the vehicle test data was used to perform the optimization approach. By comparing results from both rule-based and optimization-based strategies, the areas for further improving rule-based strategy are discussed. Furthermore, recent development of OBD raises a concern about the increase of energy consumption. This paper investigates the energy consumption increase with extensive OBD usage.

Key words: *energy management strategy, rule-based, dynamic programming, OBD, hybrid electric vehicles*

1. Introduction

As a key tool in the race to continuously reduce energy consumption in transportation, electrification has emerged as the primary means to achieve this goal. Hybrid electric vehicles (HEVs) play a significant role in the family of electrified vehicles. Unlike conventional vehicles and battery electric vehicles (BEVs), hybrid electric vehicles have a greater complexity and take advantage of operating dual propulsion systems to meet the load on the road. The dual propulsion system usually consists of a high voltage (HV) battery pack, a traction motor, an engine, and a generator. The combination of the HV battery pack and the motor provides customers with pure electric vehicle (EV) driving experience. When the state of charge (SOC) falls below a certain threshold, the engine will engage to charge the HV battery pack and/or provide additional power to meet the instantaneous load. Because HEVs can allow some or all the powertrain components to operate at a time, the operation is more complex than conventional vehicles and BEVs. The control strategy that manages these components to achieve the lowest energy consumption is the energy management strategy.

The energy management strategy can be divided into three categories: rule-based strategies, optimization-based strategies, and a mix of the two. The rule-based strategy is often also called an online strategy and employs control laws and rules to achieve a local optimal point [1, 11, 14, 15, 17, 19, 21]. One advantage of rule-based strategies is that they require less computational power to make decisions. Another advantage is that it does not require future information about the trip. A group of researchers used ADVISOR software to study several rule-based strategies [1]. They suggested the charge depleting (CD) and charge sustaining (CS) strategies along with electric assist strategy are more effective. Another group of researchers built a co-simulation platform using CANoe and MATLAB/Simulink to study a rule-based strategy which allows the vehicle to switch between CD mode and CS mode [14]. Generally, once entering CS mode, a plug-in hybrid electric vehicle (PHEV) does not switch back to CD mode until it is charged via alternative current (AC). A blended rule-based strategy was proposed in [11]. This strategy does not consider a specific vehicle speed or acceleration but rather vehicle energy. Comparing to a conventional rule-based strategy, the authors claimed that the fuel economy was improved by 18.4%.

The optimization-based strategies such as nonlinear programming, genetic algorithm, and dynamic programming (DP) require prior knowledge of the trip [9, 12, 15, 20]. In addition, they are more computationally intensive than rule-based strategies. Usually, they are used offline to find the global optimal point that could have been achieved after the fact.

Mixed strategies such as the equivalent consumption minimization strategy (ECMS) take advantage of both rule-based strategies and optimization-based strategies [5, 6, 10, 13]. The operating parameters are determined by using optimization techniques. After this determination, these pre-determined parameters are used by rule-based algorithms in real-time controllers within the vehicle. Therefore, the computational burden in the vehicle is avoided.

Recent research on the optimization-based strategies has focused on utilizing knowledge from modeling and simulation to make the optimization results more representative. Two dynamic programming algorithms were studied in [20]. The deterministic dynamic algorithm solves the optimization problem by sequentially calculating every state at every time step in a backwards order. Unlike the deterministic dynamic algorithm, the stochastic dynamic programming algorithm approach results in a control which depends on a specific state [20]. A stochastic model of a vehicle's drive missions was used in their study and the strategy was validated in hardware-in-the-loop (HIL). Another group of researchers combined DP with a neural network to perform the energy management [9]. Their method utilizes the neural network to predict the decision variable which normally is calculated by DP. A rule-based strategy was proposed

Received 19 November 2020; Received in revised form 22 December 2020; Accepted 27 December 2020
Available online 11 March 2021

based on the projection partition of composite power system efficiency in [12]. In conjunction to the rule-based strategy, a DP method was proposed on the basis of the establishment of the whole system. Some other researchers proposed a recalibration method to improve a rule-based strategy in [15]. The DP essentially helps calibrate the rule-based strategy. However, none of the above references recognizes that the measurement errors in the vehicle plays an important role in the energy management strategy. In addition, the complexity of vehicle dynamics results in a much higher energy consumption at the wheel than their models predicted. Therefore, their optimization results may not represent the energy consumption in real world.

A recent development in on-board diagnostics (OBD) suggests that more OBD services and routines may be required for future vehicles [3]. The use of deceleration fuel shutoff in conventional vehicles to diagnose powertrain faults and meet OBD regulatory requirements is replaced by spinning the gen-set in the HEV [3, 8]. The increasing number of OBD events may lead to an increase in energy consumption for HEVs. Therefore, it is important to understand if extensive OBD events have an impact on the energy consumption.

To achieve the above objectives, we propose a framework that utilizes physical test data from a series PHEV under the emission and energy consumption (E&EC) drive cycle to get more representative DP result. The E&EC drive cycle represents real world driving in the US. After that, the DP result is analyzed to identify where the rule-based strategy can be improved. At last, the impact of recent OBD development on the energy consumption is assessed.

The remainder of this paper is organized as follows. The Method section is divided into five subsections. We first review the E&EC drive cycle test. After that, we discuss the vehicle architecture and specifications. Following that powertrain component models are discussed. Later, we visit both the rule-based strategy and the optimization-based strategy used in this study. Most importantly, our discussion sheds light on how the test data from the rule-based strategy is used to improve the optimization-based strategy. We also discuss how the optimization via dynamic programming is fed back to improve the rule-based strategy. In the last subsection, we talk about the method used to calculate energy consumption. In the Results and Discussion section, we begin with discussing the result from the drive cycle analysis. Following that, we review the energy consumption from both the vehicle test and simulations. Finally, we conclude this paper in the Conclusions section.

2. Method

The proposed framework has four steps. The first step is to analyze the drive cycle(s). The result from the analysis include propulsion energy, peak power, average positive power, and percent idle time. These four items are selected to represent the characteristics of the drive cycle(s). The second step is to perform a vehicle test in the same drive cycle(s). Vehicle test mass, vehicle velocity, power input and output from each powertrain component, and other properties need to be collected during the test. The third step is to compare the drive cycle result with the test result. The difference between the two is used to feed into DP to generate a more representative optimization result. At last, the optimization result is looped back with the vehicle test result to identify areas in the energy management strategy that can be improved.

2.1. E&EC test

The E&EC drive cycle is illustrated in Fig. 1. The E&EC drive cycle was developed by Argonne National Lab to address more real-world driving conditions on the road. The drive cycle blends four standard certification test cycles: Federal Test Procedure (FTP), Highway Fuel Economy Driving Schedule (HWFET), US06 City and US06 Highway. This drive cycle aims to have a much higher top speed with more aggressive accelerations and decelerations. The distance of the drive cycle is 22.55 km.

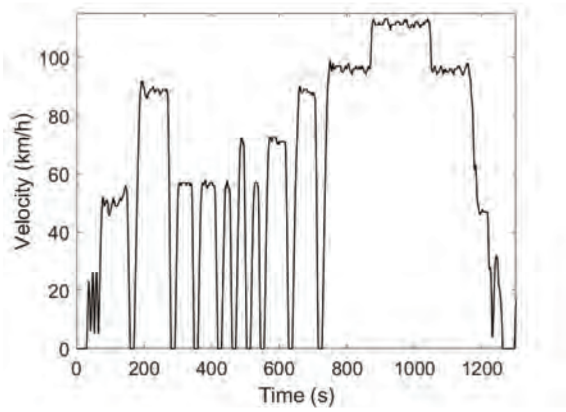

Fig. 1. E&EC drive cycle

The vehicle had one driver and one passenger during the test. The vehicle also towed a trailer in which a SEMTECH emissions analyzer was used to measure the exhaust gases from the exhaust pipe. As a result, the driver, passenger, and trailer added additional 700 kg to the vehicle in the test, which increases the energy consumption of the vehicle.

2.2. Vehicle Overview

A 2013 General Motors Malibu was used in this study as shown in Fig. 2. After the original powertrain of the vehicle was removed from the vehicle, a set of new powertrain components was selected and integrated into the vehicle to represent a series PHEV. A peak 100 kW Magna electric motor is coupled to a single speed transmission with a gear ratio 7.82:1 to power the front axle. The gen-set consists of a continuous 37 kW TM4 generator and a 33 kW Kubota diesel engine. The generator and engine are mechanically coupled through a herringbone belt drive at a ratio of 2.7:1. An 18.9 kWh HV battery pack using lithium-ion phosphate cells is electrically coupled with the motor, generator and a 3.3 kW BRUSA on-board charger in an HV junction box. The high-level vehicle architecture is illustrated in Fig. 3. This architecture advances other architectures by allowing the range extender to be completely decoupled from the wheels and run at optimal operation points. This vehicle may also be considered as an extended-range electric vehicle (EREV) that is a subcategory of HEVs. We use PHEV to emphasize the plug-in feature.

Fig. 2. The reengineered vehicle

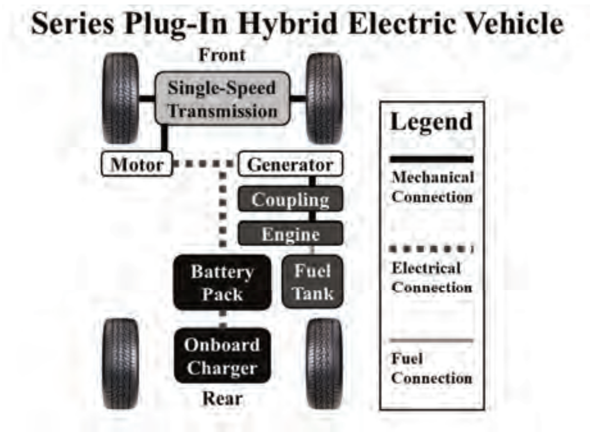

Fig. 3. Vehicle architecture

The large HV battery pack allows the vehicle to drive approximately 80 km before activating the gen-set. The total range of the vehicle is about 378 km. The mass of the vehicle is 2100 kg. The electric motor is the only powertrain component coupled with the wheels. The 0-to-100 kph acceleration is 13.2 seconds.

2.3. Vehicle model

The vehicle model consists of a vehicle dynamic model, motor model, gen-set model, and a battery model. The vehicle dynamic model was used to calculate the power and energy needed at the wheels to propel the vehicle. The model is described by the equation below:

$$m_i \cdot \frac{dv}{dt} = F_{tr} - F_{grade} - F_{aero} - F_{rr} \quad (1)$$

$$m_i = m \cdot i \quad (2)$$

where m_i is the inertial mass of the vehicle in kg, v is the vehicle velocity in m/s, F_{tr} is the tractive force at the wheels in N, F_{grade} is the force generated by a grade in N, F_{aero} is aerodynamic drag in N, F_{rr} is the rolling resistance in N, m is the vehicle mass in kg, and i is the rotating inertia factor. Substituting vehicle properties into Equation (1), the equation becomes

$$m_i \cdot \frac{dv}{dt} = F_{tr} - m \cdot g \cdot \sin\alpha - \frac{1}{2} \cdot \rho \cdot C_d A_f \cdot v^2 - m \cdot g \cdot C_{rr} \quad (3)$$

where g is the gravitational constant in N/kg, α is the road grade in degrees, ρ is air density in kg/m^3, C_dA_f is the product of air drag coefficient and vehicle frontal area in m^2, and C_{rr} is the rolling resistance coefficient. The vehicle properties used in this study can be found in Table 1.

Table 1. Vehicle properties

Parameter	Symbol	Value
Vehicle mass	m	2100 kg
Vehicle test mass	m_t	2800 kg
Drag coefficient × frontal area	C_dA_f	0.75 m^2
Rolling resistance coefficient	C_{rr}	0.009

The motor and gen-set were modeled using the black box modeling technique [22]. For the motor model, the inputs include accelerator pedal position, brake pedal position, and vehicle velocity. The outputs of the motor model are motor torque, motor speed, motor input power, motor output power, and motor losses. An efficiency map shown in Fig. 4 was developed for this model using component characterization test data such as motor voltage input, motor current input, motor torque output, and motor speed output. The following equation was used to calculate the efficiencies:

$$\eta_{motor} = \frac{T_{motor} \cdot \omega_{motor}}{V_{motor} \cdot I_{motor}} \cdot 100\% \quad (4)$$

where η_{motor} is the motor efficiency in %, T_{motor} is the torque output in Nm, and ω_{motor} is the speed output in rpm, V_{motor} is the voltage input in V, and I_{motor} is the current input in A.

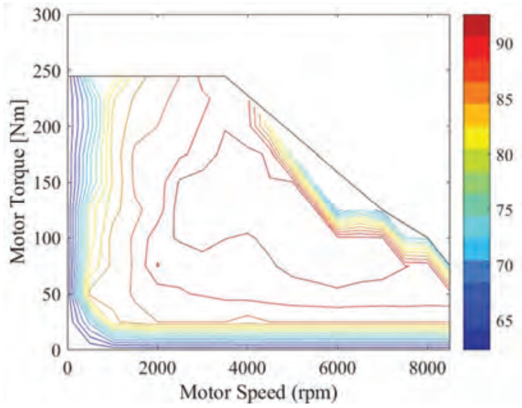

Fig. 4. Motor efficiency map

The gen-set model is similar to the motor model. The following two equations were used to calculate the engine and generator efficiencies, respectively:

$$\eta_{eng} = \frac{1}{BSFC \cdot LHV} \cdot 100\% \quad (5)$$

$$\eta_{gen} = \frac{V_{gen} \cdot I_{gen}}{T_{gen} \cdot \omega_{gen}} \cdot 100\% \quad (6)$$

where η_{eng} is the engine efficiency in %, BSFC is the brake-specific fuel consumption in g/(kWh) and LHV is the low heating value in kWh/g, η_{gen} is the generator efficiency in %, V_{gen} is the voltage output of the generator in V, I_{gen} is the current output of the generator in A, T_{gen} is the generator torque input in Nm, and ω_{gen} is the speed input in rpm. The engine and generator efficiency maps are illustrated in

Figs. 5 and 6. The efficiency map of the gen-set was created by merging the generator and engine efficiency maps together in Fig. 7.

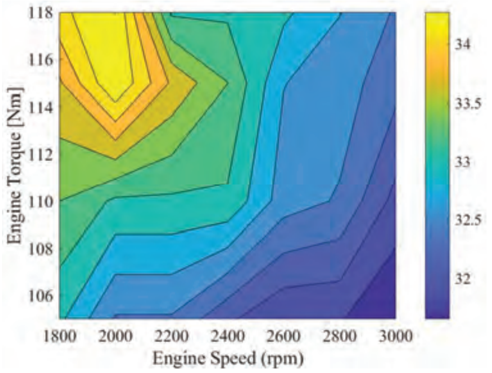

Fig. 5. Engine efficiency map

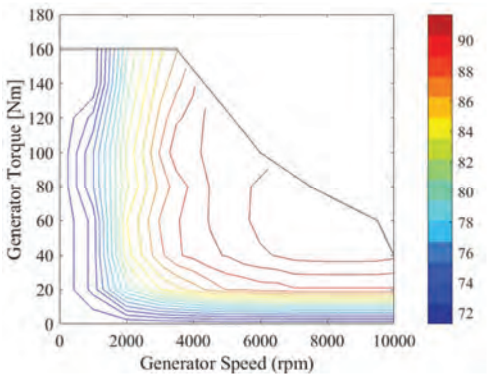

Fig. 6. Generator efficiency map

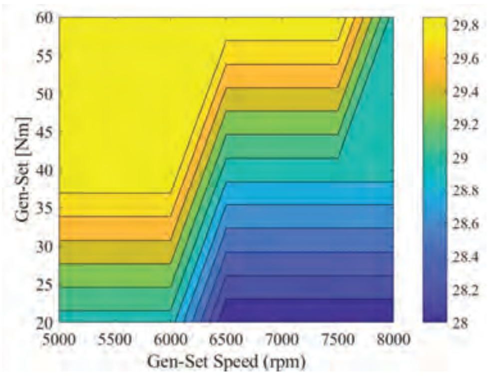

Fig. 7. Gen-set efficiency map

The battery model was represented by a simple internal resistance model. The model can calculate cell open-circuit voltage, battery pack open-circuit voltage, cell voltage, pack voltage, battery losses, and SOC. The model is described below:

$$P_{batt} = \frac{R_{in} \cdot I_{batt}^2 + V_{oc} \cdot I_{batt}}{1000} \tag{7}$$

$$SOC = \frac{\int V_{oc} \cdot I_{batt}}{3600000 \cdot C_{batt}} \cdot 100\% \tag{8}$$

where P_{batt} is battery pack power in kW, R_{in} represents the internal resistance in Ω, I_{batt} is the battery pack current in A, V_{oc} is the pack open-circuit voltage in V, SOC is the state of charge in %, and C_{batt} is the battery pack capacity in kWh.

2.4. Energy management strategies

A rule-based energy management strategy was implemented in the vehicle. The rule-based strategy has two primary operation modes: CD mode and CS mode. The CD mode was designed to take advantage of the 18.9 kWh battery pack to achieve 80 km pure electric range. Customers get the smoothest and quietest driving experience while recovering kinetic energy through advanced regenerative braking strategies. The 18.9 kWh battery pack was selected to ensure the pure electric range can satisfy 80% of consumers daily travel needs. This 80% design criterion is the result of the utility factor calculated from SAE J2841 in [18]. In this phase, the propulsion is solely supported by the motor and battery pack. Therefore, the SOC continues depleting as the vehicle travels.

The CS mode does not begin until the SOC falls below a designed threshold in the SOC CS window. After that, the gen-set is turned on to increase the battery pack SOC until the upper limit of the SOC CS window is reached. SOC_{high} and SOC_{low} are used to represent the upper and lower limits, respectively. They form the SOC window. The threshold to initiate CS mode is set slightly higher than SOC_{low} to ensure the gen-set has time to begin power generation and keep the SOC within the window while operating at optimal points. The SOC moves within the SOC window in the CS mode. One of the key advantages of this architecture is that the gen-set can be operated at any given operating point regardless of road load. To avoid turning on and off the gen-set too frequently, a 10-second ramp down time was implemented. Once the gen-set is turned on, the control strategy does not turn it off in the next 10 seconds and vice versa. Besides the gen-set ramp down, two other techniques were also implemented to provide the customer with a smoother experience. One of the two techniques is the delay torque production from the engine. After cranking the engine, the generator spins freely with the engine until the engine warms up. The other technique is the maximum current limit for regenerative braking. While the gen-set is pushing current into the battery pack, the regenerative braking algorithm continuously monitors the current on to HV bus to avoid putting the battery pack into an overcurrent condition.

The data from the vehicle test opens up an opportunity to further improve the rule-based energy management strategy through optimization. Since the vehicle depletes the battery pack to the lower limit in CD mode no matter what the driving conditions are, there is no gain to optimize the energy management strategy for the CD mode. However, if the trip information such as vehicle velocity can be either predicted or known prior to beginning the trip, optimizing the energy management strategy in CS mode can provide a noticeable energy consumption reduction. In addition, recent studies have shown interest of using the generator to perform OBD. Still, it is unclear that how the new development in OBD is going to affect the energy consumption for hybrids. Thus, an optimization-based energy management strategy considering the latest OBD techniques is proposed in the following paragraph.

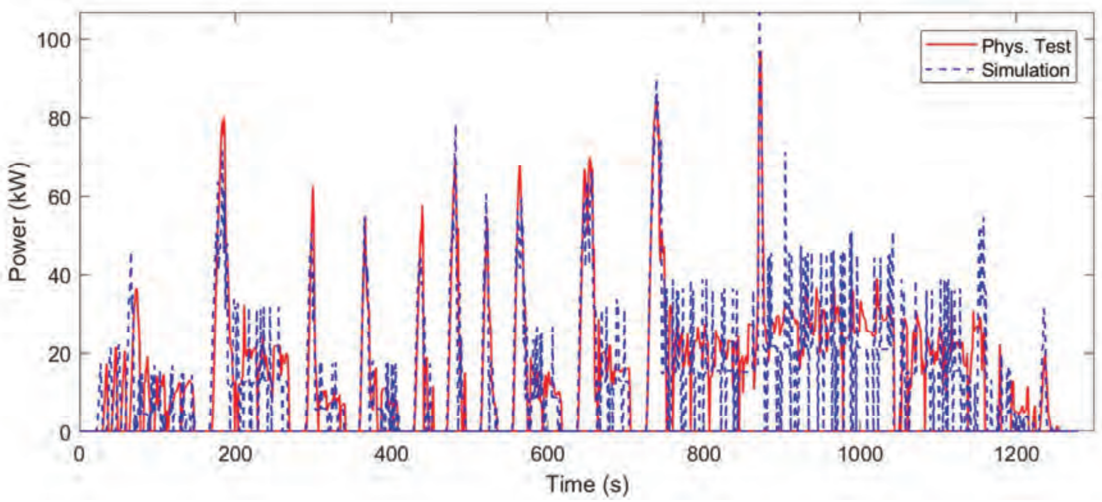

Fig. 8. Positive power from the simulation and physical test for a single E&EC drive cycle

The state equations in the discrete-time format can be expressed as:

$$x_{k+1} = f(x_k, u_k) \tag{9}$$

$$x_k = SOC_k \tag{10}$$

$$u_k = \Delta SOC_k \tag{11}$$

where x denotes the state variable, k is the step in discrete-time format, and u represents the decision variable. The cost function for minimizing the energy consumption in the general format is expressed as:

$$J_k(x_k) = \min_{u_k}\{f(x_k, u_k) + J_{k+1}(x_{k+1})\} \tag{12}$$

The constraints that should be met are as follows:

$$\begin{cases} SOC_{min} \le SOC_k \le SOC_{max} \\ 0 \le \Delta SOC_k \le \frac{P_{gen-set\_max}}{3600 \cdot C_{batt}} \cdot 100\% \end{cases} \tag{13}$$

When the rule-based strategy was first developed and implemented, there was not enough information about the maturity of the prototype vehicle. Therefore, the operating point from the gen-set was selected conservatively. After testing the vehicle on the proving ground, all the operating points in the gen-set efficiency map are available. However, we still want to select operating points that are at the same gen-set speed as we originally selected for the rule-based strategy. Therefore, the following equations are used to make decisions in the optimization:

$$u_k = \begin{cases} a & SOC_{max} \le SOC_k + 0.567 \\ b & SOC_{min} \le SOC_k < SOC_{max} - 0.567 \end{cases} \tag{14}$$

$$a = 0 \tag{15}$$

$$b = (0.294: 0.051: 0.567) \tag{16}$$

where a and b represent SOC change in % for 10-second period.

In summary, two optimization cases were studied. The first case optimized the energy consumption for the CS portion of 3-lapse E&EC drive cycles. The travel distance for that portion is about 13.23 km. The other case optimized the energy consumption over one E&EC drive cycle with and without considering the OBD. The energy consumption from the OBD is assumed to be 0.00497 kWh per OBD event which is equivalent to the energy consumption by spinning the engine for 10 seconds. The OBD event is performed in every 10-second interval when the gen-set does not operate to generate electricity. By doing so, the energy consumption using CS mode only was estimated.

2.5. Energy consumption calculation

Understanding the energy flow and energy consumption in different operating modes is critical for HEVs [2, 4, 16]. SAE J1711 standard was used to determine the energy consumption in both CD and CS modes for each trip [7]. After that, the utility factor described in SAE J2841 was used to combine the two energy consumption values into a single energy consumption number for the trip [18]. The equation used to calculate utility factor-weighted energy consumption is expressed below:

$$EC_{UF\_weighted} = EC_{CD} \cdot UF + EC_{CS} \cdot (1 - UF) \tag{17}$$

where $EC_{UF\_weighted}$ denotes the utility factor-weighted energy consumption, EC_{CD} is the energy consumption in CD mode, and EC_{CS} is the energy consumption in CS mode. A charging efficiency of 83% was used when calculating the UF-weighted AC electric energy consumption in the Results and Discussion section.

3. Results and discussion

3.1. Drive cycle analysis

A drive cycle analysis was performed to understand the difference in both power and energy between the models and vehicle. A comparison of positive power at the wheels is shown in Fig. 8. It is observed that the peak power from the models matches the peak power from the vehicle. However, some of the vehicle dynamics are not captured by the models. We believe this is primarily due to the simplicity of the model and the measurement accuracy in the vehicle.

The differences can also be found in Table 2, where positive propulsion energy, peak power output, average positive power and percent idle time from the simulation and vehicle are compared. The vehicle consumed 15.85%

more energy than the models estimated. The average positive power from the vehicle physical test is also 16.60% higher than the average positive power from the models. Interestingly, the models reported a higher peak power output. Since the goal is to develop an energy management strategy that can be used in the vehicle, using the vehicle test data in energy management optimization provides a more representative result. That is why the physical test data was used in the optimization study.

Table 2. Drive cycle results at the wheels

Test mass: 2800 kg	Unit	Simulation	Phys. Test
Positive propulsion energy	Wh/km	223.75	259.21
Peak power output	kW	112.50	96.96
Average positive power	kW	14.04	16.37
Percent idle time	%	10.55	10.55

3.2. Energy consumption

The physical test results from the vehicle with the rule-based strategy in three E&EC drive cycles are illustrated in Fig. 9. The first optimization case for the CS mode is also plotted in Fig. 9. The subplot on the top depicts the vehicle velocity. The red and blue curves on the bottom represent the SOC throughout the trip with the rule-based strategy and optimization-based strategy, respectively. The SOC_{high} and SOC_{low} that form the SOC CS window are depicted by the magenta and cyan lines on the bottom subplot, correspondingly. The SOC_{high} and SOC_{low} are 17% and 12%, respectively. The vehicle drove 54.37 km in CD mode. Once the SOC fell below 14.00% SOC, the CS mode kicked in. With the rule-based strategy, the gen-set increased the SOC to 16.94% at the end of the third E&EC drive cycle. The SOC curve from the optimization-based strategy is like the SOC curve from the rule-based strategy. The only difference is the SOC ended at 14.00% at the end of the trip. The rule-based strategy ran the gen-set to put an additional 3.00% SOC into the battery pack, which resulted in a higher energy consumption.

The UF-weighted energy consumption values are listed in Table 3. Both strategies have the exact same energy consumption in CD mode. It is noted that the UF-weighted AC energy consumption includes an 83% charging efficiency from AC to DC. Unlike the UF-weighted energy consumption in CD mode, the optimization-based strategy has a lower UF-weighted fuel energy consumption than the rule-based strategy does in CS mode. There are two major contributors for the difference. The rule-based strategy only operates at a single operating point, while the optimization-based strategy operates at seven operating points and some operating points have a slightly higher efficiency than the operating point used in the rule-based strategy. The other contributor is due to the additional 3% that the rule-based strategy put into the battery pack. The rule-based strategy can be improved by addressing these two areas. Therefore, the rule-based strategy has higher energy consumption values for UF-weighted fuel energy consumption and UF-weighted total energy consumption.

Table 3. CS optimization

	Unit	Rule-Based	Optimization-Based
UF-weighted fuel energy consumption	Wh/km	274.90	274.90
UF-weighted AC electric energy consumption	Wh/km	194.30	160.59
UF-weighted total energy consumption	Wh/km	469.20	435.49

The results from the OBD study, which is also the second optimization case, are illustrated in Fig. 10. A single E&EC drive cycle simulation was performed for two scenarios: optimization-based strategy without using OBD and optimization-based strategy with using OBD. The black curve on the top represents the vehicle velocity. The magenta and cyan lines on the bottom represent SOC_{high} and SOC_{low}, respectively. The red curve is the case without using OBD, while the blue curve represents the case with using OBD. It is observed that both curves overlay most of the time. The SOC difference starts at around 200 seconds and becomes greater than 1% at around 580 seconds. The two curves start merging again at around 880 seconds.

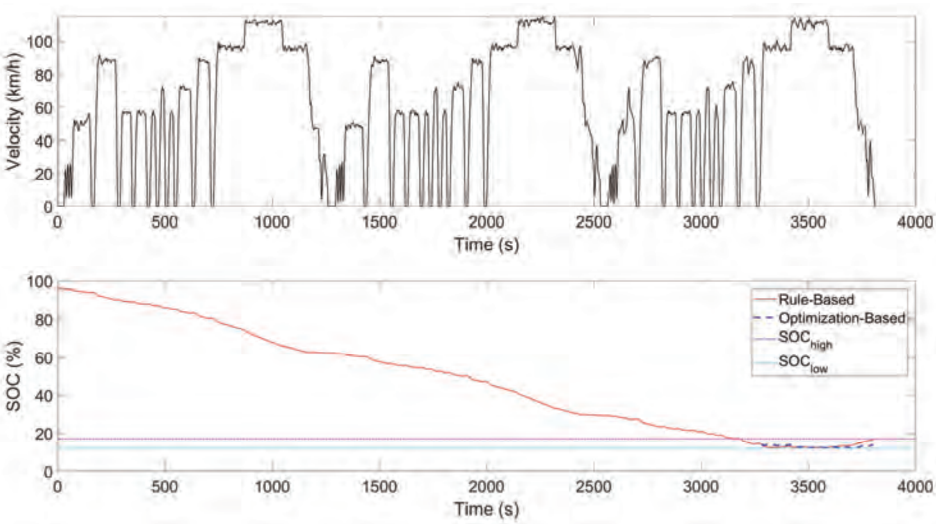

Fig. 9. A comparison of rule-based and optimization-based energy strategies in three laps of E&EC drive cycles

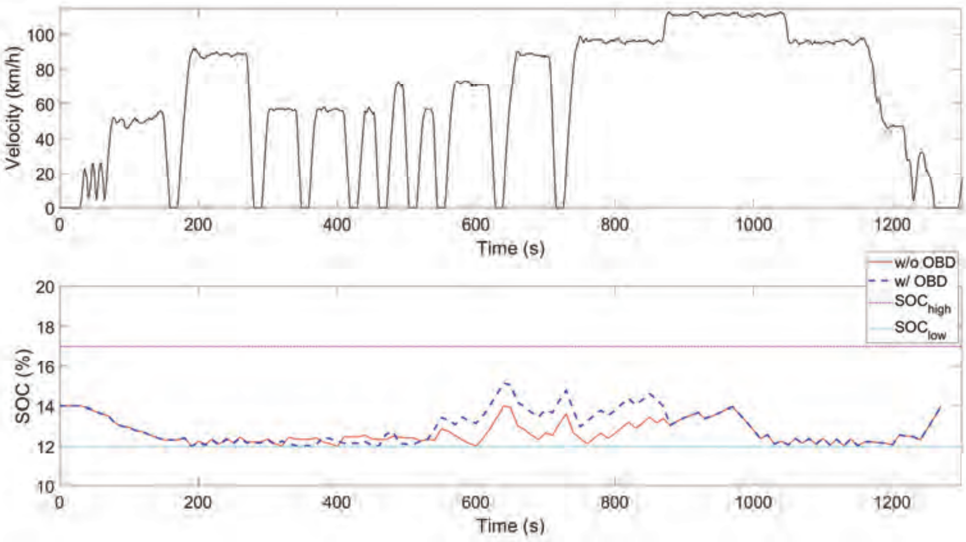

Fig. 10. A comparison of energy management strategy with and without OBD in a single E&EC drive cycle

Table 4 lists the CS energy consumption for both cases. The CS energy consumption with using OBD is slightly higher than the CS energy consumption without using OBD. However, the difference is less than 1.9%.

Table 4. Energy consumption with and without OBD

	Unit	w/o OBD	w/ OBD
CS energy consumption	Wh/km	880.22	896.10

4. Conclusions

The aim of this work was to propose and demonstrate a four-step framework. Unlike previous work, which heavily focused on modeling and simulations, this framework incorporated the utilization of real-world data in the workflow to improve the optimization result. In addition, it identifies areas in the rule-based strategy for future improvement. This work studied the energy management strategy from a different angle and proposed two hypotheses. The first hypothesis is with the measurement errors from in-vehicle measurement system and simplicity of the widely used models, incorporating the physical test data improves the optimization result. The second hypothesis is the extensive OBD events does not increase the energy consumption significantly. To prove the proposed hypotheses, a case study using a PHEV was conducted. The case study showed that the proposed framework provided a more representative optimization result for energy management strategy. In addition, the extensive OBD events only increased 1.9% energy consumption in the E&EC drive cycle.

Acknowledgements

This work was partially supported by the US Department of Energy (DOE) Advanced Vehicle Technology Competitions (AVTC).

Nomenclature

AC	alternative current
BEV	battery electric vehicle
BSFC	brake specific fuel consumption
CD	charge depleting
CS	charge sustaining
DP	dynamic programming
E&EC	emission and energy consumption
ECMS	equivalent consumption minimization strategy
EREV	extended-range electric vehicle
EV	electric vehicle
FTP	federal test procedure
HEV	hybrid electric vehicle
HIL	hardware-in-the-loop
HV	high voltage
HWFET	highway fuel economy driving schedule
LHV	lower heating value
OBD	on-board diagnostics
PHEV	plug-in hybrid electric vehicle
SOC	state of charge

Bibliography

[1] BANVAIT, H., ANWAR, S., CHEN, Y. A rule-based energy management strategy for plug-in hybrid electric vehicle (PHEV). *2009 American Control Conference.* 3938-3943. https://doi.org/10.1109/ACC.2009.5160242

[2] CIEŚLIK, W., SZWAJCA, F., GOLIMOWSKI, J. The possibility of energy consumption reduction using the ECO driving mode based on the RDC test. *Combustion Engines.* 2020, **182**(3), 59-69. https://doi.org/10.19206/CE-2020-310

[3] DADAM, S.R., JENTZ, R., MEISSNER, H. Diagnostic evaluation of exhaust gas recirculation (EGR) system on gasoline electric hybrid vehicle. *SAE Technical Paper* 2020-01-0902. 2020. https://doi.org/10.4271/2020-01-0902

[4] FLUDER, K., PIELECHA, I., CIEŚLIK, W. The impact of drive mode of a hybrid drive system on the energy flow indicators in the RDE test. *Combustion Engines.* 2018, **175**(4), 18-25. https://doi.org/10.19206/CE-2018-403

[5] GENG, B., MILLS, J.K., SUN, D. Energy management control of microturbine-powered plug-in hybrid electric vehicles using the telemetry equivalent consumption minimization strategy. *IEEE Transactions on Vehicular Technology*. 2011, **60**(9), 4238-4248. https://doi.org/10.1109/TVT.2011.2172646

[6] HAN, J., PARK, Y., KUM, D. Optimal adaptation of equivalent factor of equivalent consumption minimization strategy for fuel cell hybrid electric vehicles under active state inequality constraints. *Journal of Power Sources*. 2014, **267**, 491-502. https://doi.org/10.1016/j.jpowsour.2014.05.067

[7] HYBRID-EV COMMITTEE. J1711: Recommended practice for measuring the exhaust emissions and fuel economy of hybrid-electric vehicles, including plug-in hybrid vehicles. *Proceedings of the SAE Std. J1711_SAE World Congress*. 2010, 13-15. https://doi.org/10.4271/J1711_201006

[8] JAMMOUSSI, H., MAKKI, I., KLUZNER, M. et al. Diagnostics of individual air fuel ratio cylinder imbalance. *SAE International Journal of Passenger Cars-Electronic and Electrical Systems*. 2017, **10**(2017-01-1684), pp. 400-404. https://doi.org/10.4271/2017-01-1684

[9] LIU, J., CHEN, Y., ZHAN, J. et al. Heuristic dynamic programming based online energy management strategy for plug-in hybrid electric vehicles. *IEEE Transactions on Vehicular Technology*. 2019, **68**(5), 4479-4393. https://doi.org/10.1109/TVT.2019.2903119

[10] ONORI, S., SERRAO, L., RIZZONI, G. Adaptive equivalent consumption minimization strategy for hybrid electric vehicles. *Dynamic Systems and Control Conference* vol. 44175, pp. 499-505. 2010. https://doi.org/10.1115/DSCC2010-4211

[11] PADMARAJAN, B.V., MCGORDON, A., JENNINGS, P.A. Blended rule-based energy management for PHEV: System structure and strategy. *IEEE Transactions on Vehicular Technology*. 2015, **65**(10), 8757-8762. https://doi.org/10.1109/TVT.2015.2504510

[12] PAN, C., LIANG, Y., CHEN, L. et al. Optimal control for hybrid energy storage electric vehicle to achieve energy saving using dynamic programming. *Energies*. 2019, **12**(4), 588. https://doi.org/10.3390/en12040588

[13] PARK, J., PARK, J.H. Development of equivalent fuel consumption minimization strategy for hybrid electric vehicles. *International Journal of Automotive Technology*. 2012, **13**(5), 835-843. https://doi.org/10.1007/s12239-012-0084-6

[14] PENG, J., FAN, H., HE, H. et al. A rule-based energy management strategy for a plug-in hybrid school bus based on a control area network bus. *Energies*. 2015, **8**(6), 5122-5142. https://doi.org/10.3390/en8065122

[15] PENG, J., HE, H., XIONG, R. Rule based energy management strategy for a series-parallel plug-in hybrid electric bus optimized by dynamic programming. *Applied Energy*. 2017, **185**, 1633-1643. https://doi.org/10.1016/j.apenergy.2015.12.031

[16] PIELECHA, I., CIEŚLIK, W., FLUDER, K. Analysis of energy management strategies for hybrid electric vehicles in urban driving conditions. *Combustion Engines*. 2018, **173**(2), 14-18. https://doi.org/10.19206/CE-2018-203

[17] PRITCHARD, E., MACKEY, L., ZHU, D. et al. Modular electric generator rapid deployment DC microgrid. *2017 IEEE Second International Conference on DC Microgrids (ICDCM)*. 2017, pp. 106-110. https://doi.org/10.1109/ICDCM.2017.8001030

[18] SAE INTERNATIONAL HYBRID-EV COMMITTEE. J2841: Utility factor definitions for plug-in hybrid electric vehicles using travel survey data-SAE International. *SAE International Hybrid-EV Committee*. 2010. https://www.sae.org/standards/content/j2841_201009

[19] SONNENBERG, M., PRITCHARD, E., ZHU, D. Microgrid development using model-based design. *In 2018 IEEE Green Technologies Conference (GreenTech)*. 2018, 57-60. https://doi.org/10.1109/GreenTech.2018.00019

[20] WEGMANN, R., DÖGE, V., BECKER, J. et al. Optimized operation of hybrid battery systems for electric vehicles using deterministic and stochastic dynamic programming. *Journal of Energy Storage*. 2017, **14**, 22-38. https://doi.org/10.1016/j.est.2017.09.008

[21] ZHU, D., PRITCHARD, E. NCSU year three final technical report. *SAE Technical Paper* 2014-01-2907. 2014. https://doi.org/10.4271/2014-01-2907

[22] ZHU, D., PRITCHARD, E.G., SILVERBERG, L.M. A new system development framework driven by a model-based testing approach bridged by information flow. *IEEE Systems Journal*. 2016, **12**(3), pp. 2917-2924. https://doi.org/10.1109/JSYST.2016.2631142

Di Zhu, DEng. – FREEDM Systems Center, North Carolina State University, United States.
e-mail: *dzhu2@ncsu.edu*

Ewan Pritchard, DEng. – FREEDM Systems Center, North Carolina State University, United States.
e-mail: *egpritch@ncsu.edu*

Sumanth Reddy Dadam, MSci. – Mechanical Engineering Department, Wayne State university, United States.
e-mail: *sumanth.me03@gmail.com*

Vivek Kumar, MSci. – Mechanical Engineering Department, Wayne State University, United States.
e-mail: *mechviku@gmail.com*

Yang Xu, DEng. – FREEDM Systems Center, North Carolina State University, United States.
e-mail: *yxu17@ncsu.edu*

Article citation info:
STOECK, T. Methodology of testing common rail fuel injectors witch the use of Gauss`s formulas. *Combustion Engines*. 2021, **184**(1), 11-15. DOI: 10.19206/CE-133505

Tomasz STOECK

Methodology of testing common rail fuel injectors with the use of Gauss's formulas

The paper presents the methodology of testing common rail fuel injectors, which consisted in extending the standard diagnostic procedures with the analysis of the resulting fuel delivery fields. The calculations were carried out in a popular spreadsheet, using Gauss's formulas (the so-called shoelace formula). In this way, the necessity to modify the test bench software was eliminated, as the analytical process took place after the end of the active experiment phase. It has been shown that the proposed solution should be particularly useful in problematic situations where clear-cut verification and assessment of the technical condition of the fuel injectors is sometimes difficult, as shown in the example. In addition, implementation in a digital environment allows the presented algorithms to be reused in research with a similar profile.

Key words: *common rail fuel injectors, extension of diagnostic procedures, Gauss's formulas, resulting fuel delivery fields*

1. Introduction

In recent years, services related to the regeneration of malfunctioning common rail fuel injectors have become particularly important. Before the repair, a verification process is carried out on the test bench, which allows checking the parameters specified by the manufacturer, including mainly the correctness of fuel delivery. In most cases, standard diagnostic procedures are sufficient to assess the technical condition of the fuel injector, as they relate to critical engine operation points. Depending on the results obtained, maintenance activities may be limited to cleaning (external, internal) and possible adjustment of individual doses, or may require partial or complete disassembly, microscopic inspection and replacement of defective components with new ones [18]. However, there are problematic situations that necessitate the use of extended diagnostics [6, 9]. An additional correction is made on the basis of the fuel injection characteristics, implemented with the full spectrum of operating pressures and actuation (opening) times of the fuel injector sprayer [7]. Unfortunately, this function is available only on selected test benches, and the time consumption of the experimental phase, compared to the production procedures, increases several times [4, 16, 17].

For the above reasons, the own methodology was proposed, in which the base points were located and connected in a Cartesian coordinate system, and then the resulting fuel delivery fields of the tested fuel injector with the reference fuel injector were calculated and compared. To achieve this goal, classic Gauss's formulas, also known as the shoelace formula, were used, implementing a mathematical algorithm in a Microsoft Excel spreadsheet. This approach is convenient from the practical point of view, because it enables a very quick analysis of experimental data that may come from diagnostic tests of fuel injectors of various types or generations.

2. Methods

2.1. Test object

The tests were carried out on a Delphi DFI 1.2 electromagnetic injector, which was dismantled from the OM 646 engine of a Mercedes-Benz E Class 2.2 CDI vehicle with an operational mileage of 172 thousand kilometres (Fig. 1).

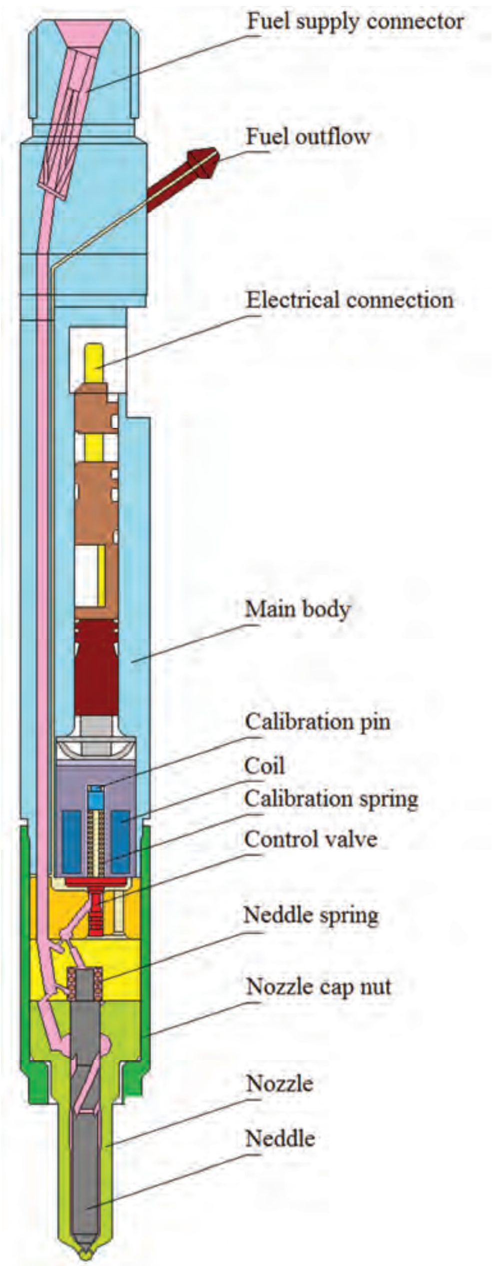

Fig. 1. Delphi fuel injector design

Received 13 December 2020; Received in revised form 4 January 2021; Accepted 20 February 2021
Available online 11 March 2021

Fuel injectors of this type operate at fuel injection pressures of up to 140 MPa [14]. A characteristic feature of their structure is the lack of a guide piston acting on the needle, which is activated by a hydraulic system consisting of chambers and a system of channels with neckings [3]. Owing to screw incisions, it partially rotates, increasing the turbulence of the supplied fuel and favouring the self-cleaning of the working surface. Moreover, the lightweight control valve affects a very short fuel injection delay time and a low value of the force needed to move the needle in the sprayer [10]. In the absence of shims, the size of the injected fuel doses depends on the preload of the electromagnetic coil spring, which is determined by the length of the calibration pin [11, 12].

2.2. Test beds

The following equipment and instrumentation were used in the regeneration process:

- Zapp CRU 2i test bench (Fig. 2),
- Meiji FL150/70 laboratory microscope,
- ultrasonic baths (Carbon Tech S15/C2, Elmasonic S10H),
- vices and tools for assembling/disassembling the fuel injector.

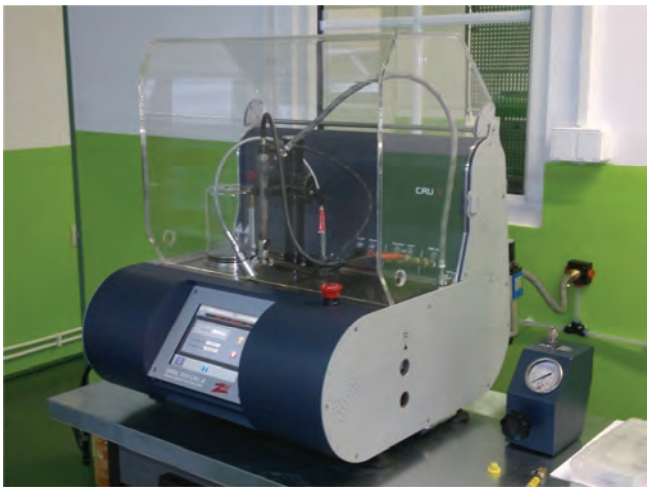

Fig. 2. Zapp CRU 2i test bench

2.3. Gauss`s formulas

In the analytical method, the surface area of a polynomial, which is presented in the Cartesian coordinate system, can be calculated on the basis of the contour corner coordinates [1]. On the assumption that the vertices (x_1,y_1), (x_2,y_2), …, (x_n,y_n) are marked clockwise, then the area of figure A is determined using the following formulas [8, 13]:

$$A=\frac{1}{2}\left|(x_1y_2+x_2y_3+\ldots+x_ny_1)-(y_1x_2+y_2x_3+\ldots+y_nx_1)\right| \quad (1)$$

and in a general form for coordinates x

$$A=\frac{1}{2}\left|\sum_{i=1}^{n} x_i(y_{i+1}-y_{i-1})\right| \quad (2)$$

and for coordinates y

$$A=\frac{1}{2}\left|\sum_{i=1}^{n} y_i(x_{i-1}-x_{i+1})\right| \quad (3)$$

where:
A – polygon surface area,
n – number of vertices,
x_i, y_i – coordinates of the i-th vertex.

Gauss's formulas should be used jointly as they serve the mutual control of calculations. In order to simplify the analytical procedure, some mathematical operations can be entered into the spreadsheet cells in the form of Table 1.

Table 1. Auxiliary table for the calculation of surface areas

Point number	x_i	y_i	$x_{i+1} - x_{i-1}$	$y_{i+1} - y_{i-1}$
1	x_1	y_1	$x_2 - x_4$	$y_2 - y_4$
2	x_2	y_2	$x_3 - x_1$	$y_3 - y_1$
3	x_3	y_3	$x_4 - x_2$	$y_4 - y_2$
4	x_4	y_4	$x_1 - x_3$	$y_1 - y_3$
1	x_1	y_1	$\sum_{i=1}^{n}(x_{i+1} - x_{i-1})$	$\sum_{i=1}^{n}(y_{i+1} - y_{i-1})$

3. Analysis results and discussion

3.1. Preliminary tests

Before starting the tests, the fuel injector was thermochemically rinsed on the diagnostic test bench, so it was subjected to the internal cleaning process at an increased temperature of the detergent. This decision was made due to the possibility of the presence of impurities and internal Diesel Injector Deposits (IDIDs), the presence of which adversely affects the method of fuel delivery, reducing the dynamics of the movement of control and actuation elements [2, 5, 15].

Table 2. Results of the preliminary tests on the Zapp CRU 2i stand

Test type			Result	
Electric test, eRLC	Coil resistance, R_c [Ω]		[0.2–0.6] **0.38**	
	Coil inductance, L [μH]		[60–110] **76**	
	Frequency, f [Hz]		**20**	
Reaction speed test, RSP [μs]			[300–495] **478**	
Nozzle opening pressure test, NOP [MPa]			[13–23] **18**	
Leak Test, LKT [MPa] 140 MPa, 120 s			Injection dosage	Return dosage
			0	[0–40] **34.86**
Injector Volume Metering, IVM				
Dose number	Injection pressure, p_{inj} [MPa]	Nozzle opening times, t [μs]	Injection dosage, d [mm³/H]	
1	40	462	[1.18–7.91] **2.02**	
2	80	600	[14.43–31.35] **16.24**	
3	140	700	[31.83–46.33] **42.46**	
4	23	573	[0.30–5.55] **0.58**	

The data presented in Table 2 show that the fuel injector passed the standard test procedure, as the obtained results are within the limits permitted by the manufacturer. After installation, however, the engine was characterised by hard, rough operation, particularly at idle and light loads, and the service indicator was illuminated on the vehicle's dashboard. For the above reasons, it was decided to implement the proposed methodology.

The results of the IVM volume measurements were located in the Cartesian coordinate system. The connection of the base points 1-2-3-4 made it possible to create an irregular quadrilateral, the surface area of which was estimated using the formulas (2) and (3). For this purpose, calculation formulas were created and entered into the spreadsheet. After substituting the numerical values constituting the vertices of the analysed figure, the resultant fuel metering field was obtained in the preliminary test A_{PT} (Table 3).

Table 3. Calculation of the resultant fuel metering field A_{PT}

Dose number	t_i	d_i	$t_{i+1} - t_{i-1}$	$d_{i+1} - di_{-1}$
1	462	2.02	27	15.66
2	600	16.24	238	40.44
3	700	42.46	–27	–15.66
4	573	0.58	–238	–40.44
1	462	2.02	Σ = 0	Σ = 0
A_{PT}				
1317.60 = ½|(27·2.02) + (238·16.24) + (–27·42.46) + (–238·0.58)|				
1317.60 = ½|(15.66·462) + (40.44·600) + (–15.66·700) + (–40.44·573)|				

The calculations for the reference fuel injector were performed in the same way, using the data provided by the manufacturer (Table 4).

Table 4. Calculation of the resultant fuel metering field A_{SI}

Dose number	t_i	d_i	$t_{i+1} - t_{i-1}$	$d_{i+1} - di_{-1}$
1`	462	4.55	27	19.96
2`	600	22.89	238	34.53
3`	700	39.08	–27	–19.96
4`	573	2.93	–238	–34.53
1`	462	2.02	Σ = 0	Σ = 0
A_{SI}				
1909.09 = ½|(27·4.55) + (238·22.89) + (–27·39.08) + (–238·2.93)|				
1909.09 = ½|(19.96·462) + (34.53·600) + (–19.96·700) + (-34.53·573)|				

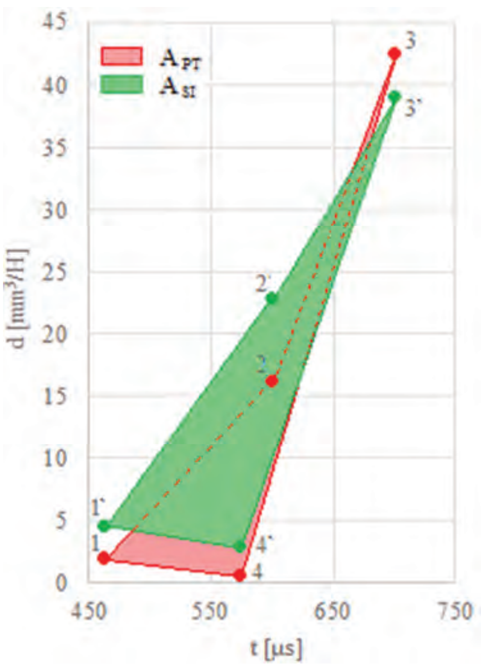

Fig. 3. Graphical interpretation of the preliminary test results

Figure 3 shows the graphic interpretation of the obtained results. The disturbance of the fuel injection process causes a clear shift of the quadrilateral 1-2-3-4, and the position of individual vertices may indicate the cause of the malfunction. The doses obtained at short actuation (opening) times of the sprayer prove that the needle is difficult to lift, which has problems with overcoming the spring tension after applying low operating pressures on the test bench. On the other hand, the discrepancies between points 2-2' and 3-3' suggest incorrect operation of the control valve, in particular the possibility of frictional wear of its guide surface. As a result, the difference between the resulting fuel delivery fields for the tested fuel injector A_{PT} and the reference one A_{SI} was significant as it amounted to 30.98%.

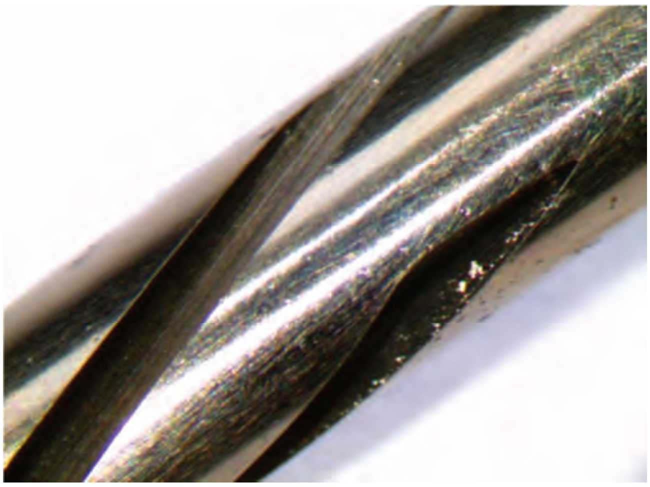

Fig. 4. Longitudinal delineation on the needle

Fig. 5. Friction wear on the guide surface of the control valve

During the disassembly phase, it was found that the control valve does not fall out of the body seat under the influence of gravitational force, which confirmed the earlier conclusions. In the next step, the components were subjected to cleaning baths in ultrasonic baths and microscopic inspection under high magnification (Figs. 4 and 5). Due to the identified signs of wear, it was decided that the repair would be limited to the replacement of the valve assembly, plunger and barrel assembly (needle and sprayer) and the solenoid coil seals, which were additionally lubricated with light liquid petrolatum. Since the results of the preliminary test were within the limits specified by the manufacturer, no additional correction of the fuel metering was carried out by changing the length of the control pin. The fuel injector was assembled and mounted on the test bench for further testing.

3.2. Main tests

Tables 5 and 6 show the results of the main tests that were carried out after the fuel injector regeneration process.

Table 5. Results of the main tests on the Zapp CRU 2i stand

Test type			Result	
Electric test, eRLC	Coil resistance, R_c [Ω]		[0.2–0.6] **0.42**	
	Coil inductance, L [μH]		**[60–110]** **84**	
	Frequency, f [Hz]		**20**	
Reaction speed test, RSP [μs]			[300–495] **432**	
Nozzle opening pressure test, NOP [MPa]			**[13–23]** **15**	
Leak Test, LKT [MPa] 140 MPa, 120 s			Injection dosage	Return dosage
			0	**[0–40]** **2.06**
Injector Volume Metering, IVM				
Dose number	Injection pressure, p_{inj} [MPa]	Nozzle opening times, t [μs]	Injection dosage, d [mm^3/H]	
1``	40	462	[1.18–7.91] **4.58**	
2``	80	600	[14.43–31.35] **22.14**	
3``	140	700	[31.83–46.33] **38.86**	
4``	23	573	[0.30–5.55] **2.91**	

The repair should be assessed positively as the factory settings have been restored. As a result, the resulting fuel delivery field A_{MT} and the reference one A_{SI} are comparable, as the difference between them was only 4.37%. For this reason, in the graphic interpretation presented in Figure 6, they practically overlap. In the absence of an injector malfunction, the vertices of both figures have a similar position, and the shifts characteristic for the preliminary test does not occur.

Table 6. Calculation of the resultant fuel metering field A_{MT}

Dose number	t_i	d_i	$t_{i+1} - t_{i-1}$	$d_{i+1} - d_{i-1}$
1``	462	4.58	27	19.23
2``	600	22.14	238	34.28
3``	700	38.86	–27	–19.23
4``	573	2.91	–238	–34.28
1``	462	4.58	Σ = 0	Σ = 0
A_{MT}				
1825.59 = $\frac{1}{2}\lvert(27\cdot4.58) + (238\cdot22.14) + (-27\cdot38.86) + (-238\cdot4.58)\rvert$				
1825.59 = $\frac{1}{2}\lvert(19.23\cdot462) + (34.28\cdot600) + (-19.23\cdot700) + (-34.28\cdot573)\rvert$				

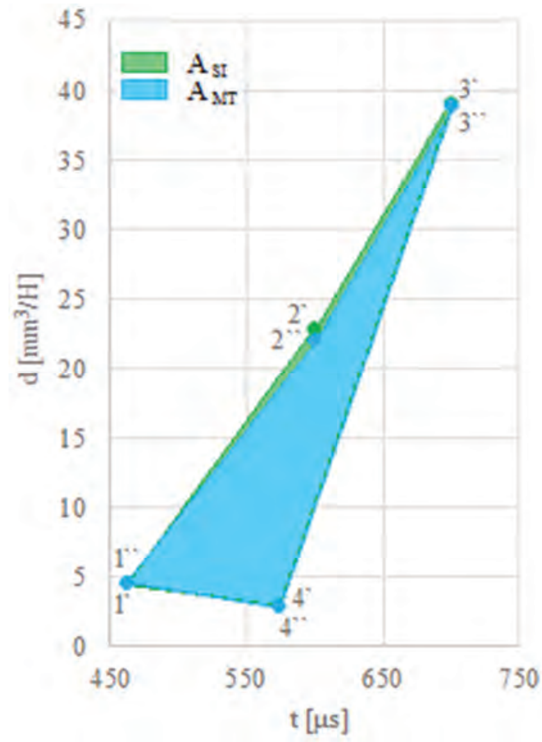

Fig. 6. Graphical interpretation of the main test results

4. Conclusions

The proposed methodology makes it possible to consider specific cases of failure of common rail fuel injectors that operate incorrectly despite meeting the required diagnostic criteria. As standard base points are taken into account in the calculations, its implementation does not require additional measurements on the test bench, which is an unquestionable advantage. There is also no need to modify the test bench software, as the analytical process was completely transferred to the popular spreadsheet environment. Algorithms created once in this way can be reused in the analysis of other cases and easily modified, adapting them to the procedures of a given manufacturer. In addition, in laboratory and repair shop conditions, graphic interpretation of the final results is not required, and the drawings presented in this paper are for illustrative purposes only.

It is also worth emphasising that the resulting fuel delivery fields should be treated purely hypothetically, as they do not reflect the actual fuel injection method at intermediate points, i.e. beyond the vertices of the generated figures. Nevertheless, their mathematical estimation allows for verification and assessment of the technical condition of the fuel injectors in problematic situations, as shown in a specific example. In view of the above, the presented methodology is an effective solution to the needs of the modern service market of fuel injection equipment, which have been signalled in recent years.

Nomenclature

A polygon surface area

A_{MT} the resulting fuel delivery field in the main test

A_{PT} the resulting fuel delivery field in the preliminary test

A_{SI} the resulting fuel delivery field of the reference fuel injector

CDI Common Rail Direct Injection

d injection dosage

eRLC Electric test
f frequency
IDID Internal Diesel Injector Deposit
IVM Injector Volume Metering
L coil inductance
LKT Leak Test
n number of vertices
NOP Nozzle Opening Pressure test
p_{inj} Injection pressure
R_c coil resistance
RSP Reaction Speed test
t nozzle opening times
x_i, y_i coordinates of the i-th vertex

Bibliography

[1] BALDIN, N. Estimating the volume of a convex body. *Snapshots of modern mathematics from Oberwolfach*. 2018, **15**, 1-12. https://doi.org/10.14760/SNAP-2018-015-EN
[2] BERNDT, S., SCHÜMANN, U., SADLOWSKI, T. et al. Development of a laboratory test for the deposit forming tendency of diesel fuels. *ATZ offhighway worldwide*. 2018, **11**, 50-55. https://doi.org/10.1007/s41321-018-0006-2
[3] BORZA, E.V., BĂLDEAN, D.L. Studiul posibilitătii de implementare a evaluării asistate de calculator în analiza injectoarelor common-rail Delphi. *Stiintă Si Inginerie*. 2018, **33**, 33-35.
[4] BUSZ, W., WALASZYK, A. Optimize the testing process common rail fuel injectors. *Combustion Engines*. 2015, **162**(3), 978-981.
[5] CORBETT, P.J., McINTOSH A.J.S., GEE, M. et al. Use of ionic liquids to minimize sodium induced internal diesel injector deposits (IDIDs). *Molecular Systems Design & Engineering*. 2018, **3**, 397-407. https://doi.org/10.1039/C7ME00110J
[6] KARPIUK, W., BOR, W., SMOLEC, R. Possibilities of analysis of condition and repair of common-rail system injectors. *Journal of KONES Powertrain and Transport*. 2018, **23**(4), 209-216. https://doi.org/10.5604/12314005.1217208
[7] KNEBA, Z., STRASZAK, P., JAKÓBCZYK, K. The effectiveness of fault detection in common rail injectors examination methods. *Combustion Engines*. 2017, **170**(3), 49-56. https://doi.org/10.19206/ CE-2017-308
[8] OCHILBEK, R. A new approach (extra vertex) and generalization of Shoelace Algorithm usage in convex polygon (Point-in-Polygon). *14th International Conference on Electronics Computer and Computation (ICECCO)*. 2018, 206-212. https://doi.org/10.1109/ICECCO.2018.8634725
[9] OLSZOWSKI, S., CHOJNACKI, T., OLSZOWSKI, T. Nieprawidłowa praca wtryskiwaczy common rail pomimo pozytywnego wyniku badania. *Autobusy – Technika, Eksploatacja, Systemy Transportowe*. 2017, **6**, 1003-1007.
[10] OSIPOWICZ, T., ABRAMEK, K.F. Diagnosing methods common rail fuel injectors. *Combustion Engines*. 2017, **168**(1), 56-61. https://doi.org/10.19206/CE-2017-109
[11] OSIPOWICZ, T., PRAJWOWSKI, K. Possibilities of research electromagnetic fuel injectors. *Journal of KONES Powertrain and Transport*. 2017, **24**(3), 167-176. https://doi.org/10.5604/01.3001.0010.2928
[12] PUNOV, P. Research the fuel injection characteristics of a common-rail solenoid injector. *Scientific conference on aeronautics, automotive and railway engineering and technologies – BulTrans2015*. 2015, 153-158.
[13] PURE, R., DURRANI, S. Computing exact closed-form distance distributions in arbitrarily shaped polygons with arbitrary reference point. *The Mathematica Journal*. 2015, **17**, 1-27. https://doi.org/doi:10.3888/tmj.17-6
[14] SCHÖPPE, D., ZÜLCH, S., HARDY, M. et al. Delphi Common Rail system with direct acting injector. *MTZ Worldwide*. 2008, **69**, 32-38. https://doi.org/10.1007/BF03226918
[15] STĘPIEŃ, Z. A study of factors influencing the formation of harmful deposits in the diesel engine injectors. *Eksploatacja i Niezawodność – Maintenance and Reliability*. 2017, **19**(3), 331-337. https://doi.org/10.17531/ein.2017.3.3
[16] STOECK, T. Methodology for Common Rail fuel injectors testing in case of non-typical faults. *Diagnostyka*. 2020, **21**(2), 25-30. https://doi.org/10.29354/diag/122034
[17] STOECK, T. Simplification of the procedure for testing common rail fuel injectors. *Combustion Engines*. 2020, **180**(1), 52-56. https://doi.org/10.19206/CE-2020-109
[18] STOECK, T., OSIPOWICZ, T., ABRAMEK, K.F. Methodology for the repair of Denso common rail solenoid injectors. *Eksploatacja i Niezawodność – Maintenance and Reliability*. 2014, **16**(2), 270-275.

Tomasz Stoeck, DEng. – Department of Automotive Engineering, West Pomeranian University of Technology in Szczecin, Poland.

e-mail: *tstoeck@wp.pl*

Article citation info:
STĘPIEŃ, Z. Influence of physicochemical properties of gasoline on the formation of DISI engine fuel injector deposits. *Combustion Engines*. 2021, **184**(1), 16-23. https://doi.org/10.19206/CE-133730

Zbigniew STĘPIEŃ

Influence of physicochemical properties of gasoline on the formation of DISI engine fuel injector deposits

This paper describes the results of an engine study of the tendency for fuel injector deposits to form by gasolines of various compositions. Since the factors promoting the formation of fuel injector deposits in DISI engines have, in many cases, been insufficiently identified they require further research and investigation work, which was the greatest motivation for undertaking this project. The latest CEC F-113-KC test procedure for the most damaging deposits in DISI engine injectors was used for this purpose. The research results obtained in the framework of the conducted project indicated T90, aromatic and olefinic hydrocarbons, sulphur, ethanol, DVPE, IBP and fuel density as the most important factors causing the increase in the tendency for deposits to form on the injectors of SI type DISI engines.

Key words: *direct injection spark ignition engine, injector deposits, deposit control additives, fuel, engine tests*

1. Introduction

The problem of formation of harmful deposits on various elements of gasoline and diesel engines has been known for about 50 years. The need to prevent the formation of these deposits has forced the gradual development and implementation of various engine testing and evaluation methods as well the effectiveness of various solutions to reduce deposits formation. This is reflected in subsequent editions of the World-Wide Fuel Charter, where successively verified procedures of testing harmful engine deposits are indicated, adjusted to the requirements of changing fuel formulations, their categories and successive generations of engines. For testing deposits formed in SI engines, the World-Wide Fuels Charter (2013 edition) indicates the following American methods: ASTM D 5500, ASTM D 6201, ASTM D 5598, and ASTM D 6241 and European methods: CEC F-05-93 (M102E), CEC F-16-96 (VW Boxer), and CEC F-20-98 (M111) [1]. All the American methods assume testing in cars or engines dating back to the 1980s, with only indirect fuel injection engines. The tests include evaluation of deposits on intake valves and in fuel injectors. European methods assume that all of the above tests are conducted on port fuel injection (PFI) indirect fuel injection engines dating back to the 1990s. The evaluations concern deposits on intake valves and in combustion chambers. Therefore none of the mentioned methods are representative for the currently most widespread both in the USA and in Europe direct injection SI engines (direct injection spark ignition DISI/gasoline direct injection GDI).

The direct injection technology has allowed engine manufacturers to meet the emission and fuel consumption (engine efficiency improvement) targets imposed by progressively more stringent regulations. However, it changed the need for testing and evaluation of harmful deposits. It turned out that in this type of engines, the deposits that have the most harmful effect on the correct and reliable functioning of the engine are the fuel injector deposits. The influence of contaminated fuel injectors on the deterioration of the engine operating characteristics, its emissions and performance has been studied and described in many works [2–11]. Gradually increasing injector deposits enforce the need for constant, precise verification and tuning of the amount of fuel injected into the engine combustion chamber – Fig. 1.

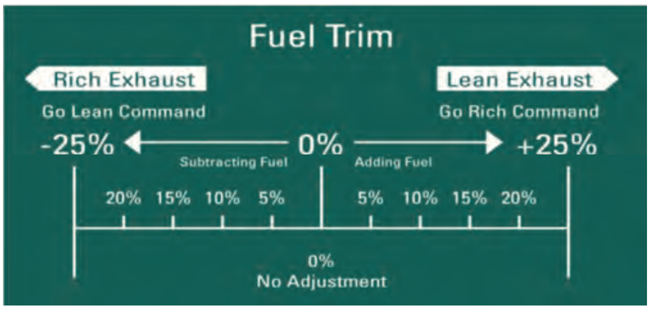

Fig. 1. Tuning the size of the fuel dose to the needs of the combustible mixture formed with an excess air ratio of $\lambda = 1$ [12]

This is necessary in order to maintain the constant excess air ratio of $\lambda = 1$ required for the correct and reliable operation of the commonly used three-way exhaust catalytic converters. For this purpose, a lambda sensor installed in the engine exhaust system constantly monitors the oxygen content of the exhaust gases. This information is transmitted to the engine's control unit (ECU), which simultaneously receives information from an air mass sensor that monitors the mass flow rate of the air supplied to the engine. On this basis the amount of fuel that should be delivered to the combustion chamber under specific engine operating conditions is calculated. This in turn is the basis for controlling the width of the electrical impulse which determines the length of the fuel injection time, varying depending on the operating conditions of the engine, but also on the degree of contamination of the injectors. Therefore, the on-board computer must immediately make corrections to the dosed fuel when changes in the excess air ratio indicate a mixture that is too lean or too rich.

These adjustments are made on average several times per second and are referred to as short term fuel trim (STFT) adjustments. The continuous change of the short term fuel trim correction is communicated to the engine's on-board computer to determine the long term fuel trim (LTFT) correction which is significantly affected by the

Received 26 January 2021; Received in revised form 24 February 2021; Accepted 26 February 2021
Available online 11 March 2021

injector deposits formed. As injector deposits increase, the engine's on-board computer gradually increases the fuel dose injection time to compensate for the decreasing fuel flow rate out of the injectors. However, when the amount of long term fuel trim correction exceeds 25%, fuel injection system dysfunction occurs and the engine stops [12].

It is anticipated that compliance with future, even stricter regulations for reducing emissions of harmful components of exhaust gases will be possible by further optimization of the processes of preparation and combustion of the combustible mixture in the engine cylinders. This will require further increasing the fuel injection pressure, reducing the diameter of fuel outlet channels in injectors and increasing their precision. As a result, counteracting the formation of injector deposits becomes even more important, as the injectors will be even more sensitive to fouling with deposits disrupting their functioning. Therefore, fuel properties and especially effectiveness of deposit control additives DCA type packages will play a decisive role in maintaining by the engine, during its lifetime, parameters and performance declared by its manufacturer. Unfortunately, DCA type additives are not always equally effective for direct and indirect injection engines. Meanwhile, both European and U.S. recognized test procedures for sediment testing and evaluation have been developed based on PFI indirect fuel injection SI engines. The results of these tests do not allow extrapolation and evaluation of the performance of DCA type additives for DISI engines. This has led to the development by automotive as well as fuel additive manufacturing companies of at least several different engine "in-house" methods to evaluate the performance of DCA-type additives [13, 14]. However, the results of evaluations carried out by these methods are incomparable due to different test conditions. The experience gained and observations made in this way allowed to determine the most important guidelines to be followed in the development of an effective, generally applicable test allowing for quick generation of the tested deposits and reliable fuel assessment as regards the tendency to keep clean the injectors of DISI SI engines and the ability to wash out the deposits after their earlier generation. These indications are detailed below [5, 15–17]:

– the most favourable operating conditions for deposit formation in a DISI engine are steady state operation at mid revs (typically 1500–2500 rpm) and medium to low load,
– temperature to which the injector tip gets heated plays a crucial role in the formation of deposits on the injectors (when T90 is higher than the injector tip temperature the propensity for deposits to form will be greater),
– apart from DCA, the rate and amount of deposit formation in the injectors is also influenced by the fuel composition (e.g. the higher the content of olefinic hydrocarbons and sulphur in the fuel, the greater the deposit formation tendency),
– the lower the injected fuel pressure, the higher the susceptibility to deposits,
– the operation of the engine under steady-state conditions keeps the temperature of the injector tips stable, i.e. it is always below or above the T90 temperature of the fuel,
– sufficient time to carry out "Clean-Up" type tests, guaranteeing repeatability of results is usually between 25 and 50 hours.

In 2016, the CEC formed a new TDG-F-113 DISI Working Group and began developing a test procedure that meets the above expectations.

In an effort to reduce the cost and time of developing the test procedure, an existing test method developed "In-house" by VW was adopted as its basis. The first "Draft" of the procedure was released in December 2017. The procedure was designated CEC F-113-KC and named VW EA111 DISI Injector Deposit Test. The VW EA111 BLG engine, widely known and used in many VW families, was used as the test tool.

It is a DISI engine, with combined supercharging system (mechanical supercharging + turbocharging) built in the "downsizing" convention. The basic parameters of the engine are shown in Table 1. The engine is equipped with wall-guided category fuel injection. For fuel injection 6-hole injectors controlled electromagnetically were used.

Table 1. Basic technical parameters of VW EA111 BLG engine

Engine Code	BLG – EA111
Type	4-cylinder in-line engine
Displacement	1390 cm³
Bore	76.5 mm
Stroke	75.6 mm
Valves per Cylinder	4
Compression Ratio	10:1
Maximum Output	125 kW at 6000 rpm
Maximum Torque	220 Nm at 1750 – 4500 rpm
Engine Management	Bosch Engine Management
Fuel	Super Plus at RON 98 (Super unleaded at RON 95 with slightly higher consumption and torque reduction in the low rev ranges)
Exhaust Gas Treatment	Main catalytic converter. Lambda control
Emission Standard	EU4

The current version of the CEC F-113-KC procedure (November 2020) allows the evaluation of fuels (DCA additives) to be conducted according to two tests, as follows:

1) "Keep-Clean" Test

This is a 48 hour test during which the engine works under constant speed (2000 rpm) and constant load (56 Nm). It allows to evaluate the base or upgraded fuel in terms of its ability to keep the injectors clean.

2) "Dirty-Up & Clean-Up" Test

Consists of a 48h part of the "Dirty-Up" test performed according to the "Keep-Clean" test and a 24h part of the "Clean-Up" test in which the engine operates under the same conditions as in "Dirty-Up" or "Keep-Clean". The test allows to evaluate cleaning properties of the fuel used in the "Clean-Up" part of the test.

The pressure of the fuel injected during the test is 77 bar.

The criterion of evaluating the tendency of the fuel to form deposits on the injectors in the conducted test is the changing width of the electric impulse controlling the time of injection of the fuel dose. This time changes (lengthens) as the amount of deposits accumulating outside and inside the injector gradually increases. Figure 2 shows the results of typical runs of "Keep-Up" and "Dirty-Up & Clean-Up" tests carried out according to the CEC F-113-KC procedure [18, 19].

2. Research aim

The aim of this study was to analyze the influence of gasoline composition and its various physicochemical properties on the tendency to form deposits on the injectors of DISI engine based on tests carried out in accordance with the procedure CEC F-113-KC (VW EA111 BLG).

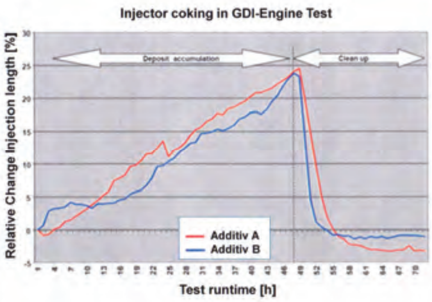

Fig. 2. Typical run of "Keep-Clean" and "Dirty-Up" & Clean-Up" tests (one fuel and two different DCA additives) [19]

3. Test method

Tests on prepared petrol samples were carried out according to test procedure CEC F-113-KC with use of test engine VW EA111 BLG at the Oil and Gas Institute – National Research Institute – Fig. 3. All tests were carried out on the same set of injectors washed after each test.

4. Materials

Seven petrols differing in physicochemical properties and amount of alcohol (ethanol) contained in them were tested in engine tests. While selecting the gasolines, the need of estimating the influence of their different physicochemical parameters and contained alcohol on the tendency to form deposits in the injectors of VW EA111 BLG engine was taken into account. In order to better distinguish the influence of different physicochemical properties on the tendency to deposit formation, fuels not containing DCA type additive packages were used for testing. The physicochemical properties of the prepared fuel samples for engine testing are presented in Table 2.

Fig. 3. General view of engine test bed with VW EA111 BLG engine

Table 2. Physicochemical properties of gasoline samples prepared for engine testing

Properties	Units	BB 95 - 1	BB 95 - 2	BB 95 - 3	BB 98 - 1	BB 98 - 2	BB 95 - 3 + 10%(V/V) ethanol	BB 98 - 1 + 10%(V/V) ethanol	Test method
		1	2	3	4	5	6	7	
Density at temperature 15°C	kg/m³	762,3 ± 0,4	751,2 ± 0,4	739,3 ± 0,4	742,5 ± 0,4	725,6 ± 0,4	744,1 ± 0,4	748,4 ± 0,4	PN-EN ISO 12185:2002^A
Research Octane Number (LOB)	-	95,7	97,6	95,3	98,8	98,8	96,8	101,0	PN-EN ISO 5164^A
Motor Octane Number (LOM)	-	85,1	86,0	85,5	87,2	89,6	86,7	88,7	PN-EN ISO 5163^A
Sulphur	mg/kg	45,6 ± 6,4	4,5 ± 1,2	7,6 ± 1,6	6,8 ± 1,5	2,8 ± 1,0	6,5 ± 1,5	6,5 ± 1,5	PN-EN ISO 20846:2020^A
Induction period	minuty	>360	>360	>360	>360	>1200	>360	>360	PN-EN ISO 7536:2011^A
Washed gums	mg/100ml	3,0 ± 2,5	2,5 ± 2,3	2,5 ± 2,3	1,5 ± 2,0	1,0 ± 1,5	1,0 ± 1,5	1,0 ± 1,5	PN-EN ISO 6246:2017-05^A
Hydrocarbon content of type									PN-EN 15553:2009^A
-olefin	%(V/V)	9,8 ± 1,4	8,5 ± 2,1	9,2 ± 2,2	4,0 ± 1,1	4,4 ± 1,1	9,1 ± 2,2	4,0 ± 1,1	
-aromatic	%(V/V)	40,6 ± 2,8	32,8 ± 2,6	26,2 ± 2,6	30,7 ± 2,6	20,8 ± 2,6	23,7 ± 2,6	26,5 ± 2,6	
Benzene	%(V/V)	0,4 ± 0.1	0,7 ± 0.1	0,5 ± 0.1	0,5 ± 0.1	0,3 ± 0.1	0,5 ± 0.1	0,4 ± 0.1	PN-EN 238:2000 +A1:2008^A
Oxygen	%(m/m)	<0,01	1,81 ± 0,21	0,77	1,96 ± 0,21	<0,01	4,6 ± 0,47	5,5 ± 0,51	PN-EN 1601:2017-09^A
Oxygen-containing organic compound content:									
-methanol	%(V/V)	<0,17	<0,17	<0,17	<0,17	<0,17	<0,17	<0,17	PN-EN 1601:2009^A
-ethanoll	%(V/V)	<0,17	<0,17	<0,17	0,2 ± 0,07	<0,17	10,4 ± 0,57	10,6 ± 0,57	
- isopropyl alcohol	%(V/V)	<0,17	<0,17	<0,17	<0,17	<0,17	<0,17	<0,17	
- tert-butyl alcohol	%(V/V)	<0,17	<0,17	<0,17	<0,17	<0,17	<0,17	<0,17	
- isobutyl alcohol	%(V/V)	<0,17	<0,17	<0,17	<0,17	<0,17	<0,17	<0,17	
- ethers (with 5 or more carbon atoms)	%(V/V)	<0,17	10,1 ± 0,57	4,8 ± 0,28	12,1 ± 0,64	10,2 ± 0,57	4,9 ± 0,28	10,4 ± 0,57	
- other organic compounds containing oxygen	%(V/V)	<0,17	<0,17	<0,17	<0,17	<0,17	<0,17	<0,17	
Vapour pressure (DVPE)	kPa	54,2 ± 1,1	74,2 ± 1,1	58,9 ± 1,1	69,2 ± 1,1	57,8 ± 1,1	65,0 ± 1,1	73,2 ± 1,1	PN-EN 13016-1:2018-05^A
Fractional composition:									PN-EN ISO 3405: 2019^A
-IBP	°C	37,4 ± 3,4	34,8 ± 3,4	37,5 ± 3,4	33,6 ± 4,8	42,1 ± 3,4	38,6 ± 3,4	28,3 ± 3,4	
- end of distillation temperature	°C	214,9 ± 5,1	196,5 ± 5,1	196,9 ± 5,1	185,0 ± 5,1	185,1 ± 5,1	194,2 ± 5,1	183,9 ± 5,1	
- distils	%(V/V)	97,3	97,1	97,5	97,6	97,9	97,5	97,5	
- residue	%(V/V)	1,0	1,2	1,2	1,0	1,0	1,0	1,0	
- losses	%(V/V)	1,7	1,7	1,3	1,4	1,1	1,5	1,5	
- evaporation temperature 10%, T10	°C	52,3 ± 2,6	48,8 ± 2,6	51,9 ± 2,6	48,8 ± 2,6	67,3 ± 2,6	49,3 ± 2,6	47,8 ± 2,6	
- evaporation temperature 50%, T50	°C	106,5 ± 3,6	93,4 ± 3,1	88,3 ± 2,9	88,2 ± 2,9	101,8 ± 3,5	67,4 ± 3,6	70,6 ± 2,9	
- evaporation temperature 90%, T90	°C	172,9 ± 4,0	156,5 ± 4,0	157,8 ± 4,1	148,4 ± 4,0	144,9 ± 4,1	153,4 ± 4,0	146,5 ± 4,0	
Volatility index, VLI (VLI=10DVPE+7E70)	-	746 ± 36	955 ± 36	830 ± 36	926 ± 36	952 ± 36	1018 ± 36	1074 ± 36	PN-EN 228 + A1:2017-06^A

5. Discussion of research results

Figure 4 shows a comparison of the results obtained for the seven fuels tested according to the CEC F-113-KC procedure. The test result is the difference in the width of the electrical pulse controlling the opening time of the fuel injectors in a single fuel injection, measured before and after the test. Since the measured pulse is unstable and varies with very high frequency and relatively large amplitude over time, calculating the pulse width increment by simply comparing its magnitude at the beginning and end of the test could be subject to large error. Therefore, a methodology based on the use of a trend function is used instead because the values calculated from the trend are more representative than those that would be based on the end points of the measurement. In this way, the computed averages of the electrical pulse widths controlling the injection timing at the beginning and at the end of the test are obtained. The difference between the two represents the test result.

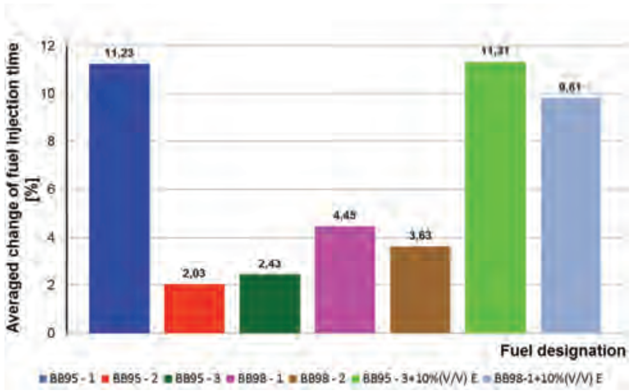

Fig. 4. Comparison of the results of the DISI engine injector deposit tendency evaluations according to the CEC F-113-KC procedure

When proceeding to the evaluation of the results, it should be stressed that each engine construction, the strategy of combustion process organization in it and the injector construction have a great influence on the intensity of the injector coking phenomenon. Therefore, they also influence the final result of fuel assessment in the sense of progression of formation, as well as the size of injector deposits produced in a specific time. The evaluations described in the paper were carried out in accordance with the CEC F-113-KC procedure on VW EA111 BLG engine. It should also be pointed out that the fuel assessments carried out so far in many European laboratories according to the procedure mentioned above allowed, within the framework of the CEC TDG F-113 Working Group, to determine the repeatability of the results obtained using this method based on the Student's t-distribution.

It was calculated that in order to distinguish the two results with 95% confidence, an absolute difference between them of the magnitude of 3.0% change in the width of the electrical pulse controlling the opening time of the fuel injectors in a single fuel injection is required. However, given that this is in practice a large change in pulse size, it was determined that a smaller confidence interval (90%) should be used in evaluating the results, for which an absolute difference between the results of the change in the width of the electrical pulse controlling the opening time of the fuel injectors in a single fuel injection of 1.8% is required. This allows sufficient differentiation and comparison of the results of the tested fuels.

Taking the above into account, the results of the evaluations of the seven fuels presented in Figure 4 can be divided into four groups. In each of these groups, fuel evaluations should be considered comparable from the statistical point of view. Thus, the same, in terms of propensity to form injector deposits, were evaluated fuels in groups: BB95-2 and BB95-3, the corresponding results of averaged fuel injection time changes are 2.03% and 2.43%, BB98-1 and BB98-2 fuels, the corresponding results of averaged fuel injection time changes are 4.45% and 3.63%, BB95-1 fuels, BB95-3 + 10% (V/V) ethanol, the corresponding results of averaged fuel injection time changes are 11.23% and 11.31% and in the last group BB98-1 + 10% (V/V) ethanol, with the result of averaged fuel injection time change of 9.81%. When considering the fuel properties that may have influenced the above variation of results in the different groups, one should refer to Table 2 which contains a summary of the physicochemical properties of the gasoline samples prepared for engine testing. In the available literature, there is a lot of information and research descriptions, which indicate that such properties of unrefined fuel as: T90, vapour pressure, density, IBP, octane number and the content of olefins, aromatics and naphthenes as well as alcohol and sulphur have large or very large effect on the processes of formation of deposits on fuel injectors of IDID type engines. Unfortunately, in different studies the magnitude of the influences of these properties is evaluated differently and not only in terms of the intensity of the effect, but even in terms of the direction. As an example, we can use the 90% fuel evaporation temperature (T90), which, according to most publications, has a very large impact on the formation of deposits of injectors [4, 20–23], although there are also some research results, according to which it has practically no impact [24]. However, speaking about the high significance of T90 on deposit formation in some publications, one can find observations (conclusions) that: high level of T90 can increase fouling of injectors due to lower volatility of fuel allowing formation of deposits in outlet channels and around injector orifices (slower volatilization leading to longer time of fuel staying on hot surfaces of injector tip and consequently faster oxidation and eventually carbonization) [20–22, 25]. In other publications it is argued that: low T90 is responsible for injector fouling due to the higher volatility of the fuel (shorter time the fuel remains on the injector surface, which limits the intensity of cleaning, and furthermore, higher volatility causes higher molecular weight components to be oxidized and carbonized on the hot injector tip surface) [14, 23]. A great difficulty in the interpretation of the obtained results is usually the significant variation of at least several properties of the evaluated fuels. The obtained test result is a resultant of interactions of various fuel properties, some of which may interact with each other in ways that are very difficult to determine and which may have various impacts on injector deposit formation. Comparing the results of injector fouling for fuels BB95-1, BB95-2 and BB95-3, i.e. petrols of LOB = 95, we see that a significantly different result was obtained for BB95-1 (11.23%). Analysing properties of these petrols (Table 2), it may be assumed that the reason of such a high result in case of BB95-1 petrol may be high sulphur content (such hypothesis is consistent with research results presented in [15, 24]), significantly higher T90 value in comparison to the two remaining petrols (it coincides with conclusions presented in [20–22, 25]), higher content of aromatic hydrocarbons (it coincides with conclusions presented in [15, 21], and higher density (such conclusions were also drawn in work [24]). The differences in the properties of BB95-2 and BB95-3 fuels contained in Table 2 were not found to be large enough to significantly affect the results of their evaluations (2.03% and 2.43%, respectively), and therefore to distinguish between these fuels at the assumed confidence interval (90%). The comparison of two gasolines with LOB = 98, i.e. gasoline BB98-1 and BB98-2, indicates gasoline BB98-1 as having a higher tendency to form injector deposits. The reason for this can be sought in higher sulfur content (hypothesis consistent with [23, 26]), higher vapor pressure (similar observations in [24]), higher aromatic hydrocarbon content (consistent with observations in [15, 21]), and higher density (similar observations in [24]). A property that could counteract the greater variation in results between these fuels could be the lower IBP value for BB98-1 gasoline, which according to e.g. [24] contributes to the reduction of injector deposits formed. However, the most interesting and surprising results were obtained when 10% (V/V) ethanol was added to BB95-3 and BB98-1 gasolines. Investigations of the samples prepared in this way, labeled BB95-3 + 10% (V/V) ethanol and BB98-1 + 10% (V/V) ethanol, showed, in both cases, a very significant increase in the propensity to foul the injectors (11.31% and 9.81%, respectively) which is a result inconsistent with those described in [15, 21, 27], but coincident with the results reported in [28]. The higher result of injector fouling by BB95-3 + 10% (V/V) ethanol fuel compared to BB98-1 + 10% (V/V) ethanol fuel may have been influenced by higher olefinic hydrocarbon content (similar observations reported in [22, 24, 29–31], higher IBP value (similar observations reported in [24]), and possibly higher T90 value (this would be consistent with observations in [20–25]).

It is also interesting to compare the course of sediment formation for all the tested fuel samples during 48 hours of the test – Fig. 5.

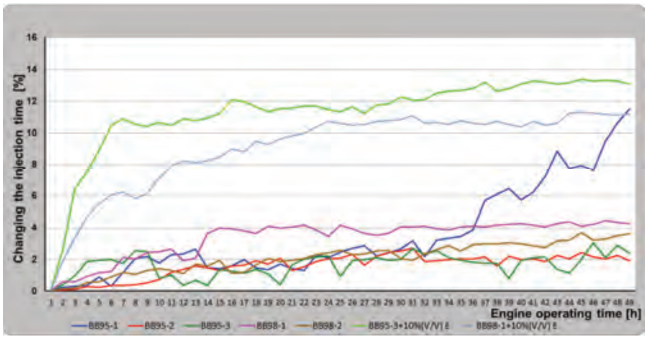

Fig. 5. Summary of fuel injection time variation results for the tested gasoline samples

All the runs presented in Fig. 5 are characterized by gradual but unstable increase in time. The results show significant fluctuations of fuel injection time changes during the test, particularly high for BB95-3, BB95-2 and BB95-1 fuels. Such a phenomenon is known e.g. in the case of deposits formation on engine intake valves [32, 33]. In order to determine the trends of changes in the processes of deposits formed in injectors by the tested petrols during the tests, the lines of their trends were presented in Fig. 6.

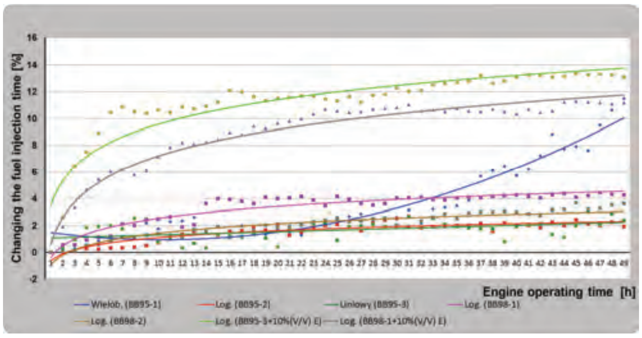

Fig. 6. Summary of trend lines of fuel injection time changes for the tested gasoline samples

As can be seen – Fig. 6, most of the fuel injection time changes for the tested gasoline samples have a logarithmic course. This is the case for BB95-2, BB98-1, BB98-2, BB953 + 10% (V/V) ethanol and BB98-1 + 10% (V/V) ethanol. Only for fuel BB95-1 the waveform is polynomial and for fuel BB95-3 the waveform is linear. The differences in trends in the formation of the size of deposits in the injectors exposed to the influence of the fuels studied result from the intensity of the processes of formation of the deposits precursors, the force of their adhesion to the surface on which they form and the simultaneous processes of self-cleaning of the injectors. Logarithmic run indicates more intensive process of sediment precursors formation at the beginning of injector contamination process, stronger sediment adhesion to the surface and/or lower intensity of sediment removal (washout) from the surface (e.g. due to higher T90). On the other hand, polynomial trend of deposits formation indicates slower process of deposits precursors formation at the beginning of injectors fouling and their weak adhesion to the surface, which can be related to parallel, intensive process of their removal (washing away) due to, for instance, low T90. In the case of linear course of action, the processes of sediment formation and sediment removal take place with constant intensity in defined proportion, with predominance of injector fouling processes. After the sediment precursors are formed and stabilized on the surface of the injectors, further injector fouling is a resultant of the processes of sediment growth and its removal.

The last evaluation of the injector deposits formed by the fuels subjected to the tests was their visual assessment, which is contained in Table 3. It is limited to the description of deposits formed on the front surface of the injector nozzles, the area of convexity of this surface, on which six fuel outlet holes are located, and deposits in the outer part of fuel channels. The evaluation was based on a description of deposits of one injector, representative for each test. It shows that the largest deposits, at the same time in the most critical areas (on the walls of the external parts of the fuel injector tubules), were formed in the BB95-1, BB95-3 + 10% (V/V) ethanol and BB98-1 + 10% (V/V) ethanol fuel tests. Such deposits cause both a reduction in the rate of fuel flow out of the injectors and a deterioration in the quality of fuel jet atomization.

Table 3. Deposits on representative injectors for each of the fuel tests performed

Fuel	Deposits on injector tip		Comment
BB95-1	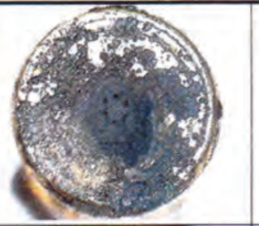		The front surface of the injector tip is covered with an uneven layer of deposits of very different thickness. In the area of the central convexity there is a clear, large thickening of deposits, especially in the vicinity of fuel hole outlets. Thick layers of deposits on the walls of the external parts of the fuel channels (pre-holes) are visible. These deposits may have impeded the outflow of fuel and distorted the pattern of fuel spray.
BB95-2	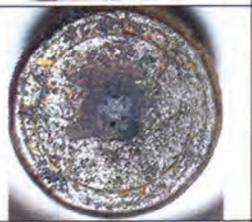		Thin layer of non-uniform (spotty) deposits covering the front surface of the injector tip. Deposits are thickened in the area of the central convexity, especially around the fuel outlet holes. Deposits that can interfere with fuel atomization are visible in some of the preholes.
BB95-3	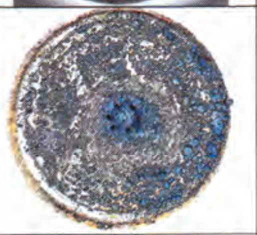	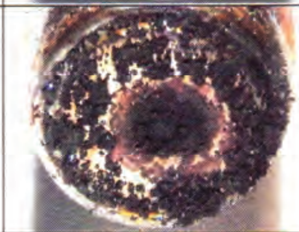	Uneven layer of deposits covering the front surface of the injector tip with local thickening in the form of darker clusters of deposits. Clear thickening of uniform deposits of varying thickness on the area of the central protuberance, especially around fuel outlet holes.
BB98 - 1			Uneven layer of sediment covering the front surface of the injector tip with localized clusters of sediment of widely varying thickness. Note the uneven distribution of deposits on the front surface, dividing it into two conventional halves. In the area of the central convexity there is a clear thickening of uniform deposits especially around the fuel outlet holes. These deposits overlap the edges of the fuel outlet holes.
BB98 - 2	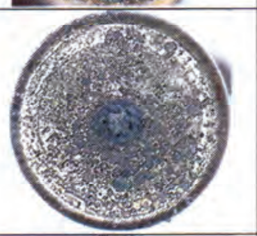		Spotty deposits of varying size and thickness evenly distributed across the nozzle face. Significant thickening of deposits in the area of the central bulge, especially around the fuel outlet orifices. These deposits overlap the edges of the fuel outlet orifices, and in the case of one of them, they significantly reduce its cross section.
BB95 – 3 + 10% (V/V) ethanol			Uniform deposits of widely varying thickness covering most of the front surface of the injector tip. Spotty deposits on the rest of the surface. Significant thickening of deposits in the area of the central bulge, especially around fuel outlet holes. Thick deposits of deposits partially restricting the outflow cross-sections of the fuel channels are visible on the walls of the external parts of the fuel channels
BB98 – 1 + 10% (V/V) ethanol	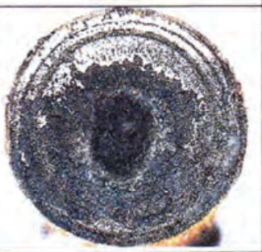		Uniform deposits of widely varying thickness covering most of the front surface of the injector tip. Spotty deposits on the rest of the surface. Significant, uneven deposit thickening around the central bulge, with much of the front face of the injector extending to its edges. Thick deposits of deposits partially restricting the outflow cross-sections of the fuel channels are visible on the walls of the external parts of the fuel channels

6. Conclusion

1) The results of the project proved that the physicochemical properties and composition of gasoline have a great influence on both the initiation, rate of formation and size of deposits formed on injectors of SI type DISI engines.
2) The rapid changes in the pulse width of the fuel injection time, observed during the tests, indicate the simultaneous processes of fuel injector deposit formation and cleaning. The final result of the injector contamination level is a resultant of these processes.
3) The results of the study showed that increased sulfur content in gasoline and increased proportion of aromatic hydrocarbons and high temperature T90 are the main factors promoting and intensifying the phenomenon of fuel injector deposit formation.
4) In the case of the fuel samples tested, an increased tendency to form injector deposits was observed in gasolines containing ethanol.
5) When gasolines with ROM 95 + 10% ethanol and ROM 98 + 10% ethanol were compared, a higher propensity for injector deposits was observed for the former. Analyzing the composition and physicochemical properties of these gasolines, higher olefinic hydrocarbon content and higher IBP and T90 values were indicated as the reason for the formation of more deposits in the case of gasoline with ROM 95 + 10% ethanol.
6) Gasoline ethanol admixture was observed to cause a rapid increase in deposit size in the first 8–10 h of the test, followed by a slow increase in the remainder of the test.
7) The extent of injector fouling is determined by the combined effect of all factors both supporting and limiting the deposit formation process. Moreover, some of the factors may interact with each other in ways difficult to determine.
8) Differences in the trends of deposit formation on the injectors exposed to the influence of the fuels studied result from the intensity of the processes of formation of deposit precursors and the force of their adhesion to the surface on which they form and then the intensity of deposit growth and simultaneous processes of injectors self-cleaning.
9) The results of tests carried out in the project according to the research procedure CEC F-113-KC indicate T90, aromatic and olefinic hydrocarbons, sulphur, ethanol, DVPE, IBP and fuel density as the most important factors causing the increase in the tendency for deposits to form on the injectors of SI engines with direct fuel injection.

Acknowledgements

This work is supported by the Ministry of Science and Higher Education Republic of Poland. Grant number INiG-PIB/0023/TE/20.

Nomenclature

SI	Spark Ignition
DISI	Direct Injection Spark Ignition
WWFCh	Worldwide Fuel Charter
PFI	Port Fuel Injection
GDI	Gasoline Direct Injection
STFT	Short Term Fuel Trim
LTFT	Long Term Fuel Trim
DCA	Deposit Control Additives
T90	Gasoline 90% Distillation Temperature
CEC	The Coordinating European Council for the Development of Performance Tests for Transportation Fuels, Lubricants and Other Fluids
IBP	Initial Boiling Point

Bibliography

[1] Worldwide Fuel Chapter, September 2013

[2] ZHAO, F., LAI, M-C., HARRINGTON, D.L. Automotive spark-ignited direct-injection gasoline engines. *Progress in Energy and Combustion Science*. 1999, **25**, 437-562.

[3] LINDGREN, R., SKOGSBERG, M., SANDQUIST, H. et al. The influence of injector deposits on mixture formation in a DISC SI engine. *JSAE Technical Paper* 2003-01-1771. 2003. https://doi.org/10.4271/2003-01-1771

[4] ARTERS, D., BARDASZ, E., SCHIFLER, E. et al. A comparison of gasoline direct injection. Part I – fuel system deposits and vehicle performance. *SAE Technical Paper* 1999-01-1498. 1999. https://doi.org/10.4271/1999-01-1498

[5] DuMONT, R.J., EVANS, J.A., FEIST, D.P. et. al. Test and control of fuel injector deposits in direct injected spark ignition vehicles. *SAE Technical Paper* 2009-01-2641. 2009. https://doi.org/10.4271/2009-01-2641

[6] CARLISLE, H.W., FREW, R.W., MILLS, JR. et. al. The effect of fuel composition and additive content on injector deposits and performance of an air-assisted direct injection spark ignition (DISI) research engine. *SAE Technical Paper* 2001-01-2030. 2001. https://doi.org/10.4271/2001-01-2030

[7] NOMA, K., IWAMOTO, Y., MURAKAMI, N. et. al. optimized gasoline direct injection engine for the European market. *SAE Technical Paper* 980150. 1998. https://doi.org/10.4271/980150

[8] SANDQUIST, H., DENBRATT, I., OWRANG, F. et. al. Influence of fuel parameters on deposit formation and emissions in a direct injection stratified charge SI engine. *SAE Technical Paper* 2001-01-2028. 2001. https://doi.org/10.4271/2001-01-2028

[9] WHITEHEAD, M.A., BUCKINGHAM, J.P., BRUNNER, J.K. The port fuel injector deposit test – a statistical review. *SAE Technical Paper* 982713. 1998. https://doi.org/10.4271/982713

[10] HIROYUKI, Y., OSAMU, A., HIDETOSHI, E. et. al. Mixture formation of direct gasoline injection engine: in-cylinder gas sampling using fast flame ionization detector. *JSAE Review*. 1999, **20**(1), 23-29. https://doi.org/10.1016/S0389-4304(98)00042-3

[11] JOEDICKE, A., KRUEGER-VENUS, J., BOHR, P. et. al. Understanding the Effect of DISI injector deposits on vehicle performance. *SAE Technical Paper* 2012-01-0391. 2012. https://doi.org/10.4271/2012-01-0391

[12] BARKER, J., REID, J., MULQUEEN, S. et. al. The investigation of the structure and origins of gasoline direct injection (GDI) deposits. *SAE Technical Paper* 2019-01-2356. 2019. https://doi.org/10.4271/2019-01-2356
[13] CHINA, P., RIVERE, J.P. Development of a direct injection spark ignition engine test for injector fouling. *JSAE Technical Paper* 2003-01-2006. 2003. https://doi.org/10.4271/2003-01-2006
[14] VON BACHO, P., SOFIANEK, J., GALANTE-FOX, J. et. al. Engine test for accelerated fuel deposit formation on injectors used in gasoline direct injection engines. *SAE Technical Paper* 2009-01-1495. 2009. https://doi.org/10.4271/2009-01-1495.
[15] ASHIDA, T., TAKEI, Y., HOSI, H. Effects of fuel properties on SIDI fuel injector deposit. *SAE Technical Paper* 2001-01-3694. 2001. https://doi.org/10.4271/2001-01-3694
[16] ARTERS, D.C., MACDUFF, M.J. The effect on vehicle performance of injector deposits in a direct injection gasoline engine. *SAE Technical Paper* 2000-01-2021. 2000. https://doi.org/10.4271/2000-01-2021
[17] ARADI, A.A., HOTCHKISS, A., IMOEHL, B. et. al. The effect of fuel composition, engine operating parameters and additives on injector deposits in a high-pressure direct injection gasoline (DIG) research engine. *Aachen Colloquium – Automobile and Engine Technology*. 2000, 187-211.
[18] BENETT, J. Gasoline direct injection engines the effects of deposit control and removal. 2018. Afton Chemical. https://www.umtf.de/pdf/vortrag_2017/04.04_04_Dr.%20Bennett%20-%20Gasoline%20direct%20injection%20engines%20and%20the%20effects%20of%20deposit%20control%20and%20removal.pdf
[19] TDG – F-113 CEC New Test Development – Proposal for a New Engine Fuels Test Procedure. CEC Materials. https://www.cectests.org/public/info_/g003/Appendix%201_CEC%20New%20Test%20Development%20-%20Terms%20of%20Reference%20-TDG-F-113.pdf
[20] HONGMING, X., CHONGMING, W., XIAO M. Fuel injector deposits in direct-injection spark-ignition engines. *Progress in Energy and Combustion Science*. 2015, 1-69. https://doi.org/10.1016/j.pecs.2015.02.002
[21] ARONDEL, M., CHINA, P., GUEIT, J. Evaluating injector fouling in direct injection spark ignition engines – a new engine test procedure to evaluate the deposit control performance of base fuels and additivated fuels. *TAE Esslingen Fuels Colloquium* 2015.
[22] ARADI, A.A., EVANS, J., MILLER, K. et. al. Direct injection gasoline (DIG) injector deposit control with additives. *SAE Technical Paper* 2003-01-2024. 2003. https://doi.org/10.4271/2003-01-2024
[23] FERNANDES, H., BRAGA, LC., MARTINS, A. et. al. Fuel sulfate content influence in the formation of inorganics components deposits in the engine injectors with technologies of gasoline direct injection. *SAE Technical Paper* 2012-36-0314. 2012. https://doi.org/10.4271/2012-36-0314
[24] PILBEAM, J., WEISSENBERGER, D. Characterisation of gasoline fuels in a DISI engine. *Afton Chemical*. Bracknell, UK. SGS S.A. Vienna, Austria. https://issuu.com/afton_chemical/docs/aftonchemical_characterization_of_g
[25] BADAWY, T., ATTAR, A.M., HUTCHINS, P. et. al. Investigation of injector coking effects on spray characteristic and engine performance in gasoline direct injection engines. *Applied Energy*. 2018, **220**. 375-394. https://doi.org/10.1016/j.apenergy.2018.03.133
[26] K-i S. The efforts to the fuel quality for the environment load reduction – compatible of the gasoline quality to the new vehicle technology. *Nippon Mitsubishi Oil Vehicle Symposium*. 2000.
[27] TANIGUCHI, S., YOSHIDA, K., TSUKASAKI, Y. Feasibility study of ethanol applications to a direct injection gasoline engine journal. *SAE Technical Paper* 2007-01-2037. 2007. https://doi.org/10.4271/2007-01-2037
[28] RUSSELL, M., CUMMINGS, J., CUSHING, T. et. al. Cellulosic ethanol fuel quality evaluation and its effects on PFI intake valve deposits and GDI fuel injector plugging performance. *SAE Technical Paper* 2013-01-0885. 2013. https://doi.org/10.4271/2013-01-0885
[29] ARADI, A.A., IMOEHL, B., AVERY, N.L. et. al. The effect of fuel composition and engine operating parameters on injector deposits in a high-pressure direct injection gasoline (DIG) research engine. *SAE Technical Paper* 1999-01-3690. 1999. https://doi.org/10.4271/1999-01-3690
[30] UEHARA, T., TAKEI, Y., HOSHI, H. et. al. Study on combustion chamber deposit formation mechanism – influence of fuel components and gasoline detergents. *SAE Technical Paper* 971722. 1997. https://doi.org/10.4271/971722
[31] ARADI, A.A., COLUCCI, W.J., SCULL, H.M. et. al. A study of fuel additives for direct injection gasoline (DIG) injector deposit control. *SAE Technical Paper* 2000-01-2020. 2000. https://doi.org/10.4271/2000-01-2020
[32] STĘPIEŃ, Z. Deposit in spark ignition engines – formation and threats. *Combustion Engines*. 2015, **160**(1), 36-48.
[33] STĘPIEŃ, Z. Types of internal diesel injector deposits and counteracting their formation. *Combustion Engines*. 2015, **163**(4), 79-91.

Zbigniew Stępień, DSc., DEng., Prof. of INIG-PIB – The Oil & Gas Institute – National Research Institute in Krakow.
e-mail: *stepien@inig.pl*

Article citation info:
MILEWICZ, J., MOKRZAN, D., SZYMAŃSKI, G.M. The assessment of the technical condition of SO-3 engine turbine blades using an impulse test. *Combustion Engines*. 2021, **184**(1), 24-29. https://doi.org/10.19206/CE-133872

Julia MILEWICZ
Daniel MOKRZAN
Grzegorz M. SZYMAŃSKI

The assessment of the technical condition of SO-3 engine turbine blades using an impulse test

The paper presents the effects of the application of an experimental impulse test as a method of diagnosis of the technical condition of an SO-3 engine turbine blade fitted in a TS-11 Iskra aircraft. The aim of the test was to investigate the frequency characteristics of the blades and discuss differences between the frequency spectrum of the investigated component before and after its damage. The acoustic response measurements were performed to the signal generated by an impact hammer on the fully functional and intentionally damaged blades. The recorded signals were converted from the domain of time to the domain of frequency using the Fast Fourier Transform (FFT). The results of the FFT were the Frequency Response Functions (FRF) of the sound of the blades, based on which the statistical analysis of the resonance frequencies was carried out. The influence of the mechanical damage of the blade on the shape and characteristics of the frequency spectrum was confirmed, which substantiated the effectiveness of the impulse test in the diagnostic assessment of jet engine components.

Key words: *jet engine, turbine, modal analysis, resonance*

1. Introduction

Turbine as the fundamental component of a jet engine is a rotor flow machine, converting the enthalpy of the working medium to mechanical work subsequently taken off by the compressor and other engine aggregates [4]. Reducing the turbine efficiency results in a reduction of the engine thrust and increased unit fuel consumption. Therefore, its high durability and operational reliability are required, both directly depending on the geometry of the turbine subcomponents constantly subject to thermal and mechanical loads. The unwanted consequences of these loads are not always easy to identify [5] and the blades operating under severe conditions (resonance vibration) are prone to damage in a short time. Material fatigue and turbine blade deformation, apart from reducing the engine efficiency, may lead to its malfunction and, as a consequence, an air disaster [7, 13].

Among the vibroacoustic methods of diagnosing the jet engine rotors we may distinguish, in particular, the vibration spectrum analysis as well as investigations of the mo dal properties. The first method consists in determining the discrete components of frequencies that are compared with the characteristic frequencies, resulting from the design of the engine and its operating conditions at a given speed. The other method is based on precise measurement of the object vibration, through an electrodynamic exciter or, mechanically, with an impact hammer and allows determining the relation between the geometry of the turbine and its technical condition. In both cases, thanks to the application of the Fast Fourier Transform (FFT) we may switch from the function of time, in which the measurements are made, to the function of frequency, which aside from the general assessment of the condition of the component, also allows identification of the sources of the malfunction [8].

The aim of the investigations was the determination of the frequency signature of selected turbine blades (SO-3 jet engine) as well as the assessment of the effectiveness of the impulse test in comparing the damaged blades with the undamaged ones. In order to obtain the expected results, the measurements were preliminarily performed on 11 undamaged blades and then certain modifications were imposed on two of them. The intentional damage locally modified the rigidity of the component and resulted in changing the parameters of the modal model, significantly influencing the components of the vibration spectrum and the resonance characteristics. On this basis, the authors determined the general areas and characteristics of the spectrum denoting the structural flaws.

2. Methodology

2.1. The object of investigations

The SO-3 jet engine, from which the turbine components were taken for the investigations, was manufactured specifically for the PZL TS-11 Iskra training aircraft by Polskie Zakłady Lotnicze in Mielec. The turbine is a single stage, axial flow reactive one with a constant outer and inner channel diameter. The diameter of the rotor disc holding 83 blades with groove locks is 760 mm [10]. The aerofoil part of a single blade is 64 mm long and the chord of its profile – 28 mm. The blade is made from a refractory alloy of steel and nickel and weighs 73 grams. An undamaged blade has been shown in Fig. 1a, while Figs. 1b and 1c present the intentionally damaged structures simulating failure in operation such as overheating or excess torsional-flexural vibration leading to material fatigue [1, 13].

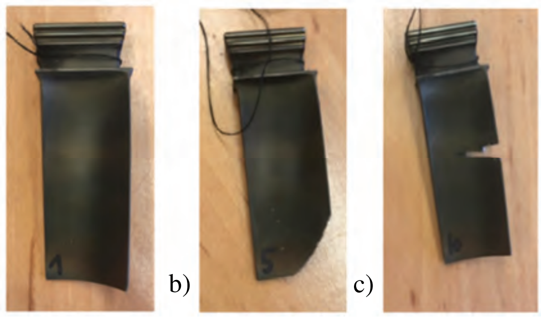

Fig. 1. Turbine blade: a) undamaged, b) damage simulating separation of the tip, c) damage simulating crack of the aerofoil part

Received 27 February 2021; Received in revised form 2 March 2021; Accepted 3 March 2021
Available online 11 March 2021

2.2. The test stand

The diagram of the test stand has been shown in Fig. 2 and the image of the stand in Fig. 3. The tested blades were hanging freely. The blade, when hit by the impact hammer (B&K type 8206), moved slightly around its axis of rotation, which is why it was necessary to use two microphones (B&K type 4189-A-021 ½-inch free-field microphones with type 2671 preamplifier) set perpendicularly to each other on the same plane, in order to limit the errors of the response to the impact and increase the efficiency of the measurement.

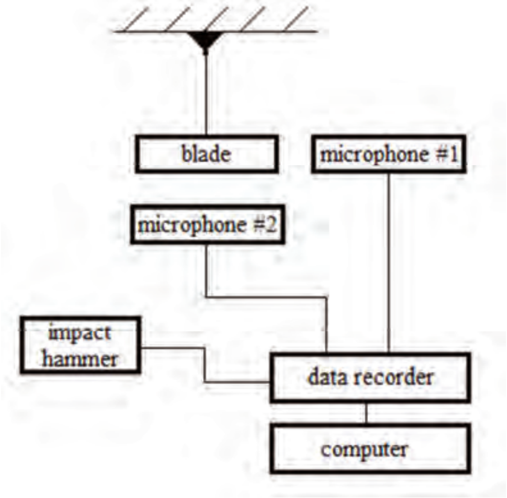

Fig. 2. Diagram of the test stand

Fig. 3. Positioning of the microphones

All blades hung at the same distance from the microphones (270 mm) on the same height and were hit with the hammer on the same spots (on the blade face near the edge). The microphones and the impact hammer were connected directly to the measurement cassette (B&K Input Module LAN-XI 51.2 kHz type 3050) and the data were recorded with the Pulse Time Data Recorder.

2.3. Parameters of the signal analysis

The BK Connect software used for the analysis and visualization of the results utilizes a FFT analysis converting the function of vibration from time to frequency. In order to obtain the interpretable results, it was necessary to determine the ratio of the output signal spectrum, i.e. vibration response of the blade to the impact of the hammer. This relation is mathematically described by the signal-independent descriptor referred to as the Frequency Response Function (FRF), defined by the formula:

$$H(\omega) = \frac{X(\omega)}{F(\omega)} \qquad (1)$$

where: $X(\omega)$ – output signal in the domain of frequency, $F(\omega)$ – input signal in the domain of frequency. Linearity and constancy of the model was assumed [6].

Depending on the nature of the noise and distortions, during the measurement, a predefined estimator of the FRF analysis is applied to minimize the errors. For the case of the hammer impacts, the H_1 estimator was applied for noises in the input signal [3, 8], described with the formula:

$$H_1(\omega) = \frac{G_{FX}(\omega)}{G_{FF}(\omega)} \qquad (2)$$

where: $G_{FX}(\omega)$ – the cross spectrum, between the response and force, $G_{FF}(\omega)$ – the autospectrum of the force.

The signal conversion scheme in this analysis is presented in Fig. 4.

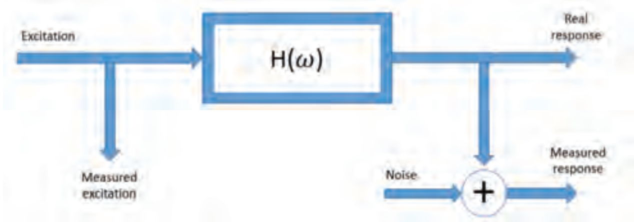

Fig. 4. Scheme for estimating the FRF function

The input parameters of the FFT analysis, selected to properly process the signal with sufficient accuracy have been shown in Table 1.

Table 1. Selected parameters of the FFT analysis

Parameter name	Value
Signal Type	transient
Frequency Range	25.6 kHz
Frequency Resolution	32 Hz
FFT Lines	800
Average Domain	spectrum averaging
Time Weighting	uniform
Reference Signal	impact hammer excitation
Minimum reference signal level	50 N

The resolution of the spectrum and the accuracy of the FFT analysis when processing the signals were selected based on [9] for the conditions of the investigations and expected results, to make the interpretation as convenient as possible. Already at this stage, spectrum averaging of 4 impacts on each of the blades was performed.

2.4. Results of analyses

Throughout the tests, the authors obtained a total of 15 characteristics: 11 for potentially undamaged blades, 2 for the intentionally damaged blades and 2 comparative ones in order to determine the differences in the vibration spectrums.

Based on the characteristics, one may observe a relation between the values of the FRF function in the y-axis, expressed in Pa/N and the frequency of vibration in the x-axis (in kHz). They are a result of averaging (already at the stage of the FFT analysis) of the response from series 4 of the impacts for each blade. The amplitudes have a varied size because the FRF values are directly dependent on the impact force of the hammer that was not the same for all the measurements. 'Linear magnitude' visualization form was selected showing only the positive values of the spectrum in the linear scale. The analyses of the frequency spectrums of the responses received by both microphones were merged into a single spectrum. An example of the sound spectrum as a function of transmittance of the blade identified as undamaged based on a visual inspection has been shown in Fig. 5.

It was observed that the natural frequency, corresponding to the local amplitude maximums is similar for all 11 spectrums, though their general shapes and dominating frequencies vary.

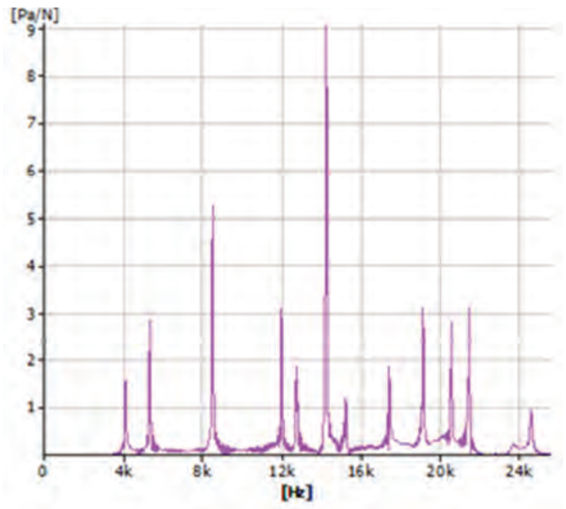

Fig. 5. Sound spectrum of the undamaged turbine blade no. 3

The comparative characteristics of the spectrum for the damaged blades no. 5 and 10 have been shown in Fig. 6.

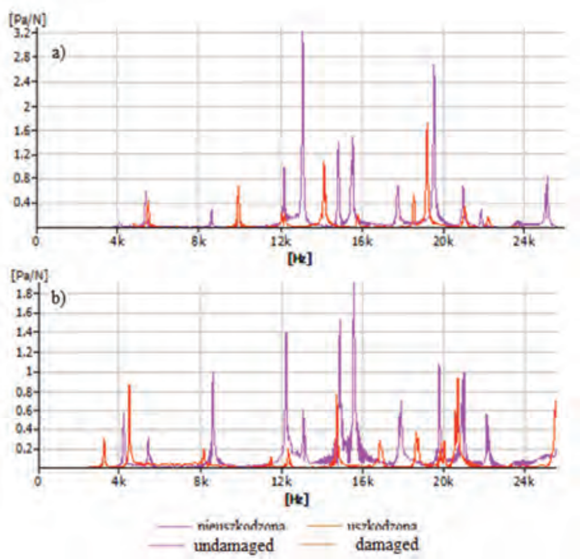

Fig. 6. Comparison of the sound amplitude spectrums: a) blade no. 5 before and after damage, b) blade no. 10 before and after damage

Already at the stage of visual comparison of the spectrums, it was observed how significantly the damage of the structure influenced the characteristics of the natural vibration of the blades. The frequency modes shifted and the amplitudes of the corresponding FRF values changed.

2.5. Statistical analysis of the results

The amplitude criterion was used to determine the resonance frequencies. It determines the natural frequency corresponding to the maximums of the amplitude in a given spectrum [12]. Upon comparing the natural frequency of the subsequent blades corresponding to the maximums of the FRF values, 12 main frequencies were observed and a sideband between mode XI and XII, appearing for the damaged blade no. 5 and the potentially undamaged blade no. 2. In the spectrum of blade no. 2, an additional band was found between modes VII and VIII.

For the statistical analysis, it was assumed that the investigated natural frequencies are a sample from the population of 84 blades of the turbine rotor; For the majority of the mode frequencies of the sample count n = 11, for 5 of them n = 10, due to a lack of a given frequency in the spectrum of the blade. When creating the statistics, the natural frequencies of the damaged blades were not included similarly to the additional sidebands of the spectrum of the blade no. 2. The following statistical measures were applied: arithmetic average $\bar{x}$, average square deviation s^2, mean deviation u, coefficient of variability v, median x_m, range r and center of range c. The results of the calculations of the statistical measures corresponding to the individual modes have been shown in Table 2.

The values of the arithmetic average, median and center of the range are similar for most of the modes, but the average square deviation, range and coefficient of variability are increasingly higher for higher frequencies. This confirms an increasing variation of the resonance frequencies for a given mode while maintaining the expected average values.

In order to assess the confidence intervals, in which the expected value of the subsequent modes μ is found, given the small size of the sample and unknown standard deviation σ, the following model of the interval was used assuming a normal distribution of the population [2]:

$$P\left(\bar{x}_n + t_{\frac{\alpha}{2}} * \frac{s}{\sqrt{n-1}} < \mu < \bar{x}_n + t_{1-\frac{\alpha}{2}} * \frac{s}{\sqrt{n-1}}\right) = 1 - \alpha \qquad (3)$$

where: $t_{\frac{\alpha}{2}}, t_{1-\frac{\alpha}{2}}$ – quintiles of the Student distribution for (n–1) degrees of freedom, α – coefficient of confidence, $\bar{x}_n$ – average value from the sample of count n, μ – expected value.

Initially, the confidence intervals were determined, within which the probability of falling of the expected frequency of a given mode in the intervals is 95% (coefficient α = 0.05), yet, not all natural frequencies obtained from the tracings fell in these intervals. This may have resulted from the assumption of a normal distribution, small size of the sample or non-representativeness of the sample (e.g. as a result of unexpected material flaws or fatigue). Upon changing of the confidence level to 99% (coefficient α = = 0.01) the intervals extended and comprised the majority of the investigated frequencies. Table 3 presents the comparison of the natural frequencies of the damaged blades with the average values of the natural frequencies and the boundary values of the confidence intervals (at the confidence level of α = 0.01). The amber color represents those frequencies of the damaged blade modes that fall in the confidence intervals.

Table 2. Statistical measures for the frequencies of 12 modes

Statistics	f_1 [kHz]	f_2 [kHz]	f_3 [kHz]	f_4[kHz]	f_5 [kHz]	f_6 [kHz]	f_7 [kHz]	f_8 [kHz]	f_9 [kHz]	f_{10} [kHz]	f_{11} [kHz]	f_{12} [kHz]
$\bar{x}$	4.148	5.405	8.547	12.134	12.806	14.575	15.375	17.501	19.340	20.672	21.647	24.807
s^2	0.005	0.002	0.008	0.010	0.029	0.063	0.042	0.049	0.079	0.043	0.075	0.255
u	0.063	0.033	0.078	0.076	0.141	0.194	0.182	0.184	0.257	0.169	0.199	0.383
v	1.75%	0.77%	1.04%	0.81%	1.33%	1.72%	1.34%	1.26%	1.46%	1.01%	1.27%	2.04%
x_m	4.128	5.408	8.576	12.144	12.720	14.640	15.424	17.504	19.264	20.704	21.568	24.800
r	0.224	0.096	0.288	0.256	0.480	0.640	0.672	0.768	0.864	0.640	0.832	1.664
c	4.144	5.392	8.560	12.096	12.848	14.544	15.344	17.504	19.344	20.640	21.536	24.704

Despite serious damage to the blade structure and a change in their rigidity, the frequency of mode IX of the spectrum of blade no. 5 and the frequencies of modes VI and X of the spectrum of blade no. 10 fall in the confidence intervals, hence, a separate analysis of these modes does not provide sufficiently reliable diagnostic information related to the technical condition of a component.

Even though the FRF values, corresponding to the frequencies dominating in the spectrums, are different for the subsequent blades, upon comparing of the modes with the highest amplitudes it was observed that the maximum amplitudes of the transmittance function for the investigated components most frequently fall in the interval f = 12.806–17.501 kHz (between mode V and VIII) deemed as mid-positioned in the vibration spectrum.

3. Interpretation of the results

In the case of the turbine blades whose visual inspection did not reveal any damage, the impulse test allowed measuring the resonance frequencies in the amplitude spectrum of the FRF function and a statistical analysis of their values. The analysis also allowed the determination of the confidence intervals for the determined values of the frequencies. Locally, sudden surges of amplitudes confirming the phenomenon of resonance appeared in the majority of the spectrums 12 times for the following frequencies (the presented results are an arithmetic average with an estimate error for the standard confidence level of 95%):

– f_1 = (4.148 ±0.049) kHz
– f_2 = (5.405 ±0.030) kHz
– f_3 = (8.547 ±0.060) kHz
– f_4 = (12.134 ±0.070) kHz
– f_5 = (12.806 ±0.122) kHz
– f_6 = (14.575 ±0.179) kHz
– f_7 = (15.375 ±0.138) kHz
– f_8 = (17.501 ±0.149) kHz
– f_9 = (19.340 ±0.189) kHz
– f_{10} = (20.672 ±0.140) kHz
– f_{11} = (21.647 ±0.184) kHz
– f_{12} = (24.807 ±0.361) kHz

The frequencies of the vibroacoustic response to the impact are in the range f = 4–26 kHz whereas the densification of the resonance frequencies falls in the range f = 12–18 kHz. In addition, in the same range, the frequencies dominate in the entire spectrum. Such a composition of the spectrum components may indicate a similarity to a normal distribution.

In the spectrums of some of the blades less than 12 modes were read, which may indicate small structural changes, which resulted in a lack of a given natural frequency. The appearance of additional bands $f_{7'}$ and $f_{11'}$ in the spectrum of blade no. 2 most likely identifies microcracks that provide additional resonance [11].

It was observed that along the increase in the vibration frequency the spread of the results around the average value increased, which resulted in a wider confidence interval for the expected value and a greater estimate error. Particularly the frequency of mode XII significantly differed for each spectrum. This may be the consequence of the Doppler's effect distorting the measurement of the vibroacoustic response recorded by the microphones. The most 'unchanging' appear to be the first four modes, therefore their observations may be treated as the most reliable diagnostic information during the analysis of the spectrums for the assessment of the diagnostic condition.

The investigated deformation of the structure and the change in the rigidity of the blade following an intentional tear of the blade tip significantly modified the vibration spectrum of the component, thus changing the characteristic natural frequencies. This resulted in an increase in the majority of the natural frequency values and a decay of the mode from the center band as well as the final mode, which reduced the spectrum range. The highest FRF value, corresponding to the main dominating frequency falls in the middle of the second part of the spectrum range, only to make the resonance frequency amplitude drop rapidly. Therefore, the damaging of the right side of the blade (in relation to the point of impact) caused a left side asymmetry of the vibration spectrum.

Cutting the blade in the middle of its length caused a clear spread of the first (I–V mode) and second (VII–IX mode) part of the vibration spectrum, while maintaining the almost unchanged middle (VI mode) and final (XII mode) value of the natural frequency. In the case of such damage, the vibrations of both 'halves' of the blades have a mutual impact, thus augmenting the resonance (the dominating frequencies are clearly distinguished through their amplitude against the outstanding bands and fall in the beginning, middle and end of the spectrum range, while in the spectrum of the same undamaged blade, the frequencies have a distribution similar to normal with the maximum amplitude for the center (VI mode).

Table 3. Comparison of the boundary values of the confidence interval and the average value of the natural frequency of the undamaged blades with the frequencies of the damaged blades modes

Mode frequency	Frequencies of the undamaged blades			Frequencies of the damaged blades	
	Lower confidence limit	Mean $\bar{x}$	Upper confidence limit	Blade no. 5 damaged	Blade no. 10 damaged
f_1 [kHz]	4.079	4.148	4.218	4.768	3.232
f_2 [kHz]	5.362	5.405	5.448	5.504	4.480
f_3 [kHz]	8.462	8.547	8.632	9.920	8.160
f_4 [kHz]	12.034	12.134	12.235	12.032	11.488
f_5 [kHz]	12.631	12.806	12.981	-	12.320
f_6 [kHz]	14.29	14.575	14.800	14.88	14.720
f_7 [kHz]	15.178	15.375	15.571	15.808	16.864
f_8 [kHz]	17.29	17.501	17.712	18.560	18.656
f_9 [kHz]	19.071	19.340	19.609	19.200	20.032
f_{10} [kHz]	20.473	20.672	20.871	21.056	20.704
f_{11} [kHz]	21.385	21.408	21.91	22.208	–
f_{12} [kHz]	24.288	24.807	25.326	–	25.536

4. Conclusions

Diagnostic methods utilize both the data coming from the vibroacoustic residual processes, generated by the engine and those contained in the response to controlled vibration impacts. The modal analysis allows observing the relation between the vibration impacts and the change in the natural frequency and determine the resonance characteristics for a specifically structurally determined blade. As a non-destructive method it may be used at the design as well as the overhaul stages of the engine life cycle.

The applied method of vibration analysis was an impulse test on a turbine blade (SO-3 engine) based on the assumptions of a modal analysis, yet, its results are limited to the interpretation of the vibration frequency spectrum obtained following the Fast Fourier Transform. Aside from the vibration frequency, the measured value was not the basic vibration parameter (e.g. acceleration) but a ratio of the vibroacoustic response to the force of the impact determined by the transmittance function referred to as FRF.

The performed investigations of the vibration characteristics of the turbine blades of an SO-3 jet engine have proven the effectiveness of the impulse test as a diagnostic method of the technical condition. An impact force and the measurement of the vibroacoustic response of the blades allowed the determination of the frequency signature with a certain confidence level for a given statistical sample.

The turbine blade of given own parameters has 12 main resonance frequencies in the range 4–26 kHz, whereas the dominating frequencies in the spectrum most often come from the range 12–18 kHz. The spread of values around the average in the sample was particularly high for higher natural frequencies. The average, the median and the center of the spread were similar for all the modes. The coefficient of variability reached the lowest values for modes II and IV (below 1%) and the highest values for modes XI and XII (above 2%), which confirms a significant variation of the distribution in the end of the spectrum range and a lower certainty in its diagnostic use. Besides, lack of some of the modes in the spectrums or the existence of additional sidebands are deviations from the set standard that may indicate interior micro-cracks and deformations of the blade structure that is undetectable without specialized equipment.

The influence of mechanical damage of the aerofoil part of the blade dramatically changed the distribution of the modes in the spectrum and the amplitude values. Upon shifting the modes towards higher or lower frequencies one may identify the location and type of damage. When the tip of the blade is torn the distribution of the natural frequencies is asymmetrical, and for the crack along the central part of the blade, the first and the second part of the spectrum get separated, and the dominating ranges have an amplitude unproportionally high compared to the outstanding ones.

Such significant changes in the vibroacoustic response of a damaged component confirm the applicability of the impulse test for the diagnostic assessment of a technical object.

Acknowledgements

The presented results have been co-financed from the subsidies appropriated by the Ministry of Science and Higher Education – 0416/SBAD/0001.

Nomenclature

$F(\omega)$ input signal in the domain of frequency

FFT fast Fourier transform

FRF frequency response function

$G_{FX}(\omega)$ the cross spectrum

$G_{FF}(\omega)$ the autospectrum of the force

$X(\omega)$ output signal in the domain of frequency

Bibliography

[1] BŁACHNIO, J., BOGDAN, M., ZASADA, J. Increased temperature impact on durability of gas turbine blades. *Eksploatacja i Niezawodnosc – Maintenance and Reliability.* 2017, **19**, 48-53. https://doi.org/10.17531/ein.2017.1.7

[2] BOBROWSKI, D., MAĆKOWIAK-ŁYBACKA, K. Selected Statistical Inference Methods. *Poznań University of Technology Publishing House*, Poznań 2006 (in Polish).

[3] DØSSING, O. Structural testing, mechanical mobility measurements. *Katalog Bruel & Kjaer* 1988.

[4] DŻYGADŁO, Z., ŁYŻWIŃSKI, M., OTYŚ, J. et al. Rotor assemblies of turbine engines. *Transport and Communication Publishers*. Warszawa 1982 (in Polish).

[5] GOLEWSKI, P. Thermo-mechanical loads on turbine engine blades with ceramic protective coatings. *Doctoral Thesis*. Lublin University of Technology. Lublin 2015. http://bc.pollub.pl/publication/12481 (in Polish).

[6] JACOBSEN, N.-J. Seminar and Workshop on Structural Dynamics. *Poznan University of Technology Publishing House*. Poznań 2018.

[7] LIPKA, J. Strength of Rotating Machinery. *Scientific and Technical Publishing House*. Warszawa 1967 (in Polish).

[8] MERKISZ, J., WALIGÓRSKI, M. Numerical method of vibroacoustic estimators analysis in a frequency domain for IC engine. *Combustion Engines*. 2013, **154**(3), 25-33. http://yadda.icm.edu.pl/yadda/element/bwmeta1.element.baztech-1dc7a641-04c4-4100-b2f3-8b7185e08934

[9] MITCHELL, L.D. Improved methods for the FFT calculation of the frequency response function. *Journal of Mechanical Design*. 1982, **104**, 277-279. https://doi.org/10.1115/1.3256336

[10] Engine description, no. 17.0.248. *Transport Equipment Manufacturing Plant PZL-Rzeszów*. 1977 (in Polish).

[11] WILK, A., MADEJ, H., ŁAZARZ, B. The application of time-frequency analysis of vibration for gears diagnostics. *Scientific Journal of Silesian University of Technology*. Series Transport. Katowice 2001, **42** (in Polish). http://www.obrum.gliwice.pl/upload/downloads/spg/101/07_WILK_MADEJ_LAZARZ.pdf

[12] WIŚNIEWSKI, W. Ground vibration tests of flying objects – methods and results analysis. *Transactions of the Institute of Aviation*. Warszawa 2010, 7 (in Polish). http://yadda.icm.edu.pl/baztech/element/bwmeta1.element.baztech-article-BSW4-0096-0015

[13] WITOŚ, M. On the modal analysis of a cracking compressor blade. *Research Works of Air Force Institute of Technology*. Warszawa 2008, **23**, 5-20 (in Polish) http://yadda.icm.edu.pl/baztech/element/bwmeta1.element.baztech-article-BWM4-0022-0049

Julia Milewicz, BSc., Eng. – Faculty of Civil and Transport Engineering, Poznan University of Technology.

e-mail: *julia.milewicz@student.put.poznan.pl*

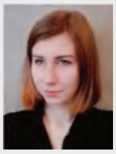

Daniel Mokrzan, BSc., Eng. – Faculty of Civil and Transport Engineering, Poznan University of Technology.

e-mail: *daniel.mokrzan@student.put.poznan.pl*

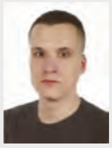

Grzegorz M. Szymański, DSc., DEng., Prof. PUT – Faculty of Civil and Transport Engineering, Poznan University of Technology.

e-mail: *grzegorz.m.szymanski@put.poznan.pl*

Article citation info:
PIELECHA, I., SIDOROWICZ, M. Effects of mixture formation strategies on combustion in dual-fuel engines – a review. *Combustion Engines*. 2021, **184**(1), 30-40. https://doi.org/10.19206/CE-134237

Ireneusz PIELECHA
Maciej SIDOROWICZ

Effects of mixture formation strategies on combustion in dual-fuel engines – a review

The article presents an overview of technical solutions for dual fuel systems used in internal combustion engines. It covers the historical and contemporary genesis of using two fuels simultaneously in the combustion process. The authors pay attention to the value of the excess air coefficient in the cylinder, as the ignitability of the fuel dose near the spark plug is a critical factor. The mixture formation of compression ignition based systems are also analyzed. The results of research on indirect and direct injection systems (and their combinations) have been presented. Research sections were separated based to the use of gasoline with other fuels or diesel oil with other fuels. It was found that the use of two fuels in different configurations of the fuel supply systems extends the conditions for the use of modern combustion systems (jet controlled compression ignition, reactivity controlled compression ignition, intelligent charge compression ignition, premixed charge compression ignition), which will enable further improvement of combustion efficiency.

Keywords: *dual fuel engine, excess air coefficient, multi-fuel mixture forming*

1. Introduction

Combustion engines are the key element in global transport nowadays. Since decades they have been subjected to improvements, which increase their efficiency. One of the development path of this power source is the research on supplying them with different fuels.

The main aim of this article is to put together the dual fuel technology applications and their critical review.

The overview has been divided into three groups:

– historical solutions using dual fuel supply,
– modern dual fuel systems in a mixed configuration (using both direct and indirect injection),
– modern dual fuel systems using a direct injection only.

In this review the main emphasis was put on the excess air coefficient value inside a combustion chamber. The overview contains the results of author's original research concerning dual direct injection system supplying various light hydrocarbon fuels.

2. The history of dual-fuel systems

Dual fuel supply systems in combustion engine were first invented in the United States in 1944, when Barnaby and Russell [4] patented a technical solution enabling stationary engines, usually operating on gas fuel, to also be supplied with an additional liquid fuel. The purpose of this solution was to supplement the temporary shortages of gaseous fuel in the combustion chamber, which could disrupt the continuity of engine operation.

The use of the dual-fuel supply system in diesel traction engines had its beginnings only a couple of years later, as it was tested already in 1946. Then, in the pages of the Popular Mechanics magazine [42], the concept by the Socony-Vacuum Oil Company was presented, in which a carburetor system was used, mixing two different fuels fed from two separate tanks with air. The authors of the design employed this solution to use two types of gasoline with different octane numbers. They showed that the use of gasoline with an octane number of 70 for 95% of the test run was sufficient to prevent knocking, whereas the commonly used gasoline at that time was the more expensive type with an octane number of 80. Even then, the economics of transport played a significant role in the development of these new technologies.

In addition to the cost-effectiveness of using different fuels simultaneously to power engines, other aspects were also analyzed, such as the environmental impact or increasing performance in different operating conditions.

One of the classic applications of a dual-fuel system is the simultaneous use of natural gas and diesel oil in compression-ignition (CI) engines. The main energy carrier in this system is natural gas supplied by indirect injection, while a small dose of diesel fuel ensures compression-ignition of the mixture can be reliably achieved.

Such modification of the classic compression ignition diesel engine brings with it a number of advantages. Methane (the main component of natural gas) is cheaper than diesel oil, that it partially replaces. In addition, its combustion, provided the right conditions, results in a smaller amount of carbon dioxide and nitrogen oxides being produced as well as an increase in the indicated pressure at full engine load [38]. Due to the different densities of the fuels used in this system, it is not possible to premix them, therefore they are supplied by separate systems.

There are many publications (including [6, 35, 41]) on premixing fuels before feeding them to the proper supply system. This method is suitable for fuels with a similar chemical composition and physical state. At the same time research mainly focuses on the influence of different proportions of fuels in the mixture on the increase of combustion efficiency [10, 13, 32], engine knock reduction [3, 28, 40] and the emission of harmful compounds in exhaust gases [1, 17, 24].

In Brazil [11] the FlexFuel system is widely used in passenger cars. It is possible to fill the vehicle's fuel tank with more than one type of fuel, most commonly unleaded gasoline along with ethanol. It is possible thanks to the constant adaptation of the engine control algorithm to the quality of the supplied fuel or fuel mixture.

Xu et al. [44] have proven that the addition of natural gas as a second fuel to power a diesel engine increases the engine's resistance to knock combustion, which may allow

Received 18 February 2021; Received in revised form 12 March 2021; Accepted 12 March 2021
Available online 13 March 2021

the use of a higher compression ratio. Moreover, an increase in indicated thermal efficiency was observed, as well as a reduction in CO and HC emissions at the expense of increased emissions of soot and nitrogen oxides.

Lata et al. [25] observed the dependence of the combustion parameters on the type of admixing gas fuel in the engine originally powered with diesel oil. A 30% share of LPG (liquified petroleum gas – a mixture of propane and butane) in the fuel mixture resulted in an increase in the rate of pressure rise by 1.37 bar/°CA, the maximum pressure in the combustion chamber by 6.95 bar and the combustion time by 5°CA. The same proportion of hydrogen in the fuel mixture resulted in an increase in these indicators by 0.82 bar/°CA, 8.44 bar and 5°CA, respectively. The mixture of three fuels: diesel oil, LPG and hydrogen resulted in an increase in the rate of pressure increase by 0.88 bar/°CA. and maximum pressure by 5.25 bar, and a reduction of the combustion time by 4°CA.

Yüksel et al. [46] added hydrogen to a gasoline engine in their research. It was found that the thermal losses to heating the coolant were decreased, while the losses due to exhaust gases did not change, compared to the use of only gasoline for engine supply.

Commonly known are dual indirect injection systems (PFI-PFI), but they are mainly used to deliver one fuel simultaneously (mainly motorcycle engines) or in a classic configuration of an engine powered by unleaded gasoline with a 4th generation LPG system [33].

A dual fuel injection system is defined in this paper as a system that supplies two different fuels via separate supply systems to the intake manifold or directly into the combustion chamber. The previously mentioned dual-fuel system: natural gas-diesel oil meets this criteria, because, due to the physicochemical properties of fuels, it is not possible to create a stable fuel mixture before delivering them to a controlled combustion process. To implement such a system, the PFI-DI system (port fuel injection-direct injection) is used. One fuel (natural gas) is delivered through the injection system to the intake manifold and the other (diesel) is delivered directly to the cylinder.

The PFI-DI system is also used for other fuel configurations, e.g. unleaded gasoline-LPG, as well as for an injection of a single fuel type from both systems.

3. Effect of the excess air coefficient in the cylinder of a dual-fuel direct and indirect injection systems

3.1. Injection of diesel fuel and natural gas

The use of two fuels in the form of diesel oil in combination with gaseous fuels is a subject of intensive research and wide industrial implementation. Diesel fuel is delivered directly and a part of its base dose is replaced by one of the gaseous fuels (LPG, CNG) supplied to the inlet duct.

Dose division is also analyzed when using dual fuel injection. Gilowski and Stelmasiak [14] proved that splitting the dose of diesel oil in a dual-fuel system (with natural gas) has a positive effect on increasing the efficiency of the engine for low and medium engine loads (by 1–3%) and may improve the durability parameters of the engine by limiting of the rate of combustion pressure increase. However, the cited research lacks the direction of further improvement possibilities of the combustion efficiency, hence it is impossible to clearly state about the potential of the used technology.

Research on creating a mixture in this way (natural gas – PFI, diesel fuel – DI) was carried out by, among others You et al. [45]. Various conditions of natural gas injection into the inlet channel were analyzed – Fig. 1a. It was found that increasing the gas injection advance, at different values of the excess air coefficient, first improves and then worsens the engine operating stability identified by CoV(IMEP) – Fig. 1b). The best conditions for the combustion process occur at gas injection angles in the crank angle range of 300–350° before TDC, regardless of the excess air coefficient value. Increasing the share of fuel in the dose (reducing λ value towards the stoichiometric mixture) leads to an improvement in the quality of the combustion process as indicated by the CoV (IMEP). The research points that during formation of multi-fuel mixture the optimal conditions of both fuels injection exist.

Another outcome of these studies was the conclusion that greater homogenization of the CNG and air mixture, achieved by placing the CNG injector further away from the intake valve, improves the combustion quality and lowers exhaust emissions. There is a growing trend towards analyzes related to the injection of two liquid fuels, with diesel oil being the main fuel.

a)

b)

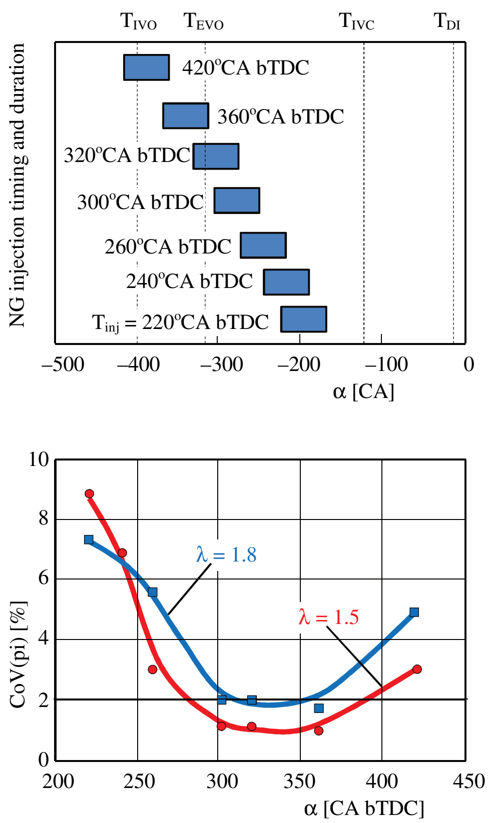

Fig. 1. Analysis of gas injection (a) and combustion process conditions (b): CNG injection into the inlet channel and DF injection into the cylinder at different values of the excess air coefficient [45]

3.2. Injection of diesel fuel and gasoline

Research on this application was conducted by Lee et al. [26]. Using a single-cylinder 395 cm^3 engine, they analyzed the combustion process when powered by direct diesel injection and indirect gasoline injection. The research used engine operation modes generating high indicated efficiency of about 45%. This value was obtained by combining diesel fuel injection and a large mass fraction of gasoline (up to 70%) – Fig. 2. Injection of diesel fuel at the angle of 6°CA before TDC resulted in a typical heat release rate and was similar to the values observed when done with gasoline – Fig. 2a.

Increasing the DF injection advance angle results in a different heat release rate characteristic – Fig. 2b. This is due to injection of DF, which extends the mixing phase of the two fuels. This results in the appearance of the second peak of the heat release rate (at around 368°CA) and a rapid increase in cumulative heat release.

Significant advance of the DF injection results in RCCI combustion – Fig. 2c. In relation to the DF injection itself, this causes the maximum cumulative heat release being reached before TDC, which leads to a faulty combustion process. In a dual-fuel system, the combustion center (CA50) is observed at around 8°CA after TDC. This is due to the significant advance of DF injection, amounting to about 50°CA. However, there are visible areas of low-temperature heat release – indicated as a slow increase in the observed heat release rate. The heat release rate is slowed down and at the same time it is the lowest among the three variants of DF injection. The tests were carried out for three values of the excess air coefficient: $\lambda = 1.72$, 2.72 and 2.77. The maps showing the three engine operation modes described above were shown in Fig. 3.

Applying two basic fuels simultaneously clearly shows the potential of increasing the combustion efficiency. Combining this solution with RCCI system requires further research on elaborating the implementation potential in transportation sector.

3.3. Injection of gasoline with other fuels

The research on dual-fuel systems where the base fuel is gasoline and supplied additionally with alcohols has been analyzed quite thoroughly in the literature. Especially in terms of the excess air coefficient being $\lambda = 1$. Kalwar et al. [22] is an example of such studies. However, in this case, it is not possible to analyze changes in the excess air coefficient and make it dependent on the conditions and amount of individual fuels injected.

In SI engines, the topic currently being explored is the use of LPG in combination with gasoline injection or its complete replacement in the engine supply [36]. Mitukiewicz et al. [31] carried out research on creating a mixture of LPG with air (via indirect injection) and using it to replace gasoline supplied to the engine (via direct injection). When determining the dose of LPG fuel to be supplied, the authors made an assumption that the engine would operate at the same global excess air coefficient as for gasoline alone.

Research on the possibilities of creating a stratified mixture with the use of LPG was carried out by Boretti and Watson [8]. The authors found that combustion of the stratified mixture with the use of direct LPG injection is possible and leads to a reduction in fuel consumption at full engine load, with a global excess air coefficient of $\lambda = 1.65$. However, they assume that enabling the LPG engine to work for lean mixtures under all load conditions would be possible with the use of turbulent ignition and a pre-chamber. The formation of a mixture in such a chamber is distinct from the formation of a stratified mixture in the combustion chamber as the aim is to create a homogeneous mixture in a smaller volume.

The popularity of applying LPG results from the low price of this fuel and the possibility of relatively easy adoption of the original single fuel supply system.

Research conducted by Ji et al. [20] concerned petrol and hydrogen fuel supply systems with indirect injection of both fuels. Combustion was carried out until the content of hydrogen reached 6%. It was found that the engine's thermal efficiency increased significantly from 26% (using gasoline) to over 31% with the addition of 6% hydrogen. At the same time, the use of lean mixtures was increased from 1.5 (petrol) to over 1.65 (petrol + hydrogen → 6%) – Fig. 4a). The use of hydrogen, despite making the fuel mixture more lean, improves the stability of the combustion process. It has been shown that in the entire range of hydrogen combustion at 6% of content the CoV(IMEP) does not exceed 1% – Fig. 4b. Despite the fact that the research direction on the enriching the mixture with hydrogen seems promising, the authors did not take into account the changes adopting the ignition point to the lambda value of the mixture. It can lead to the illusory observation of the loss of combustion stability of lean mixture without hydrogen.

An analysis of gasoline and hydrogen injection using the indirect and direct injection technique was carried out by Sun et al. [39]. Two variants of fuel injection were used in that research: indirect and direct injection with gasoline (PFI + GDI), and indirect injection with gasoline with direct injection of hydrogen (PFI + HDI → hydrogen direct injection). In both cases, the observed value of the excess

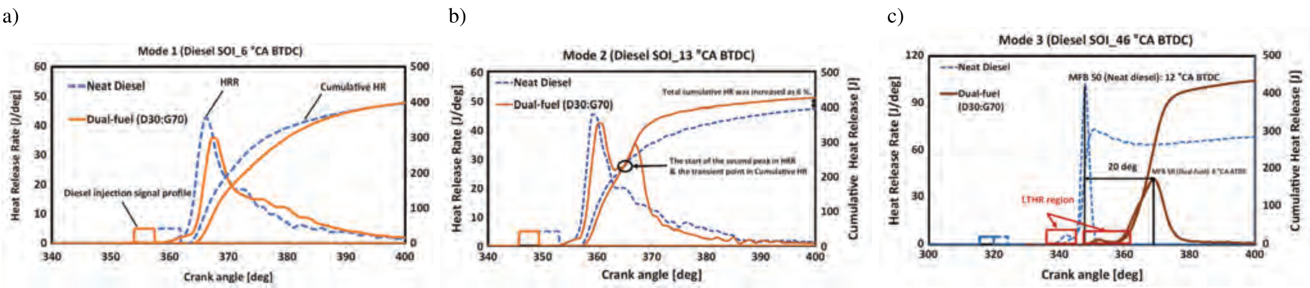

Fig. 2. Combustion process conditions for single-fuel and dual-fuel (DF and gasoline) for an engine with different fuel supply modes: a) mode 1, b) mode 2, c) mode 3 (reproduced from [26])

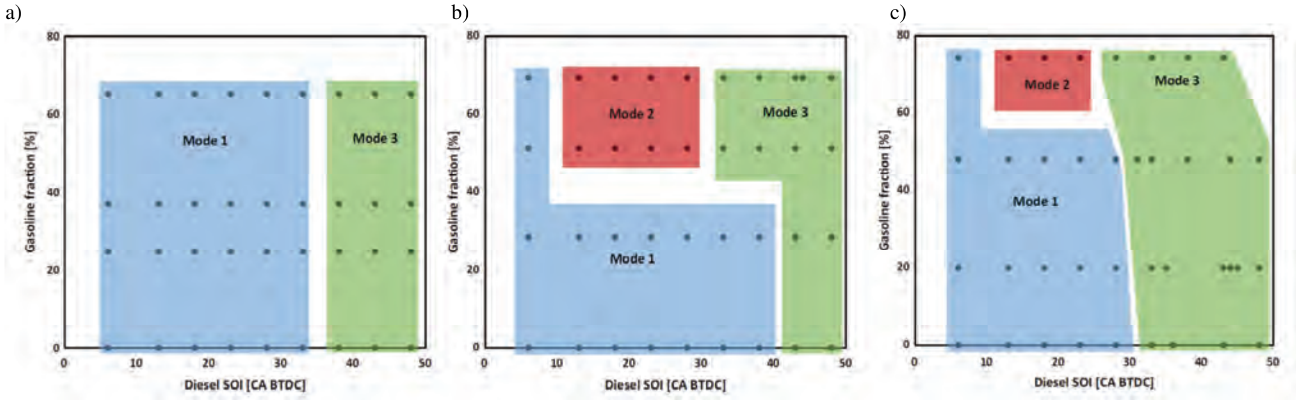

Fig. 3. Dual-fuel engine operating points maps: diesel and gasoline at different values of the excess air coefficient: a) λ = 1.72, b) λ = 2.72, c) λ = 2.77 (reproduced from [26])

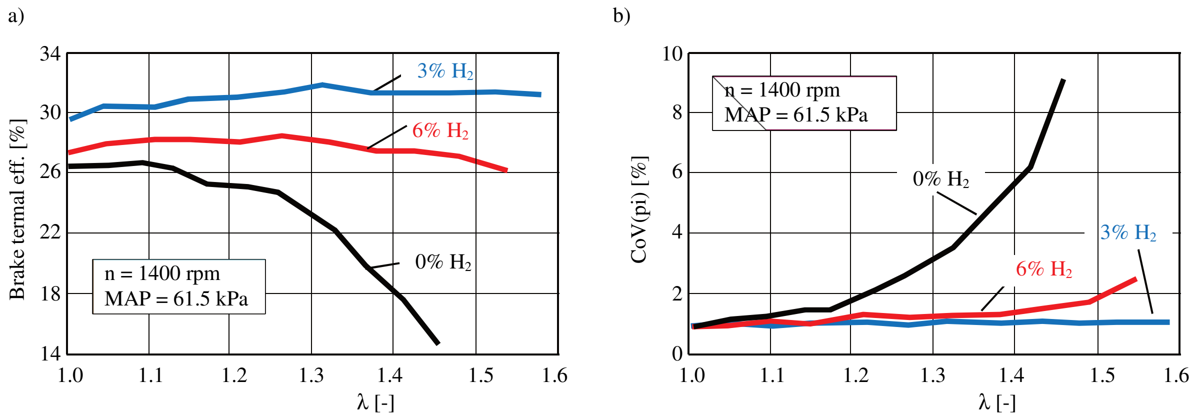

Fig. 4. Change of dual-fuel engine operating indicators: a) thermal efficiency, b) engine combustion instability coefficient [20]

air coefficient was the resultant value of λ = 1. It was found that the increase in the share of direct gasoline injection in the PFI + GDI system led to a slight decrease in the engine power output (by about 2%). However, when using the PFI + HDI system (with direct hydrogen injection), an increase in power of up to 5% was found in the same scenario. This is mainly due to the need to allow the fuel dose time to mix (gasoline fed in the compression stroke), where reducing

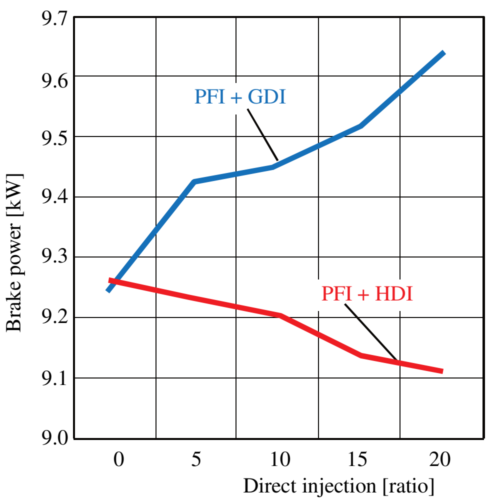

Fig. 5. The change in engine power output as a result of different dual fuel engine supply methods [39]

that time leads to a deterioration of the combustion process – Fig. 5.

Slightly different studies were published by Huang et al. [19]. They performed ethanol direct injection (EDI) and gasoline port injection (GPI). By comparing direct gasoline injection and EDI + GPI injection methods, the distribution of the excess air coefficient was analyzed (Fig. 6).

Knowing that the ignitability of the fuel dose in the vicinity of the spark plug is a critical factor, and the value of the excess air coefficient was 2 < λ < 0.66 [27], analyzes of the spark plug cross-section were performed.

It was found that during the combustion of just gasoline injected into the intake duct (GPI), the value of the excess air coefficient in the vicinity of the spark plug was λ = 1.15.

In the case of EDI + GPI injection, this value was λ = = 1.66. Both are within the above-mentioned critical flammability range of the fuel dose in a SI engine.

Similar studies were conducted by Guo et al. [16] using a mixture of acetone, butanol and ethanol as fuel, and with the second fuel being gasoline. Direct and indirect injection methods were also used. The following variants were analyzed: a) ADI + GPI – acetone and others as direct injection (ADI – acetone direct injection) and indirect petrol injection (GPI), b) API + GDI (gasoline direct injection) and c) GDI + GDI.

The research was carried at 50% share for each fuel (energy differences were up to 0.56%). It was found that for each of the mixtures it is possible to carry out the combustion process in the lambda range of λ = 0.9–1.3. The most critical is burning lean mixtures; the lowest CoV(IMEP) values were found in the GPI + ADI configuration, reaching below 1.3%. Also in this fuel supply configuration, the highest values of torque and the highest value of thermal efficiency were obtained. This configuration was also the best in terms of the number and mass of solid particles emitted (especially when burning lean mixtures for λ = = 1.3).

a) b)

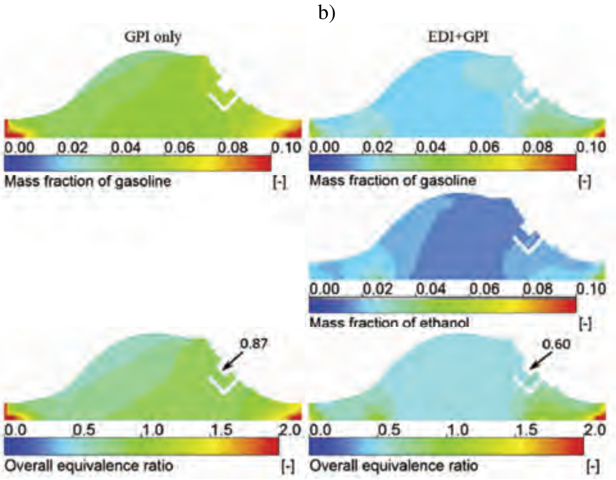

Fig. 6. Distribution of gasoline and ethanol mass (a) in the combustion chamber, and the excess air coefficient (b) when supplying the engine with gasoline (GPI) and ethanol with gasoline (EDI + GPI) (reproduced from [19])

3.4. Injection of methanol with other fuels

The research on dual fuel supply, in which the primary fuel was methanol (direct injection) with the addition of hydrogen (PFI) was conducted by Gong et al. [15]. Knowing the general properties of hydrogen related to increasing the combustion rate, especially in combination with lean mixtures, it was used as an additive in a small quantity (3–6%). A strategy of delayed injection of methanol into the cylinder was used. It was found that the addition of hydrogen (in the 3–6% range) extends the possibilities of burning lean mixtures from λ = 1.6 when burning pure methanol to λ = 2.2. The necessity to adjust the ignition angle depending on the excess air coefficient was also confirmed. With a 6% addition of hydrogen and at λ > 2 the CoV(IMEP) value was found to be below 3.5%.

4. Effect of the cylinder excess air coefficient in a dual fuel DI system

4.1. Injection of gasoline with other fuels

Previous solutions of gasoline and ethanol injection concern mainly mixtures of E85 (ethanol – 85% and gasoline – 15%) and E15 (gasoline – 85% and ethanol – 15%) [4]. The research of dual-fuel direct injection systems of gasoline and ethanol was conducted by Kang et al. [23]. The analyzes include supply with a stoichiometric mixture. Despite this, it was possible to vary the size of the doses of individual fuels in order to obtain the stoichiometric mixture as needed (Table 1).

The fuel doses presented in the table were used in experimental studies. Increasing the proportion of ethanol makes it possible to increase the start of ignition angle. This leads to an increase in combustion pressure and an increase in BMEP (Fig. 7).

Studies have also shown that increasing the proportion of ethanol reduces the CoV(IMEP). In the absence of ethanol, this ratio was approximately 4%. Increasing the proportion of ethanol to 10% resulted in a 50% reduction in CoV(IMEP) value. A further increase in the share of ethanol lead to this indicator reaching the value of 1–1.5% (with the permissible limit value being 1.5%).

Table 1. Energy shares of fuels in gasoline-ethanol blends [23]

Ethanol share	Energy content in gasoline	Energy content in ethanol	Total energy in the fuel
[%]	[MJ]	[MJ]	[MJ]
0	75.80	0	75.80
10	67.86	8.13	75.99
25	56.59	19.69	76.25
50	34.26	42.51	76.78
75	19.01	58.12	77.13
100	0	77.58	77.58

a)

b)

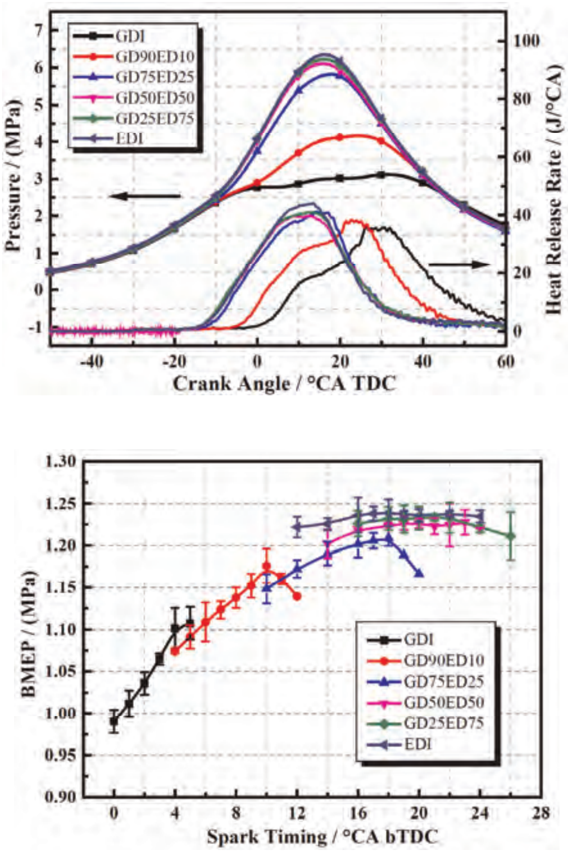

Fig. 7. Indicator tests: a) cylinder pressure curve, b) changes in BMEP as a function of the start of ignition angle (reproduced from [23])

The injection strategy of gasoline direct injection plus ethanol direct injection mode can further expand engine load range compared with the conventional direct injection. The reason is that the fuel latent heat of vaporization is more efficiently used to reduce fuel dose air temperature and increase the volumetric efficiency when both gasoline and ethanol are injected directly into cylinder.

Gasoline direct injection plus ethanol direct injection mode can increase the mean effective pressure and thermal efficiency simultaneously.

The authors of the following article conducted the research on the novel method of mixture forming using two different hydrocarbon fuels. The original dual direct injection tests relied on the injection of gasoline and other fuels (ethanol, n-butanol and n-heptane). The tests were carried out with the use of a rapid compression machine (Fig. 8).

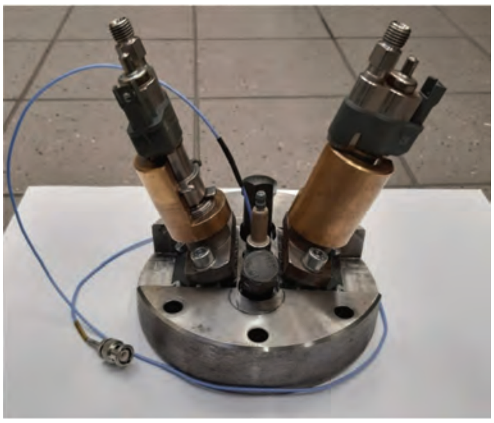

Fig. 8. The RCM head adjusted for the dual-fuel injection system

Fuel was supplied by two high-pressure injection pumps from the BMW M4 GTS. The original system was modified by disconnecting the cable connecting the two pumps, which made it possible to supply the system with two different fuels independently (Fig. 9). The system enables independent fuel pressure adjustment in the range of 5–30 MPa.

Fig. 9. High pressure pump stand with a fuel pressure regulation system

The tests were carried out in the form of injecting the same fuel (Fig. 10a) and different fuels with the two injectors (Fig. 10b).

The observed heat release loss results from the specificity of operation of such a system and the heat escape. The symmetrical piston movement causes the phenomenon, that the heat release rate is always positive [e.g. 37]. However, the application of a slider system, in which the typical cranking system does not exist, causes the different heat release rate course – it is in a certain portion of combustion – negative. The negative values of dQ lead to the heat release loss. Such results can be obtained in research using an RCEM without typical cranking system [e.g. 21, 43].

Based on the conducted research, it was found that among the analyzed fuel configurations, the gasoline + n-butanol fuel supply configuration was the most efficient; the efficiency value for this test case was 27.8% and was higher by 6.1% than for the base configuration, i.e. with the use of gasoline only.

a)

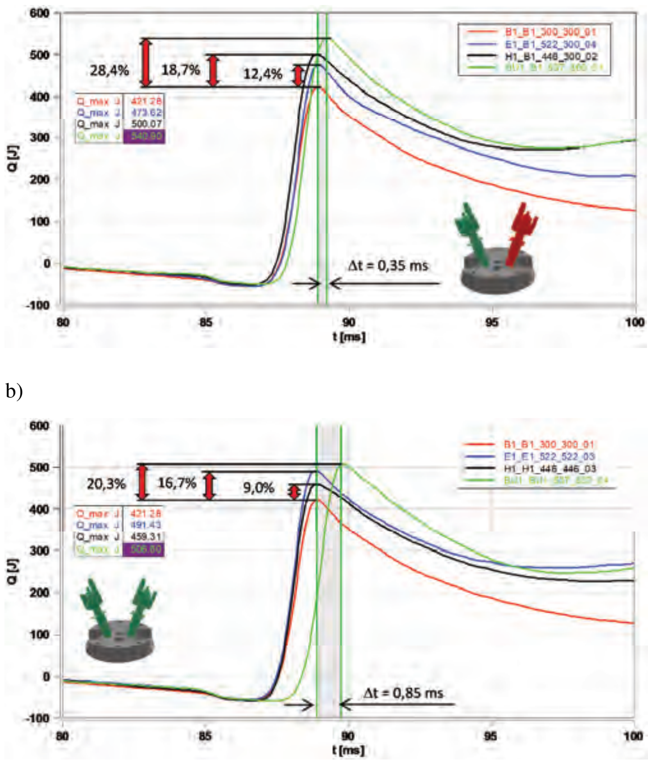

Fig. 10. Effect of fuel type on heat release: a) injection of the same fuel, b) injection of different fuels

The combustion of gasoline and n-butanol mixture in relation to the combustion of gasoline alone resulted in:

– maximum combustion pressure in the cylinder being 10% higher; changes observed for other fuel mixtures reached values up to 4%,
– the pressure increase being 17% greater; combustion of the other analyzed mixtures indicates changes in this value of up to 7% in comparison,
– maximum heat release rate being 22% greater; where other fuel mixtures generated smaller differences of up to 8% at most,
– the maximum amount of total heat released being 22% higher; changes of this indicator for other fuel mixtures compared to gasoline were: 13% (for petrol and ethanol) and 8% (for petrol and n-heptane).

4.2. Injection of diesel fuel with other fuels

Simulation tests with the use of DF and LPG fuels were conducted by Boretti [7]. The validation was used only for diesel injection in the engine. The other studies in the dual-fuel system were not validated. Simulation analyzes were performed with the use of the WAVE software, obtaining maps defining the shares of DF and LPG fuels.

Therefore, it was possible to create maps of the excess air coefficient values, which were shown in Fig. 11. It shows that with increasing engine load, the share of LPG fuel increases and the share of diesel fuel decreases. At the same time, the excess air coefficient decreases, and in the conditions of the full power characteristics it takes values in the range $\lambda = 1.1–1.2$.

Despite considerable design difficulties, Long et al. [30] used a dual-direct injection system in a compression ignition engine. This solution uses a premixed charge system prepared by the main pre-injection blended fuels of diesel and ethanol-gasoline. The system called Jet Controlled Compression Ignition (JCCI) was shown in Fig. 12. The tests were carried out with a single-cylinder engine with a cylinder diameter of 86 mm and a compression ratio of 15.5. The typical compression chamber of the diesel engine has been replaced with a flat chamber to fit the premixed combustion mode. The fuel used was a mixture of gasoline and ethanol with diesel fuel constituting 15% (D15) or 30% (D30) fuel share by mass. The injection system was equipped with two fuel injection pumps operated independently. The fuel injection pressure in the pre and main-injection systems was maintained at 60 MPa (in the case where the engine load was over 50%, the fuel injection pressure was increased to a maximum of 90 MPa). Diesel oil was supplied by the central injector (fuel injection direction being in line with the piston movement). The injector placed at an angle supplied the mixture of D15 or D30 at an angle of 10 degrees – Fig. 13.

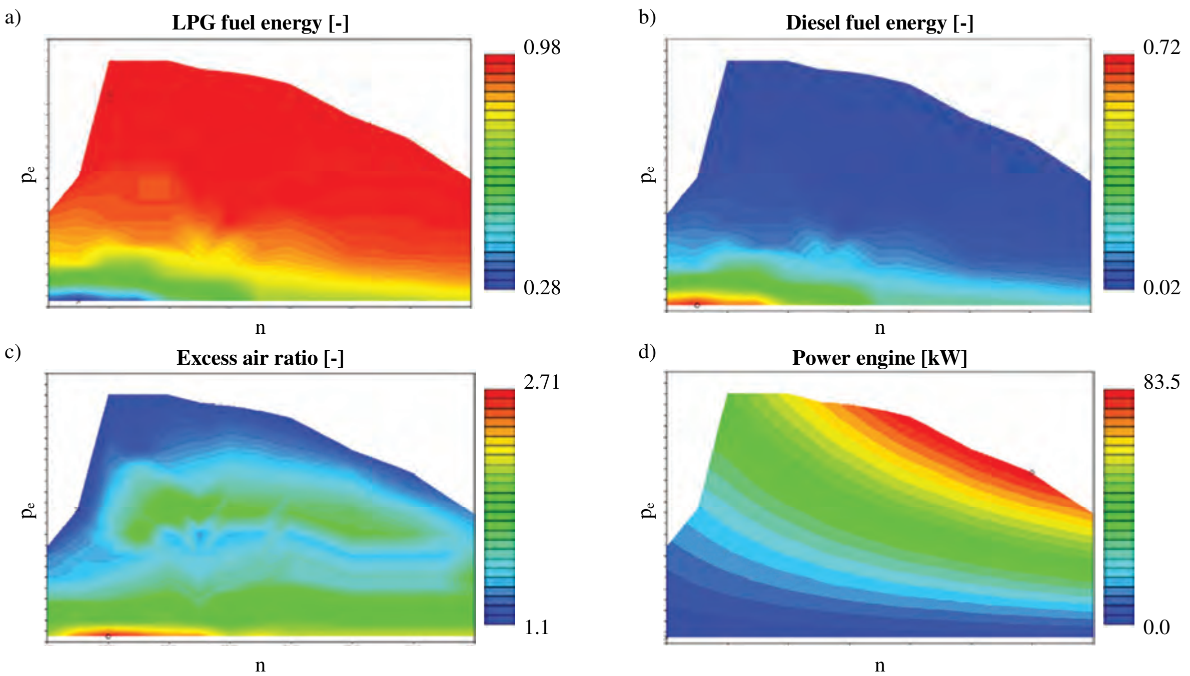

Fig. 11. Simulation analysis of the excess air coefficient overlayed on the general characteristics of an engine using a combined DF and LPG injection: a) LPG energy share, b) Diesel fuel energy share, c) excess air coefficient, d) engine power (reproduced from [7])

Fig. 12. Diagram of the JCCI combustion system design (reproduced from [30])

The experimental results and analysis demonstrated that the fuel JCCI mode with dual-direct injection strategy could effectively and robustly control the combustion event and emissions of premixed combustion mode.

Dual-fuel direct fuel injection systems currently apply – apart from the examples presented above – also to the injection of methanol and DF [12] as well as to n-butanol in combination with biodiesel [47]. The comprehensive review of different variants of powering systems and fuels has been put together by Saiteja and Ashok in [2]. In the paper by Ning et al. [34] from 2020, 10 additional publications on direct injection of two different fuels were cited, for DF and methanol mix. Simulation studies using diesel oil and n-butanol fuel were conducted by Cai et al. [9]. Various combustion systems were implemented with the simulation apparatus:

HCCI: n-butanol (PFI)
PCCI: n-butanol in-cylinder early single injection
RCCI: n-butanol (PFI) + diesel (DI)
DI^2: n-butanol (DI) + diesel DI.

An example comparison of pressure curves in a cylinder was shown in Fig. 14.

a)

b)

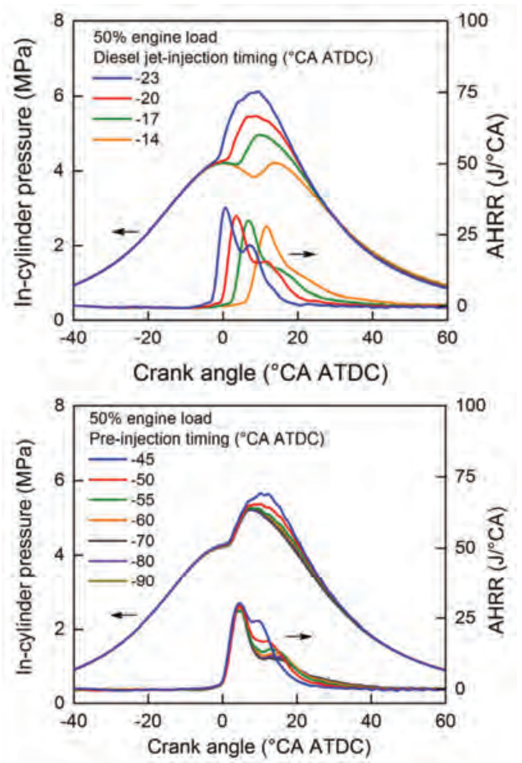

Fig. 13. Changes in cylinder pressure and heat release rate: a) during main injection, b) during pre-mixed combustion (reproduced from [30])

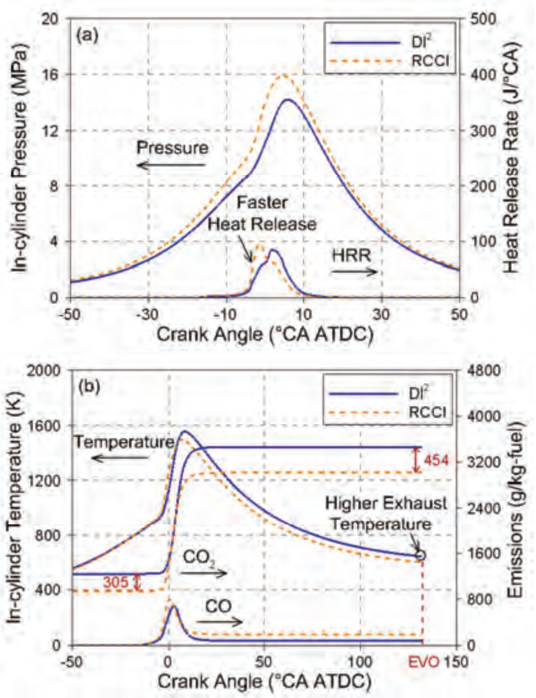

Fig. 14. In-cylinder pressure, heat release rate, temperature, CO, and CO_2 emission characteristics for representative cases of DI^2 and RCCI (reproduced from [9)]

The reason for the differences in incomplete combustion between the two strategies is primarily related to the different fuel delivery strategies. In RCCI, part of the premixed n-butanol distributes itself within the low temperature squish region near the liner, which cannot be completely oxidized due to its too low local equivalence ratio. By contrast, n-butanol and diesel with different injection timings and spray angles are directly injected into the cylinder in DI^2 by two separate nozzles, hence the in-cylinder distribution of the fuel/air mixture can be effectively modulated. As indicated in Fig. 15 for DI^2, the fuel within the squish region can also be well oxidized.

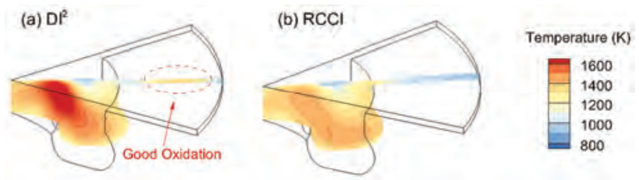

Fig. 15. Comparison of the in-cylinder temperature distribution between the representative cases of DI^2 and RCCI at CA50 (reproduced from [9])

In studies conducted by Dong et al. [12] analyzes of the injection of methanol (injected centrally in the cylinder) and diesel fuel (non-axial injection) were performed. Changes in the excess air coefficient were not analyzed. The research was conducted in the aspect of replacing diesel fuel with methanol in the range of 45% to 95%. The research results were summed up in Fig. 16.

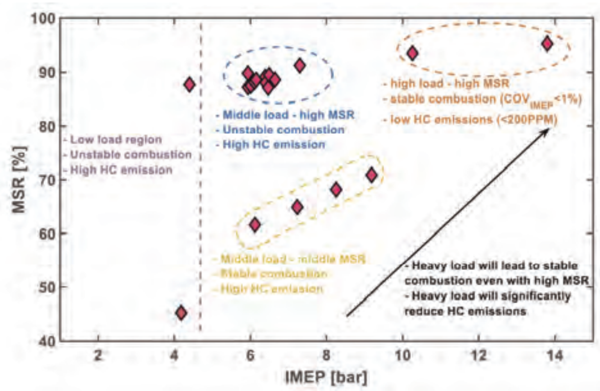

Fig. 16. Summary of studies on direct injection of MeOH and DF (reproduced from [12])

Similar studies were also conducted by Huang et al. [18]. Direct injection of two fuels was used; those being methanol and biodiesel. The tests were carried out in the ICCI (Intelligent Charge Compression Ignition) system. This combustion mode was proposed to realize flexible stratifications of concentration and reactivity with the best gradient in accordance with the engine operating conditions. In ICCI mode, most of low-reactivity fuel is directly injected during the intake stroke with a single or multiple stage split injection. Then, the rest of low-reactivity fuel and high-reactivity fuel are directly injected in succession to establish crossed stratifications of the equivalence ratio and reactivity in the cylinder.

The analysis of the combustion pressure change with the use of methanol and biodiesel was shown in Fig. 17.

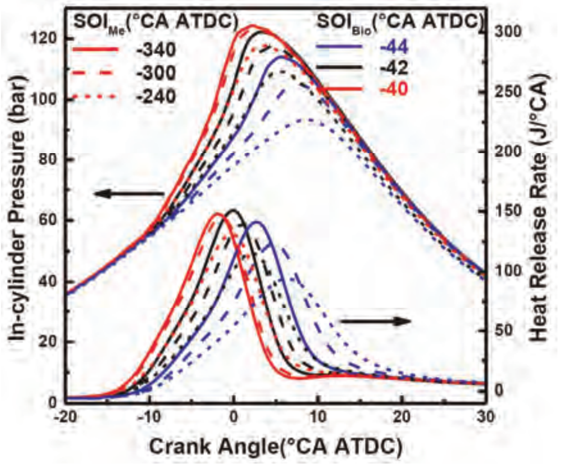

Fig. 17. Effects of fuels injection timings on the in-cylinder pressure and heat release rate (methanol energy ratios = 30%) (reproduced from [18])

Fueling the internal combustion engine with hydrogen and diesel fuel in the hydrogen-diesel dual direct injection (H2DDI) system was presented by Liu et al. [29]. Hydrogen was injected into the cylinder at a pressure of 20 MPa. The tests were carried out on a single-cylinder engine (adapted from a four-cylinder engine) with a modified compression ratio to 17.4.

The results of supplying the engine with hydrogen and diesel oil were shown in Fig. 18.

As a result of the conducted research, it was found that:

- Direct injection of hydrogen into the cylinder results in up to 10% increase in the end-of-compression pressure, which is associated with additional compression work. At later injection timings, this effect is less pronounced.
- Under the conditions of this work, the shape of the apparent heat release rate (aHRR) resembles that of the baseline diesel combustion, except when hydrogen is injected late resulting in insufficient mixing time, in which case slower aHRR indicative of a hydrogen mixing controlled combustion is observed.

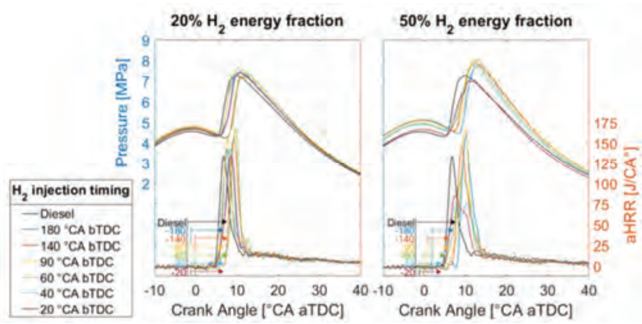

Fig. 18. Effect of hydrogen injection timing on in-cylinder pressure and apparent heat release rate (aHRR) at selected hydrogen energy fractions of 20% (left) and 50% (right) (reproduced from [29])

5. Conclusions

Direct dual-fuel injection has already been implemented with various fuels. These systems can be classified according to the dominant fuel:

- gasoline with/without other fuels,
- diesel fuel with/without other fuels,
- hydrogen with/without other fuels.

The variety of these solutions in connection with the possibility of also using indirect injection causes the implementation of combustion systems to be:

- homogeneous (HCCI): PFI,
- stratified (PCCI): PFI + DI,
- reactivity stratification combustion (RCCI): PFI + DI.

The search for new combustion systems contributes to increasing the internal combustion engines efficiency, the possibility of achieving better combustion process control (including controlling the excess air coefficient in the cylinder), as well as intensifying development works in the field of alternative fuels (butanol, methanol, hydrogen) as well as synthetic fuels.

Nomenclature

ADI	acetone direct injection
CI	compression ignition
CNG	compressed natural gas
CoV	coefficient of variation
D30	diesel (30%)
DI	direct injection
DI^2	dual direct injection
EDI	ethanol direct injection
G70	gasoline (70%)
GDI	gasoline direct injection
GPI	gasoline port injection
H2DDI	hydrogen-diesel dual direct injection
IMEP	indicating mean effective pressure
JCCI	jet controlled compression ignition
LPG	liquified petroleum gas
MAP	manifold air pressure
MeOH	methanol
MFB	mass fuel burn
NG	natural gas
PFI	port fuel injection
RCCI	reactivity controlled compression ignition
SI	spark ignition
SOI	start of injection
TDC	top dead centre
λ	excess air ratio

Bibliography

[1] ALASFOUR, F.N. NO_x emission from a spark ignition engine using 30% iso-butanol – gasoline blend: part 2 – ignition timing. *Applied Thermal Engineering*. 1998, **18**(8), 609-618. https://doi.org/10.1016/s1359-4311(97)00082-3

[2] ASHOK, B., ASHOK, S.D., KUMAR, C.R. LPG diesel dual fuel engine – a critical review. *Alexandria Engineering Journal*. 2015, **54**(2), 105-126. https://doi.org/10.1016/j.aej.2015.03.002

[3] BARAL, B., RAINE, R. Knock in a spark ignition engine fuelled with gasoline-kerosene blends. *SAE Technical Paper* 2008-01-2417. 2008. https://doi.org/10.4271/2008-01-2417

[4] BARNABY, J., RUSSELL, W. Dual fuel engine. Patent US2400219A, 15.12.1944.

[5] BENAJES, J., GARCÍA, A., MONSALVE-SERRANO, J. et al. Benefits of E85 versus gasoline as low reactivity fuel for an automotive diesel engine operating in reactivity controlled compression ignition combustion mode. *Energy Conversion and Management*. 2018, **159**, 85-95. https://doi.org/10.1016/j.enconman.2018.01.015

[6] BOGIN, G.E., LUECKE, J., RATCLIFF, M.A. et al. Effects of iso-octane/ethanol blend ratios on the observance of negative temperature coefficient behavior within the Ignition Quality Tester. *Fuel*. 2016, **186**, 82-90. https://doi.org/10.1016/j.fuel.2016.08.021

[7] BORETTI, A. Numerical study of the substitutional diesel fuel energy in a dual fuel diesel-LPG engine with two direct injectors per cylinder. *Fuel Processing Technology*. 2017, **161**, 41-51. https://doi.org/10.1016/j.fuproc.2017.03.001

[8] BORETTI, A., WATSON, H. Development of a direct injection high efficiency liquid phase LPG spark ignition engine. *SAE International Journal of Engines*. 2009, **2**(1), 1639-1649. https://doi.org/10.4271/2009-01-1881

[9] CAI, Y., JIA, M., XU, G. et al. Feasibility study of the combustion strategy of n-butanol/diesel dual direct injection (DI2) in a compression-ignition engine. *Fuel*. 2021, **289**, 119865. https://doi.org/10.1016/j.fuel.2020.119865

[10] DALHA, I.B., SAID, M.A., KARIM, A. et al. Reactivity controlled compression ignition: an advanced combustion mode for improved energy efficiency. In: Sulaiman S. (eds) Energy efficiency in mobility systems. *Springer*, Singapore 2020. https://doi.org/10.1007/978-981-15-0102-9_6

[11] DE FERREIRA GOMES, P., MENDES, C., LOPES, G. et al. High efficiency flex-fuel engines and the end of the 70% paradigm. *SAE Technical Paper* 2017-36-0162. 2017. https://doi.org/10.4271/2017-36-0162

[12] DONG, Y., KAARIO, O., HASSAN, G. et al. High-pressure direct injection of methanol and pilot diesel: A non-premixed dual-fuel engine concept. *Fuel*. 2020, **277**, 117932. https://doi.org/10.1016/j.fuel.2020.117932

[13] ELFASAKHANY, A. Gasoline engine fueled with bioethanol-bio-acetone-gasoline blends: Performance and emissions exploration. *Fuel*. 2020, **274**, 117825. https://doi.org/10.1016/j.fuel.2020.117825

[14] GILOWSKI, T., STELMASIAK, Z. Impact of symmetrical division of initial dosage diesel oil on the selected thermodynamic parameters of the working medium and operation parameters dual fuel engine fuelled CNG. *Combustion Engines*. 2013, **154**(3).

[15] GONG, G., LI, Z., YI, L. et al. Experimental investigation of equivalence ratio effects on combustion and emissions characteristics of an H_2/methanol dual-injection engine under different spark timings. *Fuel*. 2020, **262**, 116463. https://doi.org/10.1016/j.fuel.2019.116463

[16] GUO, Z., YU, X., LI, G. et al. Comparative study of different injection modes on combustion and particle emission of acetone-butanol-ethanol (ABE) and gasoline in a dual-injection SI engine. *Fuel*. 2020, **281**, 118786. https://doi.org/10.1016/j.fuel.2020.118786

[17] HOTH, A., KOLODZIEJ, C.P., ROCKSTROH, T. et al. Combustion characteristics of PRF and TSF ethanol blends with RON 98 in an instrumented CFR engine. *SAE Technical Paper* 2018-01-1672. 2018. https://doi.org/10.4271/2018-01-1672

[18] HUANG, G., LI, Z., ZHAO, W. et al. Effects of fuel injection strategies on combustion and emissions of intelligent charge compression ignition (ICCI) mode fueled with methanol and biodiesel. *Fuel*. 2020, **274**, 117851. https://doi.org/10.1016/j.fuel.2020.117851.

[19] HUANG, Y., HONG, G., HUANG, R. Numerical investigation to the dual-fuel spray combustion process in an ethanol direct injection plus gasoline port injection (EDI+GPI) engine. *Energy Conversion and Management*. 2015, **92**, 275-286. https://doi.org/10.1016/j.enconman.2014.12.064

[20] JI, C., WANG, S. Effect of hydrogen addition on combustion and emissions performance of a spark ignition gasoline engine at lean conditions. *International Journal of Hydrogen Energy*. 2009, **34**(18), 7823-7834. https://doi.org/10.1016/j.ijhydene.2009.06.082

[21] JWA, K., NAM, V.D., SETIAWAN, A. et al. Experimental study of the ignition delay of gasoline/biodiesel blends using a rapid compression expansion machine. *Energy Procedia*. 2019, **158**, 655-660, https://doi.org/10.1016/j.egypro.2019.01.178

[22] KALWAR A., SINGH, A.P., AGARWAL, A.K. Utilization of primary alcohols in dual-fuel injection mode in a gasoline direct injection engine. *Fuel*. 2020, **276**, 118068. https://doi.org/10.1016/j.fuel.2020.118068

[23] KANG, R., ZHOU, L., HUA, J. et al. Experimental investigation on combustion characteristics in dual-fuel dual-injection engine. *Energy Conversion and Management*. 2019, **181**, 15-25. https://doi.org/10.1016/j.enconman.2018.11.057

[24] KARAVALAKIS, G., SHORT, D., VU, D. et al. A complete assessment of the emissions performance of ethanol blends and iso-butanol blends from a fleet of nine PFI and GDI vehicles. *SAE International Journal of Fuels and Lubricants*. 2015, **8**(2). https://doi.org/10.4271/2015-01-0957

[25] LATA, D.B., MISRA, A., MEDHEKAR, S. Investigations on the combustion parameters of a dual fuel diesel engine with hydrogen and LPG as secondary fuels. *International Journal of Hydrogen Energy*. 2011, **36**(21), 13808-13819. https://doi.org/10.1016/j.ijhydene.2011.07.142

[26] LEE, J., CHU, S., MIN, K. et al. Classification of diesel and gasoline dual-fuel combustion modes by the analysis of heat release rate shapes in a compression ignition engine. *Fuel*. 2017, **209**, 587-597. https://doi.org/10.1016/j.fuel.2017.07.067

[27] LI, H., LI, C., MA, X. et al. Numerical study of DMF and gasoline spray and mixture preparation in a GDI engine. *SAE Technical Paper* 2013-01-1592. 2013. https://doi.org/10.4271/2013-01-1592

[28] LIU, H., WANG, Z., WANG, J. Methanol-gasoline DFSI (dual-fuel spark ignition) combustion with dual-injection for engine knock suppression. *Energy*. 2014, **73**, 686-693. https://doi.org/10.1016/j.energy.2014.06.072

[29] LIU, X., SRNA, A., YIP, H.L. et al. Performance and emissions of hydrogen-diesel dual direct injection (H2DDI) in a single-cylinder compression-ignition engine. *International Journal of Hydrogen Energy*. 2021, **46**(1), 1302-1314. https://doi.org/10.1016/j.ijhydene.2020.10.006

[30] LONG, W., LI, B., CAO, J. et al. Effects of dual-direct injection parameters on performance of fuel Jet Controlled Compression Ignition mode on a high-speed light duty engine. *Fuel*. 2019, **235**, 658-669. https://doi.org/10.1016/j.fuel.2018.08.043

[31] MITUKIEWICZ, G., DYCHTO, R., LEYKO, J. Relationship between LPG fuel and gasoline injection duration for gasoline direct injection engines. *Fuel*. 2015, **153**, 526-534. https://doi.org/10.1016/j.fuel.2015.03.033

[32] MORENO, F., MUÑOZ, M., ARROYO, J. et al. Efficiency and emissions in a vehicle spark ignition engine fueled with hydrogen and methane blends. *International Journal of Hydrogen Energy*. 2012, **37**(15), 11495-11503. https://doi.org/10.1016/j.ijhydene.2012.04.012

[33] NAYAK, V., RASHMI, G.S., CHITRAGAR, P. et al. Combustion characteristics and cyclic variation of a LPG fuelled MPFI four cylinder gasoline engine. *Energy Procedia*. 2016, **90**, 470-480. https://doi.org/10.1016/j.egypro.2016.11.214

[34] NING, L., DUAN, Q., KOU, H. et al. Parametric study on effects of methanol injection timing and methanol substitution percentage on combustion and emissions of methanol/diesel dual-fuel direct injection engine at full load. *Fuel.* 2020, **279**, 118424. https://doi.org/10.1016/j.fuel.2020.118424

[35] ROTH, P., YANG, J., PENG, W. et al. Intermediate and high ethanol blends reduce secondary organic aerosol formation from gasoline direct injection vehicles. *Atmospheric Environment*. 2020, **220**, 117064. https://doi.org/10.1016/j.atmosenv.2019.117064

[36] SAITEJA, P., ASHOK, B. A critical insight review on homogeneous charge compression ignition engine characteristics powered by biofuels. *Fuel*. 2021, **285**, 119202, https://doi.org/10.1016/j.fuel.2020.119202

[37] SCHLATTER, S., SCHNEIDER, B., WRIGHT, Y.M. et al. N-heptane micro pilot assisted methane combustion in a rapid compression expansion machine. *Fuel*. 2016, **179**, 339-352, https://doi.org/10.1016/j.fuel.2016.03.006

[38] SERRANO, D., OBIOLS, J., LECOINTE, B. Optimization of dual fuel diesel-methane operation on a production passenger car engine – thermodynamic analysis. *SAE Technical Paper* 2013-01-2505. 2013. https://doi.org/10.4271/2013-01-2505

[39] SUN, P., LIU, Z., YU, X. et al. Experimental study on heat and exergy balance of a dual-fuel combined injection engine with hydrogen and gasoline. *International Journal of Hydrogen Energy*. 2019, **44**(39), 22301-22315. https://doi.org/10.1016/j.ijhydene.2019.06.149

[40] SZYBIST, J., FOSTER, M., MOORE, W.R. et al. Investigation of knock limited compression ratio of ethanol gasoline blends. *SAE Technical Paper* 2010-01-0619. 2010. https://doi.org/10.4271/2010-01-0619

[41] TIAN, Z., ZHEN, X., WANG, Y. et al. Combustion and emission characteristics of n-butanol-gasoline blends in SI direct injection gasoline engine. *Renewable Energy*. 2020, **146**, 267-279. https://doi.org/10.1016/j.renene.2019.06.041

[42] WINDSOR, H. One car – two gas tanks. *Popular Mechanics*. 1948.

[43] XU, G., KOTZAGIANNI, M., KYRTATOS, P. et al. Experimental and numerical investigations of the unscavenged prechamber combustion in a rapid compression and expansion machine under engine-like conditions. *Combustion and Flame*. 2019, **204**, 68-84. https://doi.org/10.1016/j.combustflame.2019.01.025

[44] XU, Y., ZHANG, Y., GONG, J. et al. Combustion behaviours and emission characteristics of a retrofitted NG/gasoline duel-fuel SI engine with various proportions of NG-gasoline blends. *Fuel*. 2020, **266**, 116957. https://doi.org/10.1016/j.fuel.2019.116957

[45] YOU, J., LIU, Z., WANG, Z. et al. Impact of natural gas injection strategies on combustion and emissions of a dual fuel natural gas engine ignited with diesel at low loads. *Fuel*. 2020, **260**, 116414. https://doi.org/10.1016/j.fuel.2019.116414

[46] YÜKSEL, F., CEVIZ, M.A. Thermal balance of a four stroke SI engine operating on hydrogen as a supplementary fuel. *Energy*. 2003, **28**(11), 1069-1080. https://doi.org/10.1016/s0360-5442(03)00090-2

[47] ZHAO, W., LI, Z., HUANG, G. et al. Experimental investigation of direct injection dual fuel of n-butanol and biodiesel on intelligent charge compression ignition (ICCI) combustion mode. *Applied Energy*. 2020, **266**, 114884. https://doi.org/10.1016/j.apenergy.2020.114884

Prof. Ireneusz Pielecha, DSc., DEng. – Faculty of Civil and Transport Engineering, Poznan University of Technology.
e-mail: *ireneusz.pielecha@put.poznan.pl*

Maciej Sidorowicz, DEng. – AC S.A., Bialystok, Poland.
e-mail: *maciej.sidorowicz@ac.com.pl*

Article citation info:
ENGELMANN, D., HÜSSY, A., COMTE, P. et al. Influences of special driving situations on emissions of passenger cars. *Combustion Engines*. 2021, **184**(1), 41-51. https://doi.org/10.19206/CE-134828

Danilo ENGELMANN
Andreas HÜSSY
Pierre COMTE
Jan CZERWINSKI
Peter BONSACK

Influences of special driving situations on emissions of passenger cars

Testing of real driving emissions (RDE) offers the opportunity to collect the data about the emissions in special driving, or non-driving situations. These situations are: cold start, warm-up of the engine, stop & go and idling. In the present work, the definitions of the special driving situations were proposed, the emissions of 7 passenger cars (gasoline & Diesel) were extracted from the present RDE data and some special driving situations, particularly the stop & go operation with varying share of idling were reproduced on chassis dynamometer. As expected, the emissions of CO, NO_x and PN are in the cold start and in the first part of the warm-up phase (ca. 25 s) considerably higher than in the rest of the investigated urban phase. The singular emitting situations like "stop&go" or idling occur frequently in the warm-up phase, i.e. in the city operation when the engine and the exhaust system are still not warm enough.

Key words: *emissions at cold start, warm-up, RDE, portion of idling, stop&go*

1. Introduction

Emission factors and emission inventories are an important source of data for compiling and modelling the emissions of traffic in different situations. There is in EU a continuous work and development of emission data inventories [1–6].

Since the introduction (in 2017) of the road-testing (RDE – real driving emissions) as an obligatory element of the legal testing procedures, the increased amount of RDE-data can be used for different objectives, such as: further development of emission inventories, compliance with "In-Service Conformity" (ISC, EU regulation 2018/1832) and market surveillance activities (EU regulation 2018/858). Extensive activities of testing RDE by means of PEMS (portable emissions measuring systems) have been performed in the last years, aiming not only the emissions but also the improvements of instrumentation, of testing procedures and of evaluation [5–17].

A well-known fact is that the emissions at cold start, during the warm-up and at the low speed phases of urban operation, both in the laboratory and on the road, tend to be higher for all pollutants [13, 18–24]. This fact supports even the idea for future introduction of urban emission limits for the short trips, which are very frequent in Europe [5].

In order to enable an automatic co-evaluation of emissions from the special (non)driving situations, the necessary definitions were proposed in the present work. With these definitions, the RDE data of 7 vehicles were processed and the emissions in special driving situations were obtained (part 1). Additionally, some special situations like cold start, warm-up and stop&go were reproduced on the chassis dynamometer with cars of different ages and different technology (part 2).

This paper gives some new insights in the topic of emissions from special driving situations.

2. Analysis of present RDE data (part 1)

2.1. Data origin & processing

The emissions data originate from testing of different vehicles with Horiba PEMS (Portable Emission Measuring Systems for gaseous emissions) and with PN-PEMS (for particle number PN) at AFHB.

The Horiba OBS-ONE-PN PEMS uses two-step dilution, a catalytic volatile particle remover (350°C) and an Isopropanol-based CPC as a main measuring unit.

Figure 1 represents the PEMS installation on a vehicle.

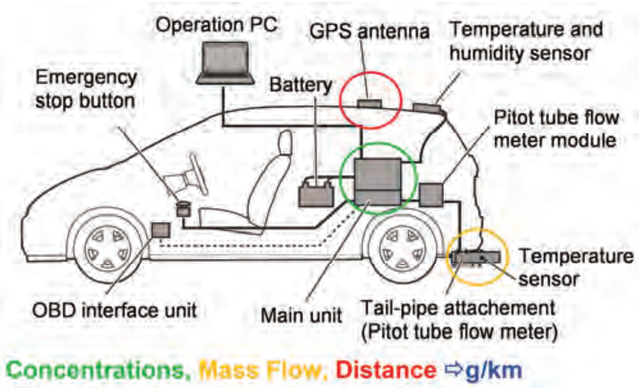

Fig. 1. Set-up of PEMS on a vehicle

The results of exhaust gas measuring devices are given as volume concentrations. Nevertheless, the legal limits are expressed in [g/km] for LDV, or in [g/kWh] for HDV.

Therefore, it is necessary to install a flowmeter at the tailpipe of the vehicle and to estimate the instantaneous exhaust gas mass flow in the transient operation.

In the data processing, the vehicle positions and speeds are required. They are usually registered from the GPS (Global Positioning System), which is installed on the vehicle. If this signal is not available, e.g. in the tunnel, the speed can be obtained from the OBD-interface (on Board Diagnose) of the vehicle.

Additionally, the parameters such as the engine coolant temperature and the engine speed are registered by the OBD.

The pollutant components measured by both PEMS (Gas & PN) are carbon dioxide CO_2, carbon monoxide CO, nitric oxides NO_x (consisting of NO and NO_2) and particle number PN (considering the invisible nanoaerosol).

Received 2 March 2021; Received in revised form 24 March 2021; Accepted 24 March 2021
Available online 24 March 2021

For the choice of data (vehicles previously measured in other projects) following criteria were taken into consideration:

– Version of the RDE route,
– The same measuring system,
– Engine cold start measured,
– Engine start measured,
– Emission components measured (CO_2, CO, NO_x, PN, HC),
– Start-stop-system (switched off).

Seven vehicles (three gasoline and four Diesel) could be chosen for the data evaluation. Table 1 summarizes the most important data of these vehicles.

Some criteria could not be completely fulfilled:

– Start-stop-system of LDV 07 was switched on,
– PN was not measured for some vehicles,
– HC was not measured for all vehicles.

Table 1. List of vehicles chosen for the data evaluation (LDV – light duty vehicle)

No.	Fuel	Displa-cement	Exhaust Aftertreatment System	Injection
LDV01	Gasoline	1.6	TWC	PFI
LDV02	Gasoline	4.0	TWC, GPF	DI
LDV03	Gasoline	6.2	TWC	PFI
LDV04	Diesel	2.0	DOC, DPF	DI
LDV05	Diesel	2.1	DOC, DPF, SCR	DI
LDV06	Diesel	3.0	DOC, DPF, SCR	DI
LDV07	Diesel	3.0	DOC, DPF, SCR	DI

2.2. Definitions of non-driving situations

Distance driven and urban part

In the legal RDE-evaluation of LDV's the parts of driving, which were performed with the speed lower than 60 km/h, are considered as "urban", even if they were performed outside of the city. In opposition, the urban part in this work is defined as the first 13.7 km of the distance driven. This was decided after investigating the speeds, distances and emission traces of the chosen vehicles. 13.7 km is the shortest distance before one of the vehicles reached the speed of 60 km/h. With this definition of urban part, it is fixed that all investigated vehicles were driven below this speed limit value (60 km/h). Furthermore, it was observed that during this 13.7 km, there were the specific driving-and emissions-situations, which are the subject of this research: cold start, warm-up, stop&go, idling.

The investigation of the high-speed driving parts – rural and highway – showed no noticeable emission events.

Cold start

The cold start is defined with the engine coolant temperature (ECT) as: (ECT +2°C) < t_{amb}, or ECT < 30°C. This means that ECT can be up to 2°C higher than the ambient temperature or it must be lower than 30°C. This definition originating from the HDV-legislation is applied in this work because it is stricter than the definition from the LDV-legislation (+7°C, 35°C).

Engine warm-up

The warm-up time is defined in two ways:

a. from the engine start (n > 500 rpm) to the instant of ECT = 70°C – this is named: "ECT 70" and
b. from the engine start (n > 500 rpm) to the duration of 5 minutes – this is named: "5 minutes".

These definitions and examples of the warm-up for two vehicles (gasoline & Diesel) are represented in Fig. 2. It can be clearly remarked that the Diesel vehicle needs a longer time to attain the ECT 70.

Figure 5 summarizes the time-traces of ECT for all investigated vehicles. For LDV1 and LDV5, there are some irregular increases of ECT. ECT of LDV1 reaches 70°C in approximately 4 minutes after start. However, it falls again below 70°C for approximately 1 minute. This 1 minute is accounted to the warm-up according to the definition.

For more detailed analyses it is useful to consider both warm-up definitions and the time-courses of the increasing ECT.

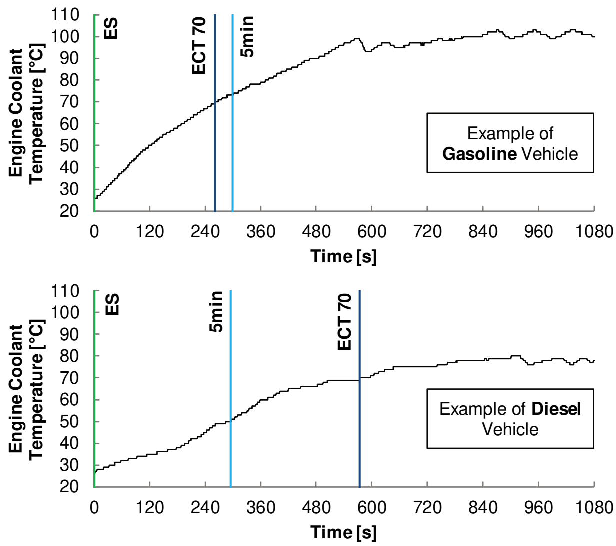

ES: Engine Start (Start of "Engine In Operation")
ECT 70: Engine Coolant Temperature (ECT) reaches 70°C
5min: 5min after Engine Cold Start

Definitions		start	end
Cold Start	state	ECT < $T_{ambient}$ +2°C OR ECT < 30°C	-
Engine in Operation	state	Engine Speed > 500 rpm	-
Warm-Up ECT 70	phase	Cold Start AND Engine in Operation	ECT > 70°C
Warm-Up 5min	phase	Cold Start AND Engine in Operation	Phase Time > 5min

Fig. 2. Definition of warm-up in RDE-test

Stop&go

According to ASTRA, the definitions of traffic congestion which are used for the public traffic information are:

– the traffic jam on the extra-urban route is given when the speed is below 10 km/h during at least 1 minute and frequent standstill occurs,
– in the city circulation, the traffic jam is considered when the loss of summary time is over 5 minutes.

These definitions are close to the stop&go operation and they gave the basis for the definition which is easy to understand and which depicts well this driving situation.

The operation of the vehicle with the driving speeds between 1 km/h and 10 km/h is considered as a "stop&go" phase. In this way, the vehicle standstill (stop) and the short acceleration by moving (go) are included in this operation mode.

Figure 3 shows the definition and example of stop&go in the urban part (13.7 km). Figure 5 summarizes the shares of stop&go in the urban part for all investigated vehicles. These shares are in the range of 13% to 19%.

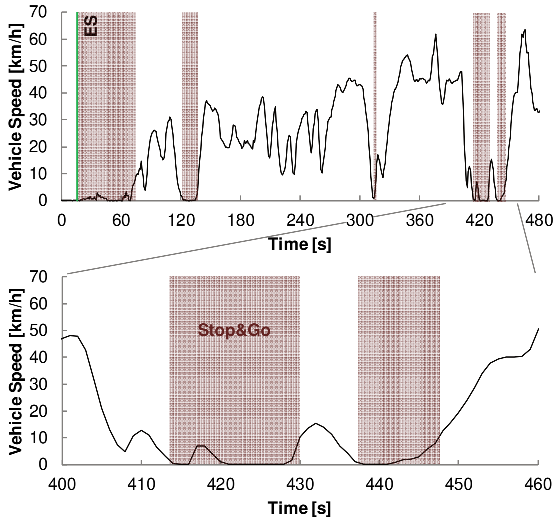

ES: Engine Start (Start of "Engine In Operation")

Definition		start	end
Stop&Go	phase	Vehicle Speed < 1 km/h	Vehicle Speed > 10 km/h

Fig. 3. Definition of stop&go in RDE-test

Idling

The idling phase is given, when the engine speed is between 500 rpm and 900 rpm and the vehicle speed is below 1 km/h.

Figure 4 shows the definition and example of idling in the urban part and Fig. 5 summarizes the shares of idling in the urban part for all investigated vehicles. These shares are in the range of 6% to 13%.

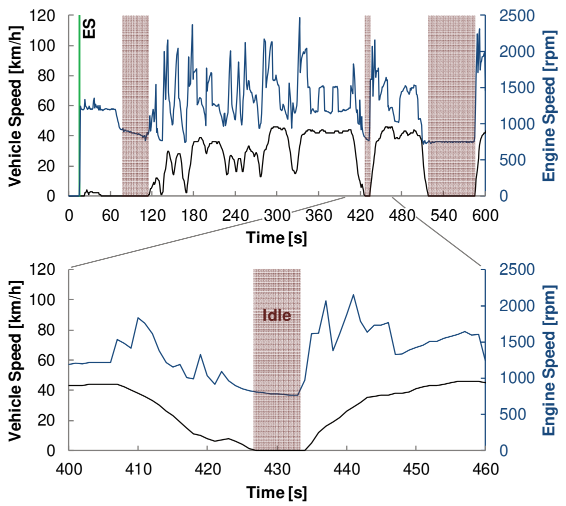

ES: Engine Start (Start of "Engine In Operation")

Definition		start	end
Idling	state	500 rpm < Engine Speed < 900 rpm	-
Idle	phase	Vehicle Speed < 1 km/h AND Idling	Idle Start Cond. False

Fig. 4. Definition of idling in RDE-test

According to these definitions, there is a certain overlapping of the data of the considered non-driving situations, see Fig. 6.

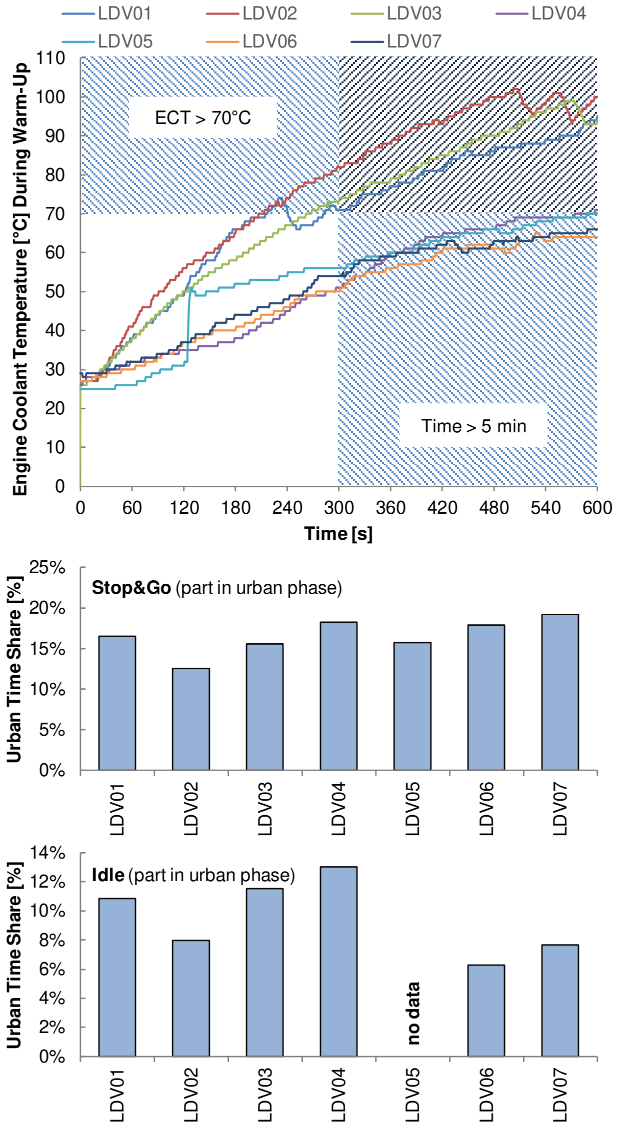

Fig. 5. Time courses of the engine coolant temperature during warm-up and time shares of stop&go and idling in the RDE-test

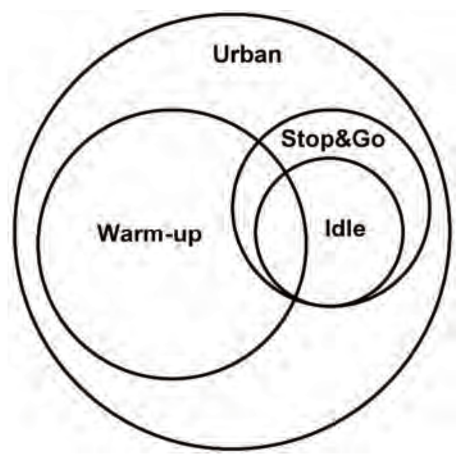

Fig. 6. Qualitative overlapping of the analyzed data

3. Results

The evaluated emissions data are expressed as total cumulated values in [g], [#], as emissions per time in [g/min], [#/min] or as specific emissions per distance [g/km], [#/km]. The specific emissions (per km) respond to the legal view, they are comparable with legal limit values, but they are not applicable for the non-driving situations, where the distance driven is zero (like idling or stop&go). These facts are considered in the data representation.

3.1. Warm-up

Figure 7 represents the cumulative emissions over time during the urban phase (13.7 km) for the gasoline vehicles. Figure 8_shows the analogous results for Diesel vehicles. It can be remarked that for the gasoline vehicles (LDV1 – LDV3), the ECT 70-warm-up happens earlier or simultaneously with the 5 minutes-point. For the Diesel vehicles (LDV4 – LDV7) inversely, the ECT 70-warm-up takes generally a longer time and it arrives after the 5 minutes-point.

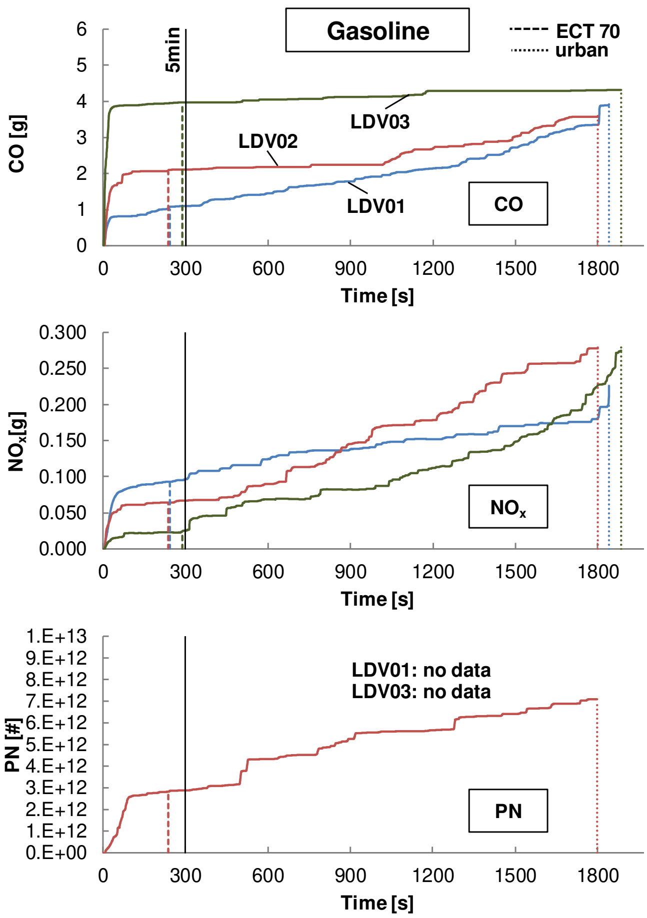

ECT 70: engine coolant temperature reaches 70°C
5min: 5 min after engine cold start
urban: part of RDE-Route (geographically defined distance: 13.7 km)

Fig. 7. Cumulated emissions of gasoline vehicles during the warm-up phase

From the comparison of vehicles, it can be stated, that:

- vehicles with smaller engine displacement produce lower CO_2-emissions,
- most emissions of CO and NO_x, especially in the "gasoline" group are produced during and shortly after cold start,
- in both vehicles' groups: "gasoline" and "Diesel", there are quite considerable emissions differences between the vehicles, resulting mostly from different efficiencies of the exhaust aftertreatment systems,
- the urban phase (13.7 km) is driven by different vehicles at different time, due to different average speeds resulting from the traffic situations.

Specific emissions (per km) and their increase factors in the warm-up phase are compared for all vehicles in the Fig. 9.

The CO [g/km] in warm-up are generally higher than in the entire urban phase (13.7 km). The "warm-up increase factor" varies between 2 & 11 for gasoline and 1 & 4 for Diesel vehicles. CO-values of LDV4 are particularly high indicating most probably some problems of engine, or of inactive DOC.

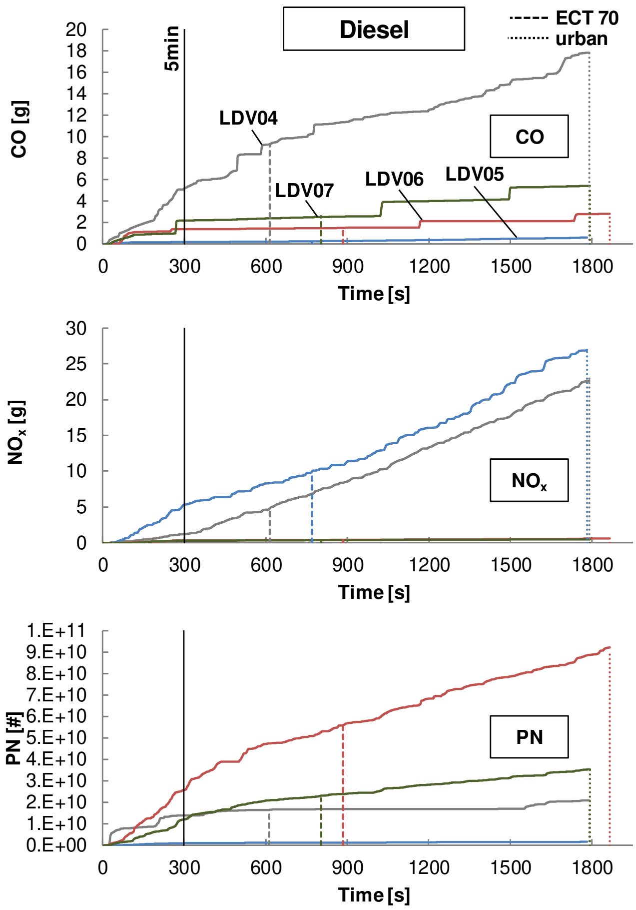

ECT 70: engine coolant temperature reaches 70°C
5min: 5 min after engine cold start
urban: part of RDE-Route (geographically defined distance: 13.7 km)

Fig. 8. Cumulated emissions of Diesel vehicles during the warm-up phase

The NO_x [g/km] values of two Diesel vehicles (LDV4 & LDV5) are very high, which particularly signalizes a misfunction of the SCR-system of LDV5 (LDV4 is not equipped with SCR). The specific emissions in warm-up are sometimes higher than in the urban phase with the "increase factor" ranging between 0.9 & 7.5 for gasoline and 0.9 & 5 for Diesel vehicles.

The nanoparticle emissions PN are efficiently eliminated by the DPF's – all investigated Diesel vehicles were equipped with a filter. In the "gasoline" group, the PN-data were available only for the LDV2, which was equipped with GPF. This GPF enables the urban PN-emission to be reduced below the limit value (6×10^{11} #/km). For the shorter warm-up phases, the emission peak of the cold start gets more weight and the distance driven is shorter. The filtration quality of this GPF, comparing to the DPF's is quite weak and the high specific PN-emission over the warm-up gets high above the limit value.

Similar experiences exist at AFHB from the previous research on GPF's [25, 26]: the PN-emissions of a gasoline car (sometimes also with PFI) can reach 10^{13} #/km in $WLTC_{cold}$. The particle count filtration efficiency of the investigated GPF's could be as low as 70%–80% in WLTC, in opposition to DPF's. With this knowledge the authors suggest that the non-measured PN-values of the other two gasoline vehicles could be in average of this "urban" phase at least in the range of 10^{13} #/km.

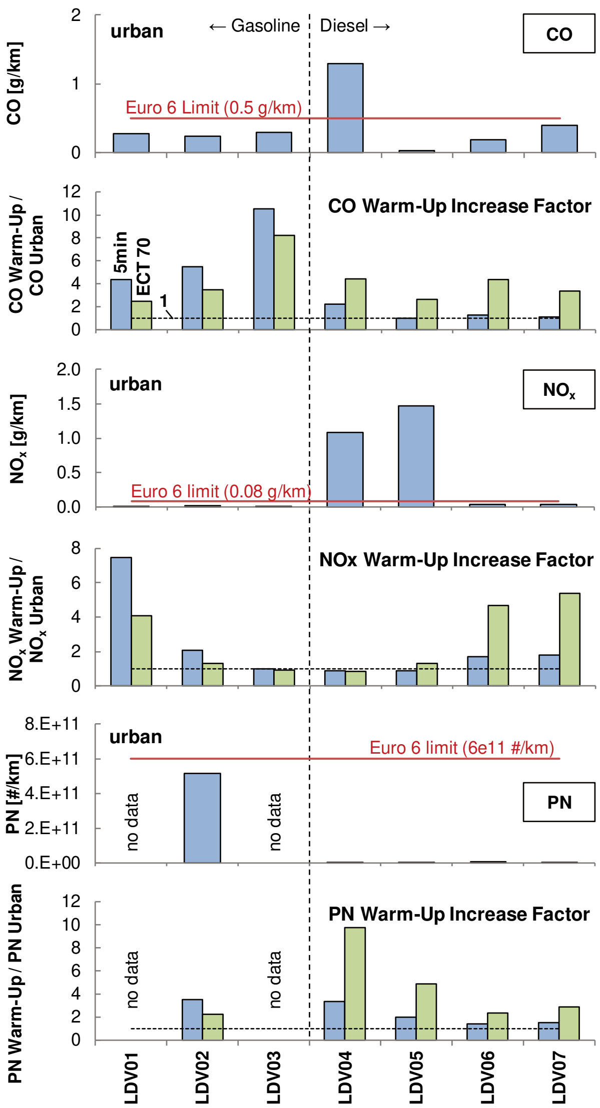

Fig. 9. Specific emissions and their increase factors in the warm-up phase

The PN warm-up increase factors for gasoline vehicle are between 2 & 4 (regarding both definitions of warm-up) and for Diesel vehicles these increase factors are between 1.5 & 10. This means that even the DPF's with the best filtration quality allow a certain penetration of the cold start PN-emission peak, of course at an absolute very low emission level.

3.2. Stop&go

The cumulated emissions in stop&go phases are summarized for all vehicles in Fig. 10.

The comparison of emissions of the single vehicles offers a similar picture, as in the previous Fig. 9.

- in the "gasoline" group: CO_2-emission is higher for bigger engines (engine swept volume increases from LDV1 to LDV3); CO-value is the highest for LDV3, which shows the slowest warm-up (see Fig. 5); the PN-values are only given for LDV2 (equipped with GPF) and they confirm the mediocre filtration quality comparing to DPF's.
- in the "Diesel" group: high CO for LDV4 (insufficiency of engine, or of DOC); high NO_x for LDV4 (no SCR) and for LDV5 (inadequacy of SCR); near-to-zero PN-emissions, thanks to right-quality DPF's.

An interesting finding is given by the higher CO- and NO_x-emissions of LDV7 relatively to LDV6. Both vehicles have the same engine displacement volume and nearly identical exhaust aftertreatment systems (DOC, DPF, SCR). LDV7 was driven with its start-stop-control switched on.

This means that during the stop&go operation, the engine was stopped and started independently on the drivers wish.

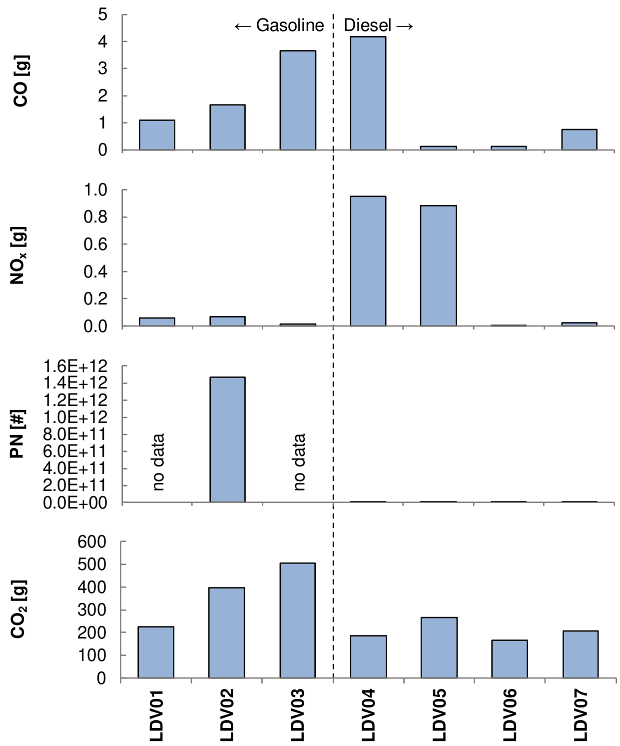

Fig. 10. Cumulated emissions in stop&go

By engine stop, there are no emissions produced, but by engine start, there is always an emission peak. The balance between the emission saving and emission over-producing depends on how long is the stop-time and how intense is the start-peak. The last one depends strongly on the thermal condition of the engine and of the exhaust system. In the present urban part (first 13.7 km) several start-stops must have been performed with not entirely warm exhaust after-treatment system and the higher emission peaks at engine restart overweighed the emissions results of LDV7.

Relatively to the urban part (13.7 km) the cumulated emissions in stop&go are increased/decreased by the following factors:

for gasoline vehicles:		for Diesel vehicles:	
CO	2–6	CO	0.2–2.2
NO_x	0.7–2.5	NO_x	0.1–0.4
PN	1.7 (1 vehicle)	PN	0.4–2.3
CO_2	0.5–0.7	CO_2	0.3–0.6

3.1. Idling

Figure 11 represents the cumulated emissions at idling for all investigated vehicles. The relationships between the vehicles and the technical explanations are similar as in the previous section for “stop&go”.

Relatively to the urban part (13.7 km) the cumulated emissions at idling are mostly decreased with the following factors:

for gasoline vehicles:		for Diesel vehicles:	
CO	0.5–2.5	CO	0.1–0.9
NO_x	0.3–1.1	NO_x	0.1–0.4
PN	0.7 (1 vehicle)	PN	0.5–1.8
CO_2	0.3–0.6	CO_2	0.3–0.4

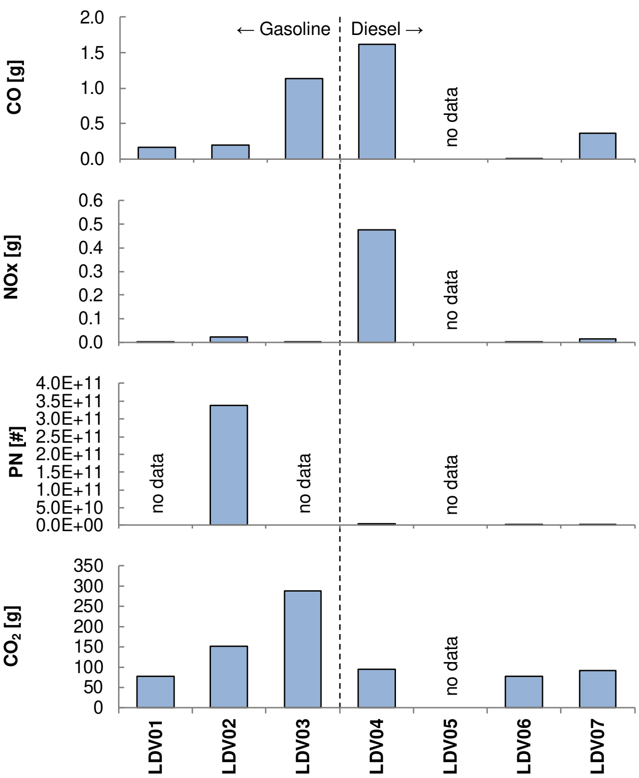

Fig. 11. Cumulated emissions at idling

4. Reproduction of non-driving situations (part 2)

4.1. Test vehicles, fuels and lubricants

The vehicles used for reproduction of special (non) driving situations are listed in the Table 2.

All vehicles were operated with the Swiss market fuels and with the lubricating oils, which actually were present in each vehicle.

Table 2. List of vehicles used for reproduction of non-driving situations on chassis dynamometer (ga – gasoline, di – Diesel)

Vehicle	Instru-ments	Fuel	Displa-cement	Emis-sion Standard	Exhaust Aftert-reatment System	Injec-tion
ga1 – “modern”	cvs	Gasoline	1.6	Euro 5	TWC	GDI
ga1 – “modern”	pems	Gasoline	1.6	Euro 5	TWC	GDI
ga2 – “dated”	cvs	Gasoline	1.6	Euro 3	TWC	MPI
di1 – “modern”	cvs	Diesel	2.1	Euro 6	DOC, DPF, SCR	DI
di1 – “modern”	pems	Diesel	2.1	Euro 6	DOC, DPF, SCR	DI
di2 – “dated”	cvs	Diesel	2.0	Euro 2	DOC	DI

4.2. Test installations and procedures

Chassis dynamometer test cell

The tests were performed on the 4WD-chassis dynamometer of AFHB (Laboratory for Exhaust Emission Control of the Bern University of Applied Sciences, Biel, CH).

The stationary system for regulated exhaust gas emissions is considered as reference. This equipment fulfils the requirements of the Swiss and European exhaust gas legislation.

The regulated gaseous components are measured with exhaust gas measuring system Horiba MEXA-7200; CO, CO_2 – infrared analysers (IR); HC_{FID} – flame ionization detector for total hydrocarbons; CH_{4FID} – flame ionization detector with catalyst for only CH_4; NO/NO_X – chemiluminescence analyzer (CLA).

The dilution ratio DF in the CVS-dilution tunnel is variable and can be controlled by means of the CO_2-analysis.

The measurements of summary particle counts in the size range 23-1000 nm were performed with the CPC TSI 3790 (according to PMP).

For the exhaust gas sampling and conditioning a ViPR system (ViPR – volatile particle remover) from Matter Aerosol was used. This system contains:

- Primary dilution – MD19 tunable rotating disk diluter (Matter Eng. MD19-2E),
- Secondary dilution – dilution of the primary diluted and thermally conditioned sample gas on the outlet of evaporative tube,
- Thermoconditioner (TC) – sample heating at 300°C.

GAS PEMS and PN PEMS

An information about the used Horiba Gas PEMS and about the gas measuring installation of the chassis dynamometer is given in Table 3.

As PN PEMS for Real Driving Emissions Horiba OBS-ONE PN measurement system (OBS-PN) was used. This analyzer works on the condensation particles counter (CPC) principle, has an integrated sample conditioning system (double dilution and catalytic stripper ViPR, 350°C) and it indicates the summary PN concentrations in the size range 23 to approximately 1000 nm. This system was used in the tests with the newer vehicles. It presents several advantages like compactness, robustness, fast on-line response and is recognized for legal testing purposes.

Table 3. Data of the used measuring systems

	HORIBA MEXA 7200	**HORIBA OBS ONE**
	4x4 chassis dyno CVS	PEMS① wet
CO	NDIR	heated NDIR
CO_2	NDIR	heated NDIR
NO_x	CLD	CLD
NO	CLD	CLD
NO_2	calculated	calculated
O_2	–	–
HC	FID	–
PN	not measured	–
OBD logger	–	yes
GPS logger	–	yes
ambient (p, T, H)	yes	yes
EFM	–	pitot tube
OBS – one H_2O monitored to compensate the H_2O interference on CO and CO_2 sample cell heated to 60°C		

Driving cycles on chassis dynamometer

The vehicles were tested on a chassis dynamometer in special, simplified driving cycles, which made possible to perform different warm-up procedures, and stop&go with different share of idling, Fig. 12. The braking resistances were set according to the legal prescriptions and responded to the horizontal road.

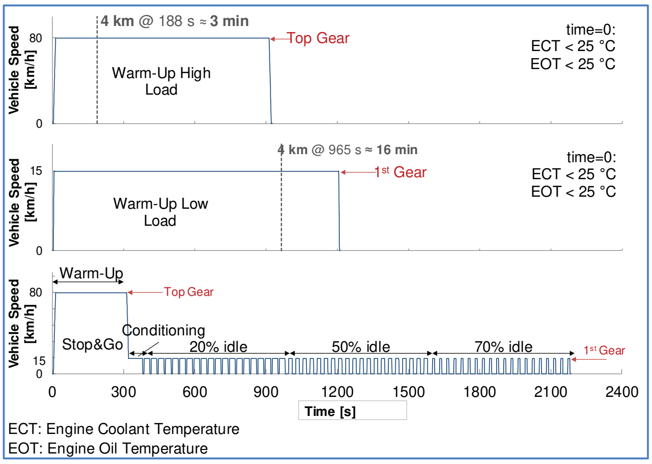

Fig. 12. Driving cycles for reproduction of warm-up and stop&go procedures on chassis dynamometer

5. Results

Figure 13 shows the cumulated emissions in the first four minutes after the cold start (25°C) with two gasoline vehicles. The newer (modern) vehicle is equipped with the engine and exhaust aftertreatment technology Euro 5 (with GDI, TWC) and the older vehicle (dated) responds to the emission class Euro 3 (with MPI, TWC). "High load" means, that after the cold start, the vehicle was driven at 80 km/h and "low load" means the same with 15 km/h (see Fig. 12).

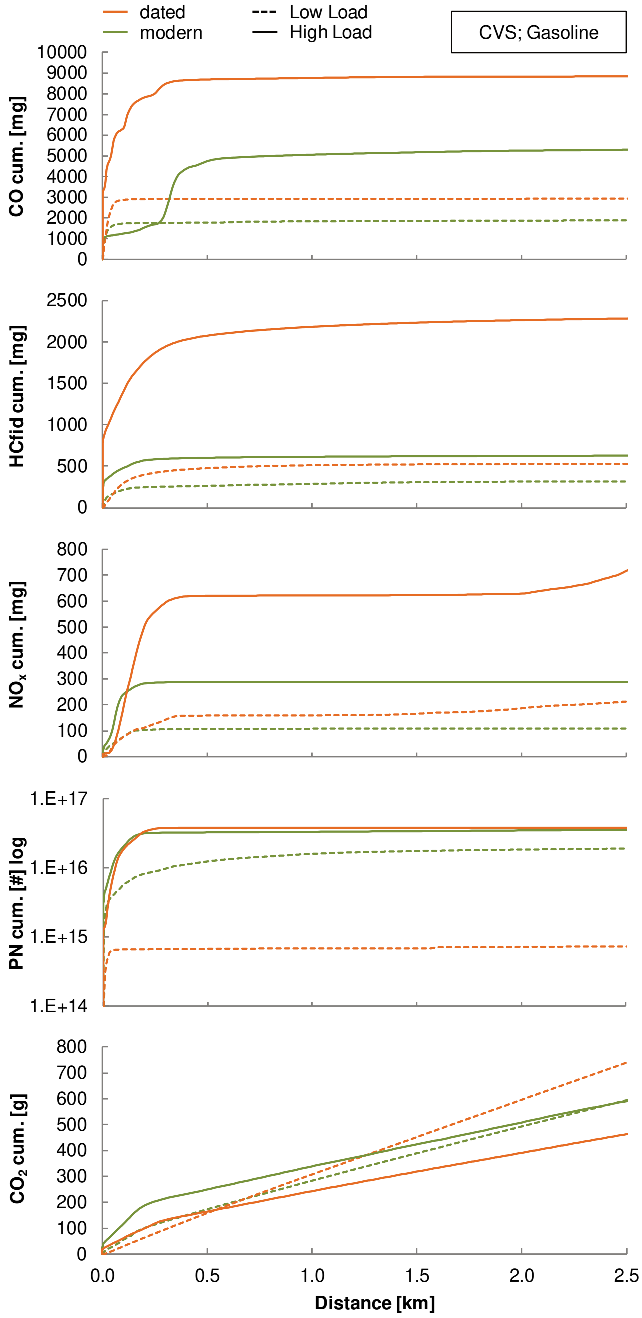

Fig. 13. Cumulated emissions during warm-up on chassis dynamometer with two gasoline vehicles and different loads

Several findings have to be mentioned:

– the emissions of CO, HC, NO_x and PN are generally higher for the older vehicle and, for both vehicles, these emissions are higher with higher load,
– the majority of these emissions is cumulated in the first 0.5 km of distance approximately; exception is NO_x of the dated vehicle: after 2 km NO_x starts to increase, es-

pecially with "high load" indicating some draw-back of the catalytic reduction,

- the emission traces obtained with PEMS (for the modern vehicle) are in a very good accordance with the emissions from the laboratory installation (CVS),
- the PN-emissions of the dated vehicle (MPI) at high load are identical with the emissions of the modern vehicle (GDI); this confirms the high PN-emissions potential of the MPI fleet as well,
- the nearly linear increase of cumulated CO_2-emissions is connected to the fuel consumption of vehicles, the relationships of slopes are influenced by the fact, that this representation is given over the driving distance and responds to different operating time. The distance of 2.5 km means for 80 km/h 1.9 minutes and for 15 km/h 10 minutes of driving.

Figure 14 represents the cumulated emissions for the Diesel vehicles. "Dated" means Euro 2 (DOC) and modern means Euro 6 (DOC, DPF, SCR). The remarkable findings are:

- the emissions of CO, HC, NO_x and PN are generally higher for the older vehicle, the emissions of CO, HC, and for the older vehicle, also NO_x, are higher with lower load (inversely to gasoline vehicles),
- the emissions of CO, HC and NO_x for the older vehicle, and particularly at low load, are cumulated not only at cold start but also in the entire represented time slot until 4 km distance driven,
- the PN-emissions of both vehicles are cumulated mainly during the cold start:
  - for the older vehicle they are significantly higher than for the newer one (up to 6 orders of magnitude) and are independent of the load,
  - for the newer vehicle (with DPF) the PN-values at low load are lower than at high load due to the lower penetration of the cold start emission peak,
- the emission traces obtained with PEMS (for the modern vehicle) are in a very good accordance with the emissions from the laboratory installation (CVS),
- the nearly linear increase of cumulated CO_2-emissions is connected to the fuel consumption of vehicles, the differences of slopes for low- and high load result from the representation of results over the distance and not over the time (see remarks to Fig. 13).

The tests of the stop&go operation with varying portion of idling were performed with warm engine and warm exhaust aftertreatment system. As a consequence, the measured emission values were very low. The exception is the older Diesel vehicle, which was equipped with a quite aged DOC only. The higher emissions which result from this vehicle allow to remark much better the effects of the idling rate.

Figure 15 represents, as example the emissions of this vehicle per distance and per time in function of the percentage of idling.

The answer to the question: how does the share of idling influence the emissions in the stop&go operation? – finally depends on the representation (consideration) over the distance or over the time. With increasing portion of idling the distance-specific emission (per km) increase and the time-specific emissions (per min) decrease.

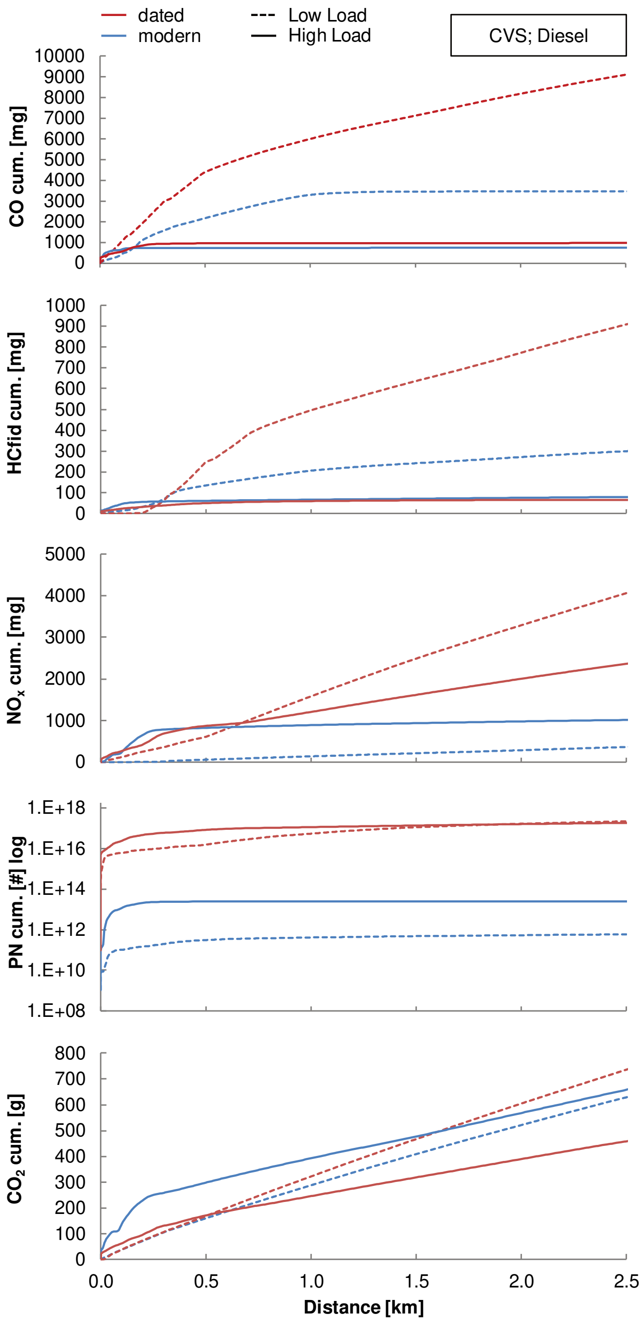

Fig. 14. Cumulated emissions during warm-up on chassis dynamometer with two Diesel vehicles and different loads

6. Conclusion

6.1. Analysis of present data

For research of emissions from non-driving or special driving situations the RDE data of 7 vehicles (3 gasoline and 4 Diesel) were analyzed.

The first 13.7 km of distance after cold start were defined as "urban" part and definitions of: warm-up (including start), "stop&go" and idling, were established in order to enable the automatic evaluation.

The most important conclusions from this research are:

- the emissions of CO, NO_x and PN are in the cold start and in the first part of the warm-up phase (c.a. 25s) considerably higher, than in the rest of the investigated urban phase (HC-data were not available),

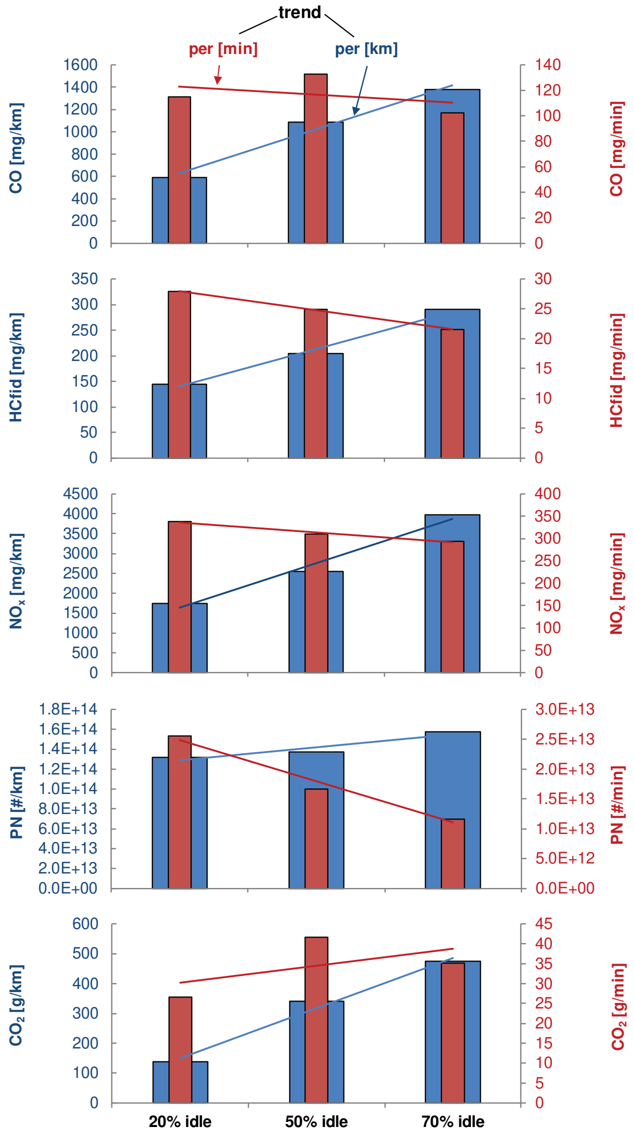

Fig. 15. Emissions of the older Diesel vehicle in the stop&go cycle depending on the share of idling; representations as distance-, and time-specific

– the special emitting situations: "stop&go" and idling are frequently given during the warm-up phase, i.e. with engine and exhaust treatment system not warm enough,
– vehicles with smaller engine displacement have lower cumulated CO_2-emissions (lower fuel consumption), they are tendentially quicker to be warmed-up,
– in both vehicles' groups: "gasoline" and "Diesel" there are quite considerable emissions differences between the vehicles, resulting mostly from different efficiencies of the exhaust aftertreatment systems,
– the specific emissions [in g/km] are in the warm-up generally significantly higher than in the investigated urban phase (13.7 km); the respective "increase factors" are in average: for CO 6; for NO_x 4; for PN 6,
– the GPF, which was applied on one of the investigated gasoline vehicles showed a weak filtration quality comparing to the DPF's which were used on the Diesel vehicles,
– the start-stop-system switched on during the warm-up is tendentially disadvantageous because the cold exhaust aftertreatment system cannot eliminate sufficiently the emissions peaks produced by restarting the engine.

6.2. Reproduction of non-driving situations

The non-driving (or special driving) situations – warm-up with different engine load and stop&go with different portions of idling – were reproduced on a chassis dynamometer with two gasoline vehicles and two Diesel vehicles. Both vehicles types were represented by a newer and an older technology.

During the cold start and warm-up in the first 2.5 km, the emissions of older type vehicles are generally higher than for the newer technology. The majority of emissions are accumulated in the first 0.5 km of the distance driven.

The PN-level of older technology gasoline vehicle (MPI) at higher load (80 km/h) is equal to the PN-level of the newer technology (GDI) – both vehicles without GPF.

The advantages and the efficiency of the modern Diesel aftertreatment (DPF) are confirmed by a significant reduction of PN.

In the stop&go operation, there are several tendencies of increasing the specific emissions [mg/km] with the higher share of idling (except of: HC for gasoline vehicles and PN for all vehicles). One of the factors taken into consideration is the shorter distance driven with the higher portion of idling in the tested time interval. The consideration of emissions per time [mg/min] results in lowering most of the emissions with higher portion of idling.

Acknowledgements

The authors express gratitude to the Swiss Federal Offices for Environment (BAFU) for the financial support of these activities.

Nomenclature

AFHB	Abgasprüfstelle FH Biel, CH
ASTRA	Federal Office of Roads
CF	Conformity Factor
CLD	Chemoluminescence Detector
DI	Direct Injection
DOC	Diesel Oxidation Catalyst
DPF	Diesel Particle Filter
ECT	Engine Coolant Temperature
EFM	Exhaust Flow Meter
EMPA	Eidgenössische Material-Prüfanstalt
EMROAD	Data processing reference software
EOT	Engine Oil Temperature
Es	Engine Start
EU	European Union
FID	Flame Ionization Detector
FOEN	Federal Office of Environment, CH
GPF	Gasoline particulate filter
GPS	Global Positioning System
HD	Heavy Duty
HDV	Heavy Duty Vehicles

ISC	In-Service Conformity	RDE	Real Driving Emission
LD	Light Duty	ResRDE	research of RDE
LDV	Light Duty Vehicles	SCR	Selective Catalytic Reduction
NDIR	Non-Dispersive Infrared	TA	Type Approval
OBD	On Board Diagnosis	TPA	Tailpipe Attachment
OCE	Off-Cycle Emissions	TWC	Three-way catalyst
PEMS	Portable Emissions measurement system	V	vehicle
PFI	port fuel injection	WHTC	World Heavy-Duty Transient Cycle
PN	Particle Number	WLTC	World Light-Duty Transient Cycle

Bibliography

[1] European Environment Agency. EMEP/EEA Air pollutant emission inventory guidebook 2016. *EEA Report*. 2016, 21. https://www.eea.europa.eu//publications/emep-eea-guidebook-2016 (accessed on 29 March 2019).

[2] FRANCO, V., KOUSOULIDOU, M., MUNTEAN, M. et al. Road vehicle emission factors development: a review. *Atmosphere Environment*. 2013, **70**, 84-97. https://doi.org/10.1016/j.atmosenv.2013.01.006

[3] NTZIACHRISTOS, L., GKATZOFLIAS, D., KOURIDIS, C. et al. COPERT: A European road transport emission inventory model. In: Athanasiadis, I.N., Rizzoli, A.E., Mitkas, P.A., Gómez J.M. (eds) Information Technologies in Environmental Engineering. *Environmental Science and Engineering*. *Springer*, Berlin, Heidelberg. https://doi.org/10.1007/978-3-540-88351-7_37

[4] BORGE, R., LUMBRERAS, J., PEREZ, J. et al. Emission inventories and modeling requirements for the development of air quality plans. Application to Madrid (Spain). *Science of the Total Environment*. 2014, **466-467**, 809-819. https://doi.org/10.1016/j.scitotenv.2013.07.093

[5] VALVERDE, V., MORA, B.A., CLAIROTTE, M. et al. Emission factors derived from 13 Euro 6b light-duty vehicles based on laboratory and on-road measurements. *Atmosphere*. 2019, **10**, 243. https://doi.org/10.3390/atmos10050243

[6] GIECHASKIEL, B., GIORIA, R., CARRIERO, M. et al. Emission factors of a Euro VI heavy-duty diesel refuse collection vehicle. *Sustainability*. 2019, **11**, 1067. https://doi.org/10.3390/su11041067

[7] ANDERSSON, J., MAY, J., FAVRE, C. et al. On-road and chassis dynamometer evaluations of emissions from two Euro 6 diesel vehicles. *SAE International Journal of Fuels and Lubricants*. 2014, **7**(3), 919-934. https://doi.org/10.4271/2014-01-2826.

[8] BIELACZYC, P., WOODBURN, J., SZCZOTKA, A. Exhaust emissions of gaseous and solid pollutants measured over the NEDC, FTP-75 and WLTC chassis dynamometer driving cycles. *SAE Technical Paper* 2016-01-1008. 2016. https://doi.org/10.4271/2016-01-1008

[9] MAY, J., BOSTEELS, D., FAVRE, C. An assessment of emissions from light-duty vehicles using PEMS and chassis dynamometer testing. *SAE International Journal of Engines*. 2014, **7**(3), 1326-1335. https://doi.org/10.4271/2014-01-1581

[10] CLAIROTTE, M., VALVERDE, V., BONNEL, P. et al. Joint Research Centre 2018, Light-duty vehicles emissions testing. *Publications Office of the European Union*. Luxembourg, 2018. https://doi.org/10.2760/289100

[11] CZERWINSKI, J., ZIMMERLI, Y., COMTE, P. et al. Experiences and results with different PEMS. TAP Paper. *International Transport and Air Pollution Conference*, May 24th-26th, 2016, Lyon.

[12] CZERWINSKI, J., ZIMMERLI, Y., COMTE, P. et al. Potentials of the portable emission measuring systems (PN PEMS) to control real driving emissions (RDE). 38. International Vienna Motor Symposium, 27-28 April 2017, *VDI Fortschritt-Bericht*. 2017, **12**(802), Vol. 2.

[13] CZERWINSKI, J., COMTE, P., ZIMMERLI, Y. et al. Research of emissions with gas PEMS and PN PEMS. *TAP Paper, International Transport and Air Pollution Conference*, 15th-16th November 2017, EMPA, Zürich.

[14] GIECHASKIEL, B., ROCCOBONO, F., BONNEL, P. Feasibility study on the extension of the Real Driving Emissions (RDE) procedure to particle number (PN). European Commission. *Joint Research Centre.* 2016. https://doi.org/10.2790/74218

[15] SUAREZ-BERTOA, R., VALVERDE, V., CLAIROTTE, M. et al. On-road emissions of passenger cars beyond the boundary conditions of the real-driving emissions test. *Environmental Research*. 2019, **176**, 108572. https://doi.org/10.1016/j.envres.2019.108572

[16] O'DRISCOLL, R., STETTLER, M.E.J., MOLDEN, N. et al. Real world CO_2 and NO_x emissions from 149 Euro 5 and 6 diesel, gasoline and hybrid passenger cars. *Science of the Total Environment*. 2018, **621**, 282-290. https://doi.org/10.1016/j.scitotenv.2017.11.271

[17] LUJÁN, J.M., BERMÚDEZ, V., DOLZ, V. et al. An assessment of the real-world driving gaseous emissions from a Euro 6 light-duty diesel vehicle using a portable emissions measurement system (PEMS). *Atmospheric Environment.* 2018, **174**, 112-121. https://doi.org/10.1016/j.atmosenv.2017.11.056

[18] KO, J., MYUNG, C.L., PARK, S. Impacts of ambient temperature, DPF regeneration, and traffic congestion on NO_x emissions from a Euro 6-compliant diesel vehicle equipped with an LNT under real-world driving conditions. *Atmospheric Environment.* 2019, **200**, 1-14. https://doi.org/10.1016/j.atmosenv.2018.11.029

[19] KAWAI, T., TSUNOOKA, T., CHIBA, F. et al. Effect of high concentration ethanol on SI engine cold startabillity and emissions. *16. Aachener Kolloquium Fahrzeug- und Motorentechnik.* 2007, **2**, 1075.

[20] CZERWINSKI, J., COMTE, P., ENGELMANN, D. et al. Non-legislated emissions and PN of two passenger cars with gasoline-butanol blends. *Combustion Engines.* 2018, **172**(1), 64-72. https://doi.org/10.19206/CE-2018-108

[21] STEPIEN, Z., CZERWINSKI, J. Cold start with ethanol-blend fuels and influences on non-legislated emissions of a GDI flex fuel vehicle. *Polish Journal of Environmental Studies*. 2017, **26**(5), 2223-2229. https://doi.org/10.15244/pjoes/69282.

[22] CZERWINSKI, J., COMTE, P., GÜDEL, M. Non-legislated emissions of a GDI flex fuel passenger car at cold start with ethanol and butanol blend fuels. TAE. *11th International Colloquium Fuels Conventional and Future Energy for Automobiles.* 2017, 199-207.

[23] BIELACZYC, P., WOODBURN, J., SZCZOTKA, A. An Investigation into cold start emissions from compression

ignition engines using EU legislative emissions test pro-procedures. *SAE International Journal of Fuels and Lubricants. 2013,* **6**(2), 466-477. https://doi.org/10.4271/2013-01-1304

[24] BIELACZYC, P., SZCZOTKA, A., WOODBURN, J. The effect of a low ambient temperature on the cold-start emissions and fuel consumption of passenger cars. *Proceedings of the Institution of Mechanical Engineers, Part D: Journal of Automobile Engineering*. 2011, **225**(9), 1253-1264. https://doi.org/10.1177/0954407011406613

[25] CZERWINSKI, J., COMTE, P., HEEB, N. et al. Nanoparticle emissions of DI gasoline cars with/without GPF. *SAE Technical Paper* 2017-01-1004. 2017. https://doi.org/10.4271/2017-01-1004.

[26] CZERWINSKI, J., COMTE, P., ENGELMANN, D. et al. PN-emissions of gasoline cars MPI and potentials of GPF. *SAE Technical Paper* 2018-01-0363. 2018. https://doi.org/10.4271/2018-01-0363

Danilo Engelmann – Professor at the University of Applied Sciences, Biel-Bienne, Switzerland.
e-mail: *danilo.engelmann@bfh.ch*

Pierre Comte, Dipl.-Ing. HTL – University of Applied Sciences, Biel-Bienne, Switzerland.
e-mail: *pierre.comte@bfh.ch*

Andreas Hüssy, BSc., BFH Automotive Engineering – University of Applied Sciences, Biel-Bienne, Switzerland.
e-mail: *andreas.huessy@bfh.ch*

Jan Czerwinski, Prof. Dr. – Professor Emeritus at the University of Applied Sciences, Biel-Bienne, Switzerland, CJ Consulting.
e-mail: *cjcons19@gmail.com*

Peter Bonsack, MSc., ME. – Federal Office for the Environment FOEN, Bern, Switzerland.
e-mail: *peter.bonsack@bafu.admin.ch*

Article citation info:
ANDRYCH-ZALEWSKA, M., MERKISZ, J., PIELECHA, J. The influence of the heating time of a catalyst-covered glow plug on the exhaust emissions from a diesel engine. *Combustion Engines*. 2021, **184**(1), 52-56. https://doi.org/10.19206/CE-134738

Monika ANDRYCH-ZALEWSKA
Jerzy MERKISZ
Jacek PIELECHA

The influence of the heating time of a catalyst-covered glow plug on the exhaust emissions from a diesel engine

The paper discusses the application of an in-cylinder catalyst allowing a reduction of the exhaust emissions from a diesel engine. Its placement in the combustion chamber, the area where the process of combustion takes place, allows reducing the emissions (carbon monoxide, hydrocarbons, particulate matter) 'at source'. The paper presents the possibilities of boosting the efficiency of catalysts in diesel engines by extending the time of heating of a glow plug (the catalyst applied on the glow plug). The tests were performed for the following conditions: no heating (marked 0+0), glow plug heating for 60 s after engine start (marked 0+60), glow plug heating prior to engine start for 60 s and glow plug heating for 60 s after engine cold start (marked 60+60). An improvement in the efficiency of oxidation of the exhaust components was observed as the glow plug heating time increased.

Key words: *combustion engine, in-cylinder catalyst, glow plug*

1. Introduction

Piston combustion engines are common sources of power in transport. They were initially used as stationary but owing to their multiple advantages, they became popular in vehicles. The attempts to obtain increasingly higher unit power outputs, improving the operating indexes and reducing the unit mass are only some of the requirements that are currently imposed by legislators and are vital in the process of improvement of the engine design, including its individual components [1]. The above requirements are also a reason for continuous changes in the engine operating routines aiming at the obtainment of the above benefits while reducing the environmental nuisance. The engine operation is characterized by the formation of harmful emissions, the source of which is to be sought in the process of combustion.

An increasing stress put on the reduction of the negative impact of motor vehicles on the environment by both the legislators in individual countries and the society forces the engineers to search for increasingly complex technical solutions that will ensure the reduction of the said impact and the fulfillment of the applicable emission standards [2-5]. Among such actions, are those that influence the emission of individual harmful exhaust components immediately after they are evacuated from the engine (aftertreatment systems). Due to the specificity of operation of aftertreatment systems (obtaining high temperatures of their operation) it is necessary to place them closer to the engine) [6, 7]. These, however, are actions aiming at reducing the already formed exhaust components [8, 9]. One should take a closer look at technologically available actions that would influence the intensity of formation of the harmful components 'at source', i.e. placing catalysts as close as possible to the combustion chamber. This is the reason for the idea of combining the in-cylinder processes with the aftertreatment systems, which allows the use of catalysts inside the cylinder.

Based on the literature data analysis, we may observe that the modification of the engine combustion area, consisting in the introduction of an active element (catalyst) most likely results in the reduction of the ignition delay by reducing the energy of activation of the preflame reactions, thus improving the engine operation and reducing the formation of harmful exhaust components inside the cylinder. The catalyst located in the combustion area may have impact on several phases of the process of combustion:

- mixture formation phase – the process of cracking of the injected fuel,
- pre-flame phase – reduction of the ignition delay,
- combustion phase – increase in the combustion rate – increasing the combustion temperature (disadvantageous increase in the concentration of nitrogen oxides),
- afterburn phase – burning of hydrocarbons in the wall layer and afterburning carbon monoxide.

The works treating on the application of an in-cylinder catalyst [10–14], clearly states the possibility of reducing exhaust emission during diesel engine operation. The fitting of the catalyst in the combustion chamber allows reducing the emission 'at source'. The presented results of the research works [10–14] under varied engine operating conditions (cold start, engine dynamometer in homologation tests and road test simulations, actual traffic operation) have confirmed that the application of an in-cylinder catalyst results in a reduction (a few percent) of the emission of carbon monoxide, hydrocarbons, carbon dioxide and particulate matter.

When analyzing the problem of engine start (cold start in particular) one needs to mind the need for the glow plugs. The duration of the glow plug heating is determined based to many parameters (engine start duration, ambient temperature, coolant temperature), yet, in this work, the following were adopted in order to determine the concentration/emission of the exhaust components (catalyst-coated glow plug only, upstream of the catalytic converter):

- no heating (marked 0+0),
- glow plug heating 60 s after engine cold start (marked 0+60),
- glow plug heating 60 s prior to engine start and 60 s after engine cold start (marked 60+60).

2. Research methodology

The objects of the research analyses were glow plugs (standard size) with a catalytic coating. The catalyst materi-

Received 13 March 2021; Received in revised form 22 March 2021; Accepted 22 March 2021
Available online 23 March 2021

al was platinum that reduces the concentration of carbon monoxide, hydrocarbons and, to a small extent, particle number in a diesel engine.

The authors performed an analysis of the glow plug heating time and its influence on the exhaust emissions: carbon monoxide, hydrocarbons, nitrogen oxides, carbon dioxide and particulate matter.

The object of the research was a Euro 4, 1.3 dm^3 turbocharged diesel engine (1.3 JTD MultiJet).

The tests were carried out on a DYNOROAD 120 kW test stand by AVL. The authors investigated the concentration of the exhaust components and, allowing for the power output/covered distance, unit emission was obtained (g/kWh) of a given exhaust component.

The main component of the test stand (Fig. 1) was a three phase asynchronous electric motor. It allows a take-off of a maximum power of up to 120 kW. During operation, a combustion engine generates mechanical work converted in the brake into electrical energy that, upon voltage-frequency transformation, is transferred to the external power grid. The software ISAC 400 interface installed on the test stand allows identifying the research cycle covering the chassis (NEDC) and engine (ESC) dynamometer tests, but primarily enables the adaptation of an individual algorithm using the function of change of the vehicle speed in time and the change of the road gradient in time.

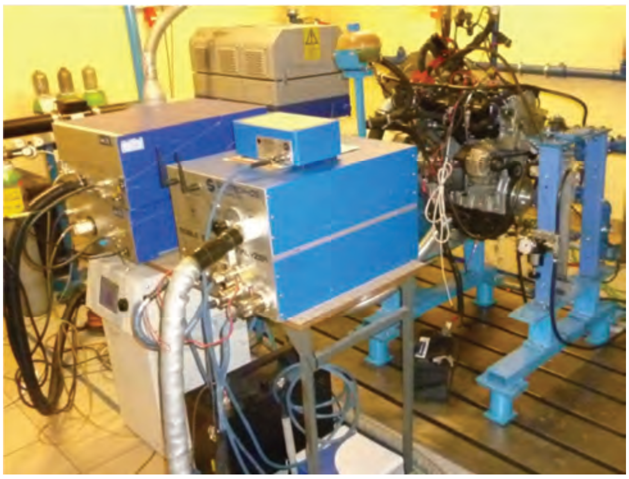

Fig. 1. View of the test stand

The measurements of the exhaust emissions were carried out according to the algorithm below.

Humid exhaust mass flow rate G_{exh} is calculated according to the formula:

$$G_{exh} = G_{air} + G_{fuel} \tag{1}$$

where: G_{air} – mass flow rate of the humid air [g/s], G_{fuel} – mass fuel consumption rate [g/s].

The emission intensity of individual gaseous exhaust components is calculated based on the relation:

$$E_{CO} = 0.000966 \cdot c_{CO} \cdot G_{exh} \cdot \beta \tag{2}$$

$$E_{NOx} = 0.001587 \cdot c_{NOx} \cdot G_{exh} \cdot \beta \cdot K_H \tag{3}$$

$$E_{HC} = 0.000966 \cdot c_{HC} \cdot G_{exh} \tag{4}$$

where: c_{CO}, c_{NOx}, c_{HC} – concentration of carbon monoxide, nitrogen oxides and hydrocarbons [ppm] in the exhaust gas, K_H – correction factor of humidity of nitrogen oxides, β – correction factor of the concentration of carbon monoxide and nitrogen oxides in dry exhaust.

The K_H factor is calculated from the formula:

$$K_H = [1 + A(H - 10.71) + B(T_{air} - 298)]^{-1} \tag{5}$$

where: $A = 0.309 \cdot G_{fuel}/G_{air} - 0.0266$, $B = -0.209 \cdot G_{fuel}/G_{air} + 0.00954$, T_{air} – temperature of the intake air [K], H – humidity of the intake air in grams (of water) per 1 kg of dry air [g/kg].

Absolute humidity of air can be calculated from the following relation:

$$H = 6.22 \cdot \varphi \cdot p/(p_a - p \cdot \varphi \cdot 10^{-2}) \tag{6}$$

where: φ – relative humidity of the intake air [%], p_a – ambient pressure [Pa], p – water vapor saturation pressure in the intake air [Pa].

Coefficient β is calculated from the formula:

$$\beta = 1 - 1.865\ G_{fuel}/G_{air} \tag{7}$$

3. Results

In the case of the evaluated concentration of carbon monoxide throughout the entire period of 1200 s, the lowest was observed for the case (60+60) and the highest for the 'no heating' case. The same effect was observed for the emission intensity of carbon monoxide (constant exhaust flow rate). As a result, the emission of carbon monoxide in the test was 7–10 g (Fig. 2).

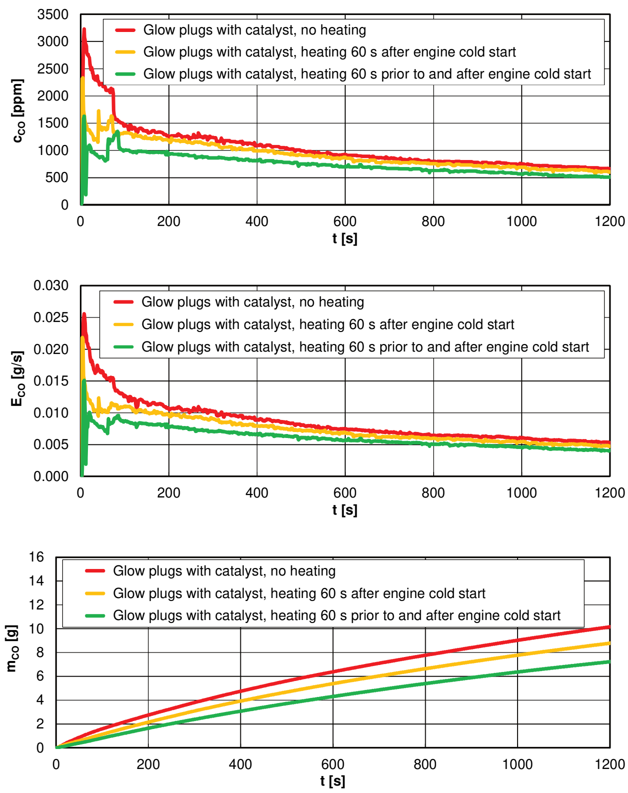

Fig. 2. Concentration, intensity of emission and emission of carbon monoxide during the tests performed on a diesel engine depending on the catalyst-coated glow plug heating time

A similar situation was observed for the concentration of hydrocarbons. The greatest increase in the concentration (over 600 ppm) was observed for the 'no heating' case (0+0). When heated only after the engine start (0+60) and for the case (60+60) this value was approx. 300 ppm. After approx. 200 s a slow decrease was observed of this concentration from 250 ppm for the cases (0+0) and (0+60) and from 200 ppm for the cases (60+60) to the value of approx. 150 ppm at the end of the measurement. The emission intensity of hydrocarbons was very similar to the course of the concentration and the final value was the same for all the cases and amounted to approx. 0.0005 g/s. The values of the emission of hydrocarbons for the three analyzed modified glow plug heating cases were in the range 0.8–1 g (Fig. 3).

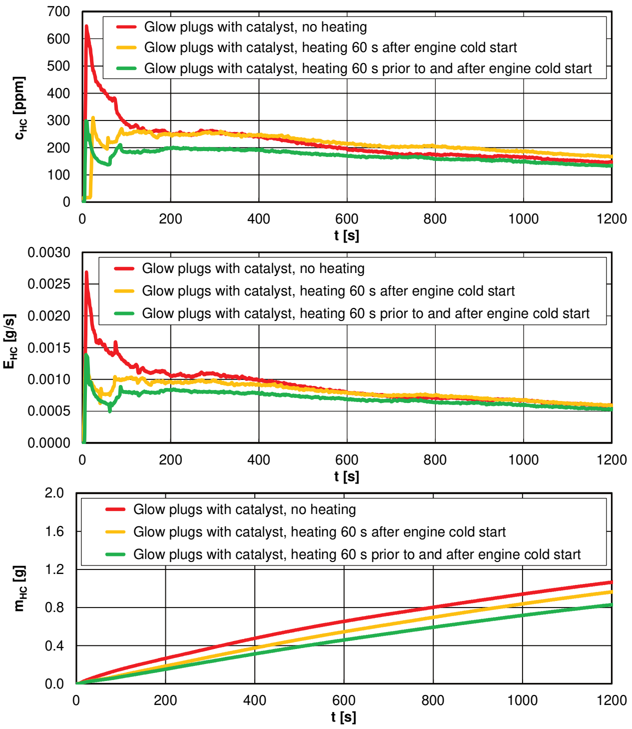

Fig. 3. Concentration, intensity of emission and emission of hydrocarbons during the tests performed on a diesel engine depending on the catalyst-coated glow plug heating time

A different situation occurred for the analysis of the concentration of nitrogen oxides. The greatest increase in the concentration of this component (over 200 ppm and the longest upkeep time) was observed for the case of glow plug heating (60+60). For the heating only after engine start (0+60), the upkeep time in the initial period of higher concentration of nitrogen oxides was shorter (the maximum is approx. 150 ppm) and for the case (0+0) a sudden increase in the concentration of nitrogen oxides was only momentary. After approx. 100 s, slow changes in the concentration were observed with a fluctuation of approx. 20 ppm. The intensity of the emission of nitrogen oxides was close to the tracing of the concentration and the final value was similar for all the cases of glow plug heating and amounted to 0.001 g/s. The final values of the emission of nitrogen oxides for the three analyzed catalyst-covered glow plug heating cases fell in the range 1–1.5 g (Fig. 4).

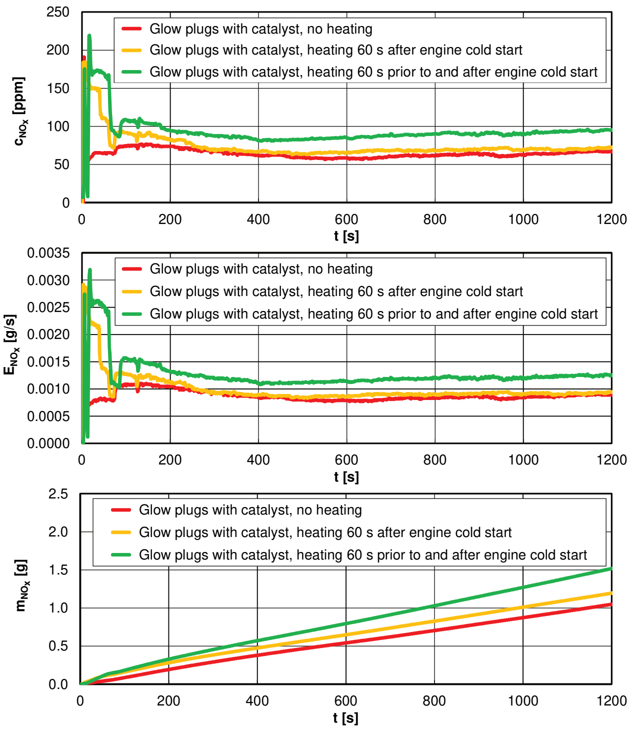

Fig. 4. Concentration, intensity of emission and emission of nitrogen oxides during the tests performed on a diesel engine depending on the catalyst-coated glow plug heating time

In the case of particle number, the test results are not varied. All tracings of the particle number intensity are similar in their nature and values and only the final values of the particle number allow a correct assessment of the environmental benefits. The particle number in the entire measurement period for different glow plug heating cases fell in the range 3–3.5·10^{11} (Fig. 5).

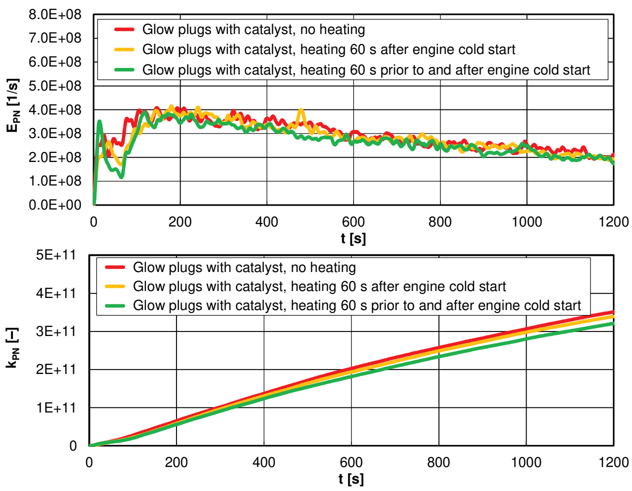

Fig. 5. Particle number intensity and particle number during the tests performed on a diesel engine depending on the catalyst-coated glow plug heating time

When analyzing the concentration of carbon dioxide for all the cases of glow plug heating, no significant differences in its values were recorded. The greatest unrepeatability occurs only in the first 100 s after engine start and the further tracings of the concentration and the intensity of emission are identical. The values of the emission of this component are close for all the heating cases (Fig. 6).

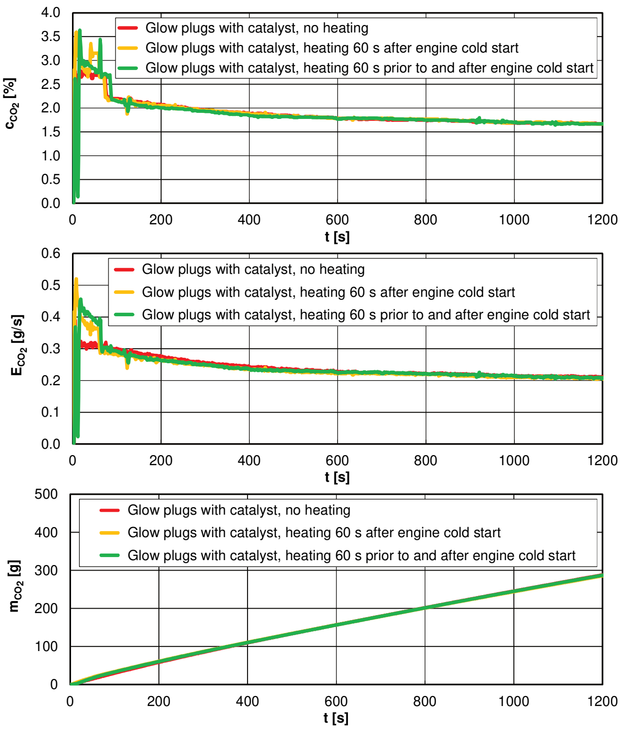

Fig. 6. Concentration, intensity of emission and emission of carbon dioxide during the tests performed on a diesel engine depending on the catalyst-coated glow plug heating time

4. Conclusions

Summarizing the performed investigations of the influence of the time of heating of the catalyst-coated glow plugs during a cold engine start on the exhaust emissions, the following final results were recorded:

1. Emission of carbon monoxide (Fig. 8a):
   - no heating condition: 10.14 g,
   - heated 60 s after engine start (0+60): 8.77 g,
   - heated for 60 s prior to and 60 s after engine start (60+60): 7.21 g.
2. Emission of hydrocarbons (Fig. 8b):
   - no heating condition: 1.06 g,
   - heated 60 s after engine start (0+60): 0.96 g,
   - heated for 60 s prior to and 60 s after engine start (60+60): 0.83 g.
3. Emission of nitrogen oxides (Fig. 8c):
   - no heating condition: 1.05 g,
   - heated 60 s after engine start (0+60): 1.19 g,
   - heated for 60 s prior to and 60 s after engine start (60+60): 1.51 g.
4. Emission of carbon dioxide (Fig. 8d):
   - no heating condition: 287 g,
   - heated 60 s after engine start (0+60): 285 g,
   - heated for 60 s prior to and 60 s after engine start (60+60): 287 g.
5. Particle number (Fig. 8e):
   - no heating condition: $3.5 \cdot 10^{11}$,
   - heated 60 s after engine start (0+60): $3.4 \cdot 10^{11}$,
   - heated for 60 s prior to and 60 s after engine start (60+60): $3.2 \cdot 10^{11}$.

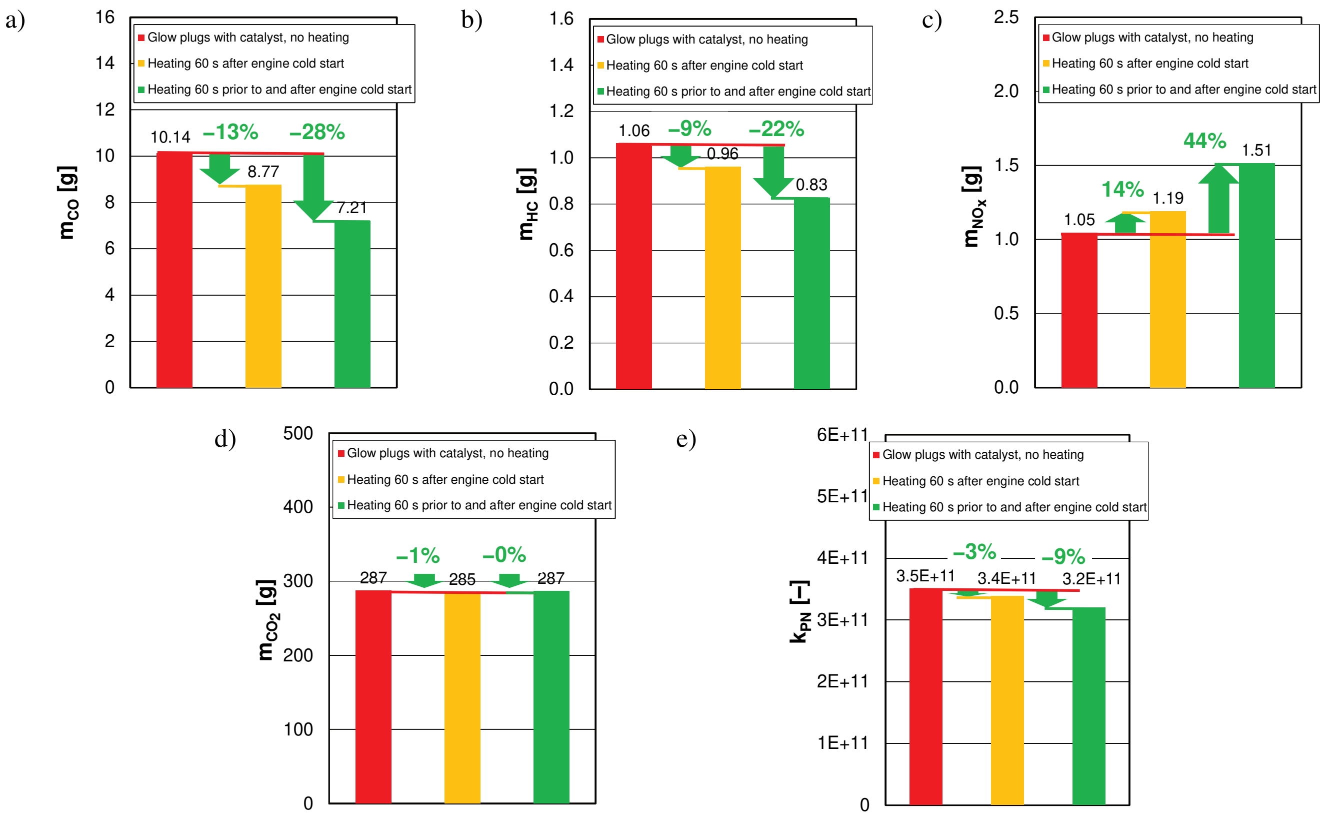

Fig. 8. Comparison of the emission of carbon monoxide (a), hydrocarbons (b), nitrogen oxides (c), carbon dioxide (d) and particle number (e) during the tests performed on a diesel engine depending on the catalyst-coated glow plug heating time

During the comparative investigations of the exhaust emissions with the application of catalyst-coated glow plugs in the measurements carried out for a cold started diesel engine, the following were obtained (values referred to the case when no glow plug heating was applied):

1. For glow plugs heated 60 s after engine start:
– relative reduction of the emission of carbon monoxide by 13%,
– relative reduction of the emission of hydrocarbons by 10%,
– relative reduction of the emission of nitrogen oxides by 14%,
– relative reduction of the particle number by 3%,
– relative reduction of the emission of carbon dioxide by 1%.

2. For glow plugs heated 60 s prior to and 60 s after engine cold start:
– relative reduction of the emission of carbon monoxide by 28%,
– relative reduction of the emission of hydrocarbons by 22%,
– relative reduction of the emission of nitrogen oxides by 44%,
– relative reduction of the particle number by 9%,
– a comparable emission of carbon dioxide.

Therefore, the authors have confirmed an improvement in the efficiency of the oxidation of the exhaust components as the heating time of the glow plug increased.

Bibliography

[1] MERKISZ, J., PIELECHA, I. *Układy mechaniczne pojazdów hybrydowych*. Wydawnictwo Politechniki Poznańskiej, Poznań 2015. https://issuu.com/wydawnictwo_pp/docs/umph

[2] KARDASZ, P., SITNIK, L., SZUBERSKI, K., HALLER, P. Ekologiczne skutki motoryzacji. *Autonaprawa.* 2010, **9**, 22–24.

[3] SKRĘTOWICZ, M., SITNIK, L., KAŹMIERCZAK, A. et al. Evaluation methods of the impact of motorization on the quality of the atmospheric air. *Journal of KONES*. 2014, **4**(21). https://doi.org/10.5604/12314005.1130507

[4] SKRĘTOWICZ, M., WRÓBEL, R., ANDRYCH-ZALEWSKA, M. Evaluation of the correlation between concentration of volatile organic compounds and temperature of the exhaust gases in motor vehicles. *International Conference on Advances in Energy Systems and Environmental Engineering* (ASEE17), Wrocław 2017. https://doi.org/10.1051/e3sconf/20172200158

[5] Worldwide Emission Standards. Passengers Cars and Light Duty Trucks. DELPHI 2017. www.delphi.com

[6] ANDRYCH-ZALEWSKA, M., SITNIK, L., WALKOWIAK, W. Modelowanie bilansu cieplnego silnika spalinowego przy zasilaniu go zróżnicowanymi paliwami. *Transport Przemysłowy i Maszyny Robocze.* 2014, **2**, 17-20.

[7] ANDRYCH-ZALEWSKA, M., SITNIK, L., WALKOWIAK, W. The heat balance of engine fed by diesel oil and BMD biofuel. Trans & MOTAUTO'14, XXII International Scientific-Technical Conference, Varna 2014. https://trans-motauto.com/sbornik/2014/1/08.THE%20 HEAT %20BALANCE%20OF%20ENGINE%20FED%20BY%20 DIESEL%20OIL%20AND%20BMD%20BIOFUEL.pdf

[8] ANDRYCH-ZALEWSKA, M. Improving the environmental performance of the internal combustion engine by the use of in-cylinder catalyst. *Combustion Engines*. 2017, **1**(168). https://doi.org/10.19206/CE-2017-120

[9] ANDRYCH-ZALEWSKA, M. The possibilities and development of in-cylinder catalytic coating. *Journal of KONES.* 2017, **3**(24). https://doi.org/10.5604/01.3001.0010.3053

[10] ANDRYCH-ZALEWSKA, M., CHŁOPEK, Z., MERKISZ, J. et al. Evaluation of the test drive cycle conditions impact on exhaust emissions from an internal combustion engine. *Combustion Engines*. 2018, **4**(175). https://doi.org/10.19206/CE-2018-401

[11] ANDRYCH-ZALEWSKA, M. Wpływ katalizatora wewnętrznego na emisję spalin w stanach pracy silnika o zapłonie samoczynnym odpowiadających jego użytkowaniu trakcyjnemu. Rozprawa doktorska. Poznań 2018.

[12] ANDRYCH-ZALEWSKA, M., MERKISZ, J., PIELECHA, J. Problemy pomiarów emisji spalin z pojazdów samochodowych. Zastosowanie metod eksperymentalnych w motoryzacji. Wybrane zagadnienia. Red. Ambroszko W. *Oficyna Wydawnicza Politechniki Wrocławskiej.* Wrocław 2020.

[13] ANDRYCH-ZALEWSKA, M., MERKISZ, J., PIELECHA, J. Analysis of the efficiency of the in-cylinder catalyst to reduce exhaust emissions during the cold start combustion engine. *Combustion Engines*. 2019, **3**(178), 38-45. https://doi.org/10.19206/CE-2019-307

[14] PIELECHA, J., ANDRYCH-ZALEWSKA, M., SKOBIEJ, K. The impact of using an in-cylinder catalyst on the exhaust gas emission in real driving conditions tests of a Diesel engine. *IOP Publishing*. 2018, **042064**. https://doi.org/10.1088/1757-899X/421/4/042064

Monika Andrych-Zalewska, DEng. – Faculty of Mechanical Engineering, Wrocław University of Technology.
e-mail: *monika.andrych@pwr.edu.pl*

Prof. Jerzy Merkisz, DSc., DEng. – Faculty of Civil and Transport Engineering, Poznan University of Technology.
e-mail: *jerzy.merkisz@put.poznan.pl*

Prof. Jacek Pielecha, DSc., DEng. – Faculty of Civil and Transport Engineering, Poznan University of Technology.
e-mail: *jacek.pielecha@put.poznan.pl*

Article citation info:
BIELACZYC, P., WOODBURN, J., JOSHI, A. World-wide trends in powertrain system development in light of emissions legislation, fuels, lubricants, and test methods. *Combustion Engines*. 2021, **184**(1), 57-71. https://doi.org/10.19206/CE-134785

Piotr BIELACZYC
Joseph WOODBURN
Ameya JOSHI

World-wide trends in powertrain system development in light of emissions legislation, fuels, lubricants, and test methods

Both the light- and heavy-duty sectors of the automotive industry are currently under unprecedented pressure from a wide range of factors, particularly in terms of environmental performance and fuel consumption. Test procedures have undergone massive changes and continue to evolve, meaning that standards are becoming much harder to meet, especially in Europe but also in other continents. Such developments force changes in testing methodology, the development of powertrains themselves and their aftertreatment systems and strategies and calibrations. This paper reports and summarises the topics of the PTNSS Congress and attempts a synthesis on the current status of the field of LD ad HD IC engines, hybrid powertrains and electric vehicles, engine fuel and oil and what the coming years may hold for the automotive and fuel industries and other allied fields.

Key words: *global LD/HD exhaust emissions, powertrain development, LD and HD IC engines, test methods, fuel development*

1. Introduction

It is widely expected that the next 20-30 years will be characterized by a high increase in the global population, especially in developing countries, with growth in the global economy and increasing urbanization. The global population is expected to increase from 7.6 to 9.2 billion by 2040. Global GDP will likely double over the same period, and several billion people are expected to join the middle class, despite unpredictable adverse events such as the Covid-19 pandemic. The expected increase in the concentration of human population in big cities worldwide will generate incremental demand for new infrastructure, distribution services for goods and local and regional transport (public as well as private): light-duty and heavy-duty vehicles (LDV and HDV) [1]. New gas, electric and hydrogen refuelling and charging stations, as well as other infrastructure, will have to be constructed to meet these needs, together with new roads, parking places and better road traffic organization, since the current vehicle fleet may even double in size over the next 30 years (or so) [2]. This will increase demand for liquid and gaseous fuels, alternative and e-fuels, electricity and hydrogen, to be met via increased production [3, 4].

Among the drivers influencing vehicular and non-road mobile machinery (NRMM) powertrain development, the field of greenhouse gases (GHG) and exhaust emissions is experiencing wide-ranging and rapid changes [4]. New emissions regulations such as Euro 6d for LDV and new test methods (RDE and WLTP) as well as Euro VI D and planned Euro VI E for HDV and the future Euro 7/VII standards are the main challenges for the automotive and powertrain industry, caused by political, socioeconomic and technical factors [5]. Air quality is very high on the political agenda and pressure remains to limit and reduce greenhouse gas emissions from the road transport sector. In addition to limits becoming increasingly stringent, the list of parameters subject to legal limits is slowly expanding – and, most importantly, these limits must be met under a wide range of conditions [6].

Discussion of GHG emissions, as well as emissions of pollutants such as NO_x and particulates – and methods to reduce such emissions, are currently underway in all the main automotive markets, as well as at the forum of UNECE GRPE Group – the World Forum for Harmonization of Vehicle Regulations [6–8]. One of important problems occurring in this area in the EU during vehicle Type Approval (TA) tests are the differences in the results of measurements of CO_2 emissions in TA tests performed using the NEDC cycle and under real driving conditions, as well as the methods of compensating for these differences after the alteration of the test procedure via the introduction of the WLTP [9, 10].

The PMP (Particulate Measurement Programme), a subgroup of UNECE GRPE, is working on a new methodology for measurements of PM/PN emissions and on the extension of the testing methodology of the number of nanoparticles (PN) for the current cut-off point of 23 nm down to 10 nm, to assess the emission of these particles which are currently not subject to limitation, which is significant especially in the case of gasoline and gaseous-fuelled engines [11–14]. The PMP team is also working on the introduction of methods testing and measuring the emission of particles generated from brake discs and brake pads used in road vehicles and the planned work for new emission standards at the post-Euro 6/VI level [15].

Fossil fuels used in the transportation sector affect Earth's climate negatively due to CO_2 emissions. Implementation of sustainable and renewable fuels for transportation has become a very important step in the reduction of the sector's carbon footprint. An effective solution for GHG reduction is the substitution of fossil fuels used in the current fleet by fuels produced from renewable sources such as biofuels, but also e-fuels and low-carbon (or even carbon-free) fuels, mainly hydrogen [16, 17].

A range of strategies are available to overcome these difficulties, as explored during the VIII International Congress on Combustion Engines organised by the Polish Scientific Society of Combustion Engines (PTNSS) and hosted at Krakow University of Technology, Poland in June 2019.

As it was presented during previous PTNSS Congresses [18] as well as International Exhaust Emissions Symposia (IEES) co-organized by BOSMAL and PTNSS [19, 20], the

Received 20 March 2021; Received in revised form 23 March 2021; Accepted 23 March 2021
Available online 24 March 2021

content of the VIII International PTNSS Congress on Internal Combustion Engines included new developments in the field of design, testing, manufacturing and maintenance of internal combustion engines for LD and HD vehicles and NRMM, hybrid and electric powertrains as well as fuel-cell development. Development of new sustainable fuel and biofuels and engine oils with low friction characteristics was also covered, as well as discussions of GHG emissions reduction efforts' influence on powertrain technology and all environmental-related issues, such as new rules and test methods, new parameters to be tested and new emissions limits.

2. Organisation of the VIII PTNSS Congress

During the years 2005-2017, the Polish Scientific Society of Combustion Engines (hereafter PTNSS), organised seven International Congresses on combustion engines, covering issues related to limiting emission of harmful exhaust emissions from automotive sources and their impact on the development of vehicle powertrain design, the development of fuel technology, engine oils, exhaust gas treatment systems and new research methods, as this subject is vitally important for the further development of the motor industry globally, in Europe generally and of course also in Poland. These Congresses were very popular among professionals in the automotive and fuel industries, both foreign and domestic, who participated extensively in their deliberations.

On 17^{th}-18^{th} June 2019, PTNSS, in cooperation with the Institute of Automobiles and Combustion Engines from Cracow University of Technology organized the VIII International Congress on Combustion Engines. VIII International Congress on Combustion Engines was held at Cracow University of Technology, at its campus on ulica Warszawska in Krakow. Other institutions were also involved in the organization of this event, such as Poznan University of Technology and BOSMAL Automotive Research and Development Institute.

The Congress covered a wide range of topics in the research fields mentioned earlier, which were explored by specialists from all over the world. The Congress also covered varied applications of combustion engines, including aviation and marine engines. It was a meeting with expert engineers and researchers sharing their new ideas, inventions, and experience. Attendees had the opportunity to add to their knowledge on a wide variety of subjects related to combustion engines and were able to enjoy, along with colleagues, friends and family, the warm welcome and hospitality afforded by the city of Krakow.

The main themes of the Congress were:

– Engine development – all engine types/sizes,
– Fuel injection systems and mixture formation,
– Combustion processes control in SI and CI engines,
– Engine thermal loading and utilization of heat released,
– Alternative fuels,
– Emission measurements and aftertreatment,
– Alternative sources of power,
– Engine testing, durability, reliability and diagnostics,
– Modelling and optimization of engine processes,
– Global trends in engine technology,
– Hybrid and electric powertrains,
– Fuels and engine oil development.

An important goal of this Congress was also the integration of the scientific and academic communities with the automotive industry (both in Poland and abroad), facilitating the establishment of new contacts, the exchange of knowledge on many issues, as well as promoting the achievements of Polish scientific and research institutions active in the fields mentioned above.

Around 200 delegates participated in the event, representing automotive and fuel industry companies, the European Commission (the EC JRC Ispra Research Centre), a key US Government Research Center (Argonne National Laboratory near Chicago), research institutes and industrial research centres from the automotive and fuel industries, and an international academic community from 16 countries (USA, Japan, China, Brazil, UK, Spain, Italy, Switzerland, Austria, Germany, Finland, France, Slovakia, Lithuania, Ukraine and Poland) representing 4 continents (Europe, North America, South America, Asia). The final programme (http://www.congress.ptnss.pl/kongres/5/final-programme) contains details of all technical presentations and other information on the event.

The VIII Congress was formally opened by Prof. Jerzy Merkisz (PTNSS, Poznan University of Technology), acting in his capacity of PTNSS president. Participants were also welcomed by Prof. Marek Brzezanski on behalf of the main Congress organizer: the Institute of Automobiles and Combustion Engines from Cracow University of Technology in Cracow, Poland.

Twenty five invited presentations were delivered during Plenary Sessions of the Congress by well-known experts on Combustion engines and powertrain system development, emissions of harmful exhausts from motor vehicles, fuels and engine oils and development of engine/vehicle testing methods. The programme for the Plenary Sessions was organised and prepared by Dr Piotr Bielaczyc and BOSMAL Automotive Research and Development Institute Ltd, Bielsko-Biala, Poland, who were involved in securing invited speakers for the Congress and preparation of the technical programme.

Presentations were delivered during five plenary sessions covering various issues of powertrain and fuel development, with the following titles:

1. Global LDV/HD exhaust emissions development.
2. Powertrain technology development (light -duty).
3. Powertrain technology development (heavy-duty & NRMM).
4. Fuel development and its impact on engine technology.
5. Testing requirements/methodologies – impact on powertrain development.

Individual sessions were chaired by well-known powertrain research experts from Poland and abroad: Les Hill (Horiba, UK), Piotr Bielaczyc (BOSMAL, Poland), Luciano Rolando (Politecnico di Torino, Italy), Andrzej Teodorczyk (WUT, Poland), Adolfo Perujo (JRC, Italy), Miroslaw Wendeker (LUT, Poland), Christopher Kolodziej (ANL, USA), Krzysztof Wislocki (PUT, Poland), David Miller (3DATX, USA) and Pawel Fuc (PUT, Poland).

In addition to the plenary presentations, around 150 technical papers that were accepted for the Congress were published in successive issues of this journal in 2019 and 2020.

The Congress was sponsored by BOSMAL & Borg Warner (Gold Sponsors), AVL, Horiba & LaVision (Silver Sponsors), 3DATX, Air Liquide, Biuro Inzynierskie M. Zajaczkowski & Motor Transport Institute (Sponsors). This journal, published by PTNSS, provided the official media patronage for the event.

More information about the congress and its organization, including the full programme, can be found at: http://www.congress.ptnss.pl/kongres/5/.

3. Congress sessions and their content

3.1. 1st session – Global LDV/HD exhaust emissions development

The first session's content related to general aspects of vehicular exhaust emissions and global standards for their reduction.

The discussions during this first session included the new method for measuring emissions under real road driving conditions – RDE, as well as the newly-introduced chassis dynamometer procedure (WLTP) described in UNECE Regulation GTR 15 and mandated in EU legislation, thus replacing the NEDC cycle which had been in use in the EU since 2000. A comparison of emissions standards in the EU, USA, China, Japan, and India was presented. Global trends in reducing emissions from vehicles using the example of the European Union, Japan, USA, China and India were also discussed, as well as the main features of new EU emission standards developed by the GRPE (UNECE) and RDE groups, which were introduced into the EU approval requirements as the emission level Euro 6d – TEMP from 1st September 2017, through Commission Regulations (EU) 2017/1151 and 2017/1154.

Les Hill (Horiba, UK) presented trends on reducing emissions on a global scale as well as their impact on measurement procedures and the requirements for test equipment and test methods. The US has introduced EPA Tier 3 and CARB LEV-III (in California) requirements, as well as regulations on GHG emissions, with procedures defined in CFR part 1065 and part 1066, which are still being continually updated.

Japan plans to introduce testing methods based on the WLTP procedure (3-phase test, without driving speeds > 100 km/h) and RDE tests for vehicles with CI engines. China and India likewise plan to introduce similar standards as in the EU, based on WLTP tests and methodology, and also RDE in the future. Thus, the precedent for RDE testing to expand from its point of origin (the EU) to other legal jurisdictions over the next few years appears clear; particularly significant are the plans for introduction of rigorous RDE requirements by the large (and growing) markets of China and India. The formation of a new UNECE Informal Working Group for Global RDE reflects this situation [21].

The second presentation on this subject was delivered by Dr. Piotr Bielaczyc (BOSMAL, Poland), who presented the most important technical, political and economic factors that currently affect the development of global road transport and propulsion system used, and current "hot topics" in powertrain development. Dr. Bielaczyc's presentation also highlighted the impact of new emission testing methods on the development of automotive engine structures and future trends in vehicular powertrains [22, 23]. His presentation examined the current situation regarding regulation of exhaust emissions and the impact on powertrains used in new vehicles across the world. Powertrain technologies which can help to overcome challenges are mentioned and key trends were analysed. Despite Diesel engines' loss of reputation according to some commentators, manufacturers of these engines have already implemented solutions based on SCR catalytic systems, together with existing filtration technology, which can ensure that this engine type has very low emissions of both PM/PN and NO_x. A new trend in engine design is "rightsizing", as well as an ongoing convergence of spark ignition and compression ignition engine technology, with differences now much smaller than in the past (turbocharging, direct injection, compression ratio) – see Fig. 1. Fundamental changes to the propulsion strategy for on-road vehicles, most notably (but not exclusively) hybrids of various types, and the development of fully electric vehicles (BEV) or fuel cell-powered vehicles represent a revolution in the industry, occurring in the context of the aforementioned effects. As development requirements are more complex than in the past and the test volume is also much higher, the challenges posed in developing, testing, approving and certifying such advanced solutions is considerable [24].

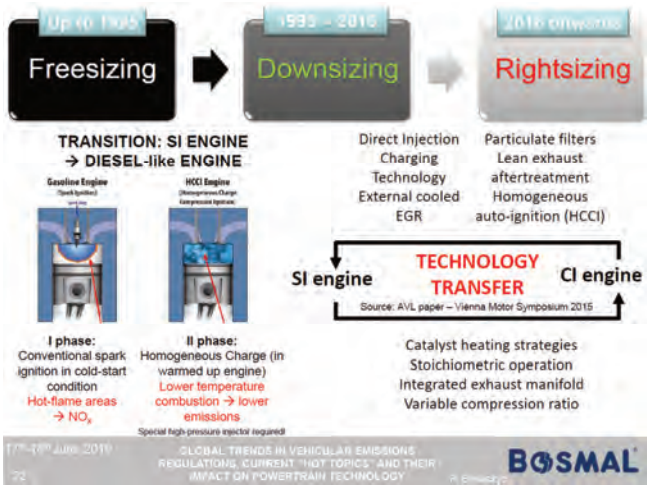

Fig. 1. Overview of engine technology trends, including the ongoing gradual convergence of SI and CI engines [24]

In the first session, which was devoted to the global regulations and methods of emission testing in the context of combustion engines, further reports were presented by Dr. Victor Valverde-Morales (European Commission, JRC) who presented the issues of air protection against pollution from automotive sources in the European Union (EU Clean air policy) and the latest data on the implementation of WLTP and RDE regulations in the European Union as tools to meet those aims, as well as market surveillance of the vehicle fleet from 2020. Recent activities on light-duty vehicles' pollutant emissions in the EU are the following:

– Amended Emissions Legislation at EU level.

- New/revised emission testing procedures: Worldwide harmonized Light vehicles Test Procedures (WLTP), Real Driving Emissions (RDE) regulation.
- In-Service Conformity (ISC) provisions.
- New type approval and market surveillance regulation adopted in 2018, in force from 2020.

Subsequent changes in research procedures will result in the fourth RDE package, which will also introduce tests of cars in use, to be performed by independent accredited laboratories as well as vehicle manufacturers. The analysis of the next emission regulations, described as 'post-Euro 6' – and even 'Euro 7' – has begun, which are to bring the same test methods and limits for all types of engines and fuels (a philosophy known as 'fuel-neutral' or 'technology-neutral', which has already been in place in the USA for many years) [25].

The last presentation in this session was delivered by Dr. Ameya Joshi (Corning Inc., USA), who spoke about the methods for limiting engine emissions from LDV and HDV through catalytic systems, also for hybrid powertrains in which the TWC and other catalytic reactors may undergo cooling when the combustion engine is not running. He also talked about the possibilities of increasing the efficiency of engines used in road transport. Thermal efficiency of 45% has already been achieved for SI engines, but further development in this field is still possible (see Fig. 2) – currently a level of 55% for the CI engines used in HD applications is being worked on. A significant part of his presentation was devoted to catalytic aftertreatment (SCR, SCRF, PNA, methane oxidation catalysts) as well as multi-component systems consisting of catalytic reactors and filters, which can allow engines to meet legal emissions requirements under a wide range of operating conditions [26]. The main conclusions from his presentations are the following.

Key summary points regarding light-duty vehicles:

- Europe has set the tightest CO_2 standards: 37.5% reduction by 2030, along with electrification mandates.
- There is still significant untapped potential for ICE technologies. Much more efficiency improvements to come. Synergistic gains with hybridization lie ahead (see Fig. 2).

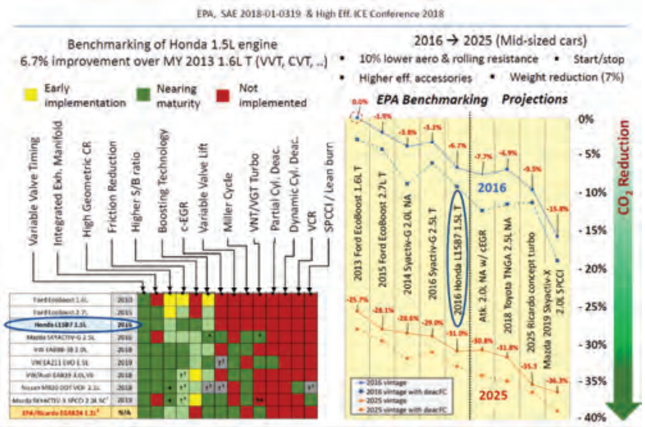

Fig. 2. Engine technology options for increased efficiency and reduced emissions [27]

- Both gasoline & diesels can comfortably meet Euro 6 norms. The path to NO_x at a level of < 10 mg/km has been shown for diesels.
- Gasoline particulate filters are being deployed in the EU/China. PFI and hybrids may also require GPFs.
- Addressing cold start emissions is critical to meet the US SULEV30 standard. TWCs continue to improve, but may require addition of HC traps.

Key summary points regarding heavy-duty vehicles:

- California is leading the development of an omnibus rule for lower in-use NO_x emissions. Various studies on evaluation technology options reviewed.
- Europe has established its first-ever HD CO_2 standards: 30% reduction required by 2030, compared to 2019.
- Super Truck II program (participants: Volvo, Navistar, Cummins, Daimler) is promising impressive gains in fuel efficiency – leading concepts were reviewed.
- Several filter-enforcing regulations in place: China VI, BS VI, non-road Tier 4, Brazil PROCONVE P8 [27].

3.2. 2nd session – Powertrain technology development – light-duty

Prof. Jerzy Merkisz from Poznan University of Technology (Poland) commenced the second session on light-duty powertrain developments with a broad yet detailed overview of the subject. To meet the goal of reducing tailpipe CO_2 by 90% by 2050, it was projected that post-2020, powertrain developments will focus heavily on electrification (hybrids to pure battery electric vehicles), as shown in Fig. 3.

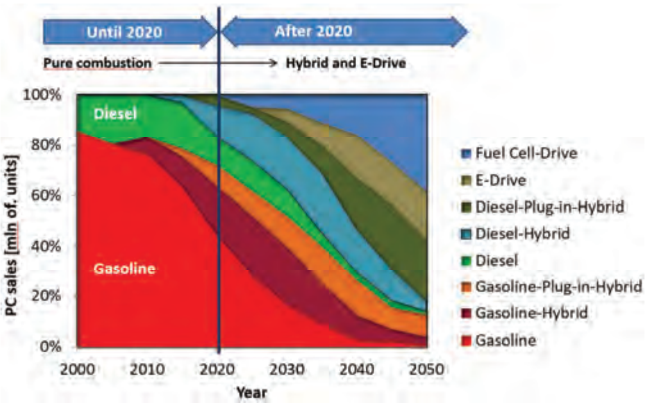

Fig. 3. Market share of various powertrains projected to 2050 [28]

However, it was cautioned that for a realistic assessment of the benefits of electrification, it is imperative for well-to-wheel emissions to be included, which can increase the tank-to-wheel emissions by as much as 30%. ICE developments will continue, and several promising technologies were reviewed. Engine downsizing is approaching its limit, and now emphasis is turning to "rightsizing" to balance efficiency and performance requirements. Recently developed advanced engine technologies are expected to proliferate, including variable compression ratio (VCR), water injection and spark assisted charge compression ignition for gasoline engines. The increased use of mild hybridization, turbocharging, exhaust gas recirculation (EGR) and optimized aftertreatment systems including filters is a common theme for both gasoline and diesel. Several new engines have been announced by major OEMs recently aimed at meeting Euro 6d emission legislation, improved fuel economy, while also meeting the core customer requirements of improved power and dynamic handling. Diesels continue to improve (i.e. lower) tailpipe NO_x emissions using SCR-coated filters, although meeting future requirements will require further reduction of cold start emissions via the addition of close-coupled lean NO_x traps, passive NO_x adsorbers or electrically heated catalysts [28].

Dr. Hubert Friedl (AVL List, Austria) highlighted various technologies which need to be developed and adopted to approach near-zero emission levels. A few examples include particulate filters for all vehicles, NO_x storage catalysts, passive SCR, electrically heated catalysts, predictive control strategies and electric drive-off. Improving battery technology is projected to reduce the cost differential between pure electric and conventional ICE powertrains by > 60% in the 2020-2025 timeframe, as shown in Fig. 4.

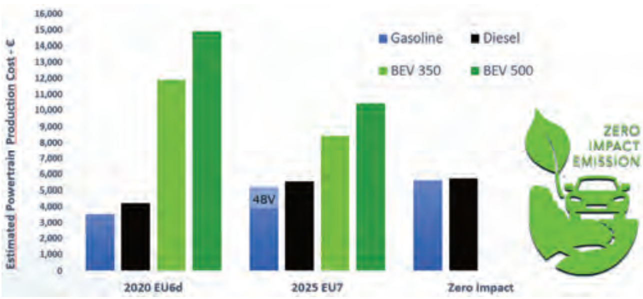

Fig. 4. Estimated production costs (in Euros) for gasoline, diesel and battery electric powertrains [29]

Nevertheless, ICEs and hybrids are expected to dominate, with 48 V mild hybrids projected to gain up to 68% market share in Europe by 2030. Brake thermal efficiencies up to 50% are now within sight, relying on various advanced gasoline technologies such as very high pressure (> 1000 bar) injection, pre-chamber ignition, VCR, ultra-lean (λ > 2) combustion and waste heat recovery, as outlined in Fig. 5 [29].

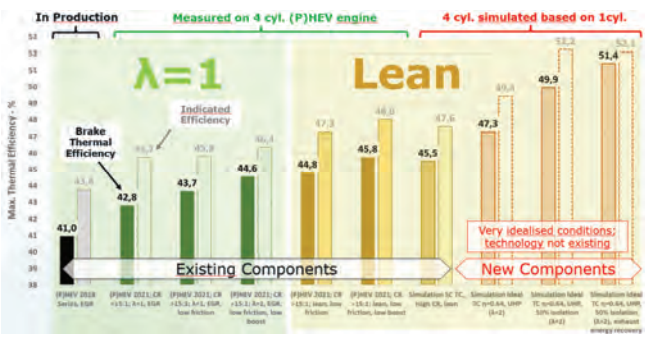

Fig. 5. Efficiency projections of a hybrid 4-cyliner engine using existing and future technologies [29]

Emissions legislation in Europe have undergone a fundamental shift since the introduction of the real-world driving emission (RDE) testing. In the presentation by Dr. Friedl and in another presentation by fellow AVL employee Kurt Engeljehringer, it was pointed out that the requirement for RDE and lower temperature (–7°C) testing has resulted (or will soon result) in > 7-fold increase in the testing time for certification, compared to pre-Euro 6 standards. Further tightening is widely expected with post Euro 6 regulations, including increasing the weighting for cold start and urban driving via shortening the urban portion of the RDE test. The utility of bringing road testing as required by RDE "back to the lab" was highlighted as a way to enhance reproducibility, perform detailed tests not possible on the road, and better analyse the influence of various parameters [30].

Steve Whelan (Horiba-Mira, UK) expanded on this idea, by discussing their work done on an integrated "RDE+ Road to rig approach" for powertrain testing and development. One gasoline and two diesel vehicles were tested over four RDE routes characterized by varying driving dynamics, and temperature and altitude boundary conditions. As expected, the CO_2 and NO_x emissions were sensitive to these conditions, although the testing showed some non-intuitive results such as higher NO_x emissions with gentler driving, hypothesized due to catalyst light-out under these conditions. The route was next replicated on a chassis dynamometer using the gasoline vehicle. A very good correlation for RDE and chassis testing was achieved for all criteria pollutant and CO_2 emissions (all within 10%) [31]. This early work promises to deliver expedited development and evaluation of the impact of various real-world driving scenarios in a lab environment at a faster pace [32].

While significant improvements are being made to lowering criteria pollutants and meeting the post Euro 6 regulations, there are unique challenges that still need to be addressed. A decrease in engine-out NO_x can lead to an increase in soot emissions due to the soot-NO_x trade-off. Marcos Alonso Baez (Nissan Technical Centre, Spain) discussed the contamination of oil with such an increase in soot and its root cause. CFD modelling was used to predict the combustion, the associated emissions of soot, and its transport from the hot combustion gas to the cold cylinder walls due to thermophoretic force. Higher soot in oil were found with increased EGR and lower injection pressures, while retarding start of injection was found to lower the soot amount. Broadly, good correlation was found between predicted trends and measured values for soot in oil, although there is room for improvement in absolute soot quantity estimations [33].

As mentioned in the opening presentation of this session, 48 V mild hybrids are expected to gain a significant market share in the coming years. Dr. Luciano Rolando (Politecnico di Torino, Italy) and discussed the potential of electric supercharging (eSC) for performance and fuel efficiency improvements of gasoline engines, when coupled with mild hybridization and Miller cycle combustion. Simulations were done for a SUV with 1.5 dm^3 turbocharged gasoline engine with a 48 V P0 architecture. The transient performance with the eSC was evaluated for accelerating from 80 to 120 km/h and 60 to 80 km/h. The eSC compensates for the engine turbo lag and improves elasticity time. While there is a small energy consumption penalty (equivalent to 2–3 gCO_2/km), when the described solution was combined with the Miller cycle, a net reduction of CO_2 by 6 g/km was obtained (via simulation) over the entire WLTC [34].

3.3 3rd session – Powertrain technology development – heavy-duty

This session mirrored the previous session, but with a specific focus on heavy-duty and NRMM.

Dr. Adolfo Perujo (EC JRC, Italy) spoke about field testing of various vehicles and pieces of machinery in the context of demonstration of compliance with EU emissions legislation. In the EU, emissions from light-duty, heavy-duty and NRMM applications (the latter not consisting of vehicles) have a long history of regulation. Changes are underway in emissions legislation for all three groups, with a strong trend towards lower limits and stricter demonstrations of compliance. On-road heavy-duty and NRMM share certain similarities, but also fundamentally different in some respects and are this dealt with in separate legislation. The European Commission's Energy, Transport & Climate directorate has been working on the steps necessary to update, expand and strengthen the aforementioned legislation. NRMM is a very broad category, with applications featuring combustion engines of power ranging from less than 10 kW to approaching 1 MW (i.e. a variation by a factor approaching 100); see Fig. 6. Applications may or may not be self-propelled (saws, cement mixers, etc. being essentially stationary; excavators, trains, boats and snowmobiles self-evidently being fully mobile). Overall, the EU strives for alignment with US EPA standards, but some PM standards are more demanding and PN represents a much more demanding requirement (no US emissions legislation currently requires any kind of particle number measurement). Furthermore, alignment with EU on-road emissions limits is also a goal for NRMM legislation. An example of such alignment is introduction of PN limits for NRMM in legislation passed in 2016. For the time being, limits are determined by engine type (compression/spark ignition) and fuel-neutral limits for NRMM seem a distant prospect. As regards in-use emissions, requirements for NRMM have been built upon the requirements for on-road heavy-duty ISC – legislation passed in 2016 requires in service monitoring (ISM) for emissions from NRMM engines when mounted in target applications tested under normal conditions of use. For NRMM, "normal conditions of use" is a broad and therefore challenging set of circumstances and conditions. Differences in usage patterns (for example, extended idling for NRMM) means that the mandatory PEMS-based emissions monitoring methods are not identical for HD and NRMM [35].

Turning to pollutant formation within the context of detailed investigations into combustion, Dr. Yuzo Aoyagi (Okayama University/New A.C.E. Institute Co. Ltd., Japan) spoke about how investigations into combustion and pollutant formation must present more information than only concentrations of pollutants in the exhaust gas. Fortunately, some well-established methods are available which provide a great deal of information on combustion and pollution formation phenomena. By combining the powerful two-colour method with further optical measurements, insight can be gained into one of the fundamental disadvantages of the Diesel engine: the PM-NO_x trade-off [36]. Aftertreatment notwithstanding, there is pressure to reduce engine-out concentrations of these pollutants, but the difficulty of optimising such a classic trade-off relationship is well known. High-resolution insights into soot formation and in-cylinder destruction and spatial distribution, as well as the thermal evolution of the mixture can provide information on the root causes of formation of these pollutants and evaluate efforts to mitigate formation (including, but by no means limited to, the use of EGR and the impact of varying fuel injection parameters) [37].

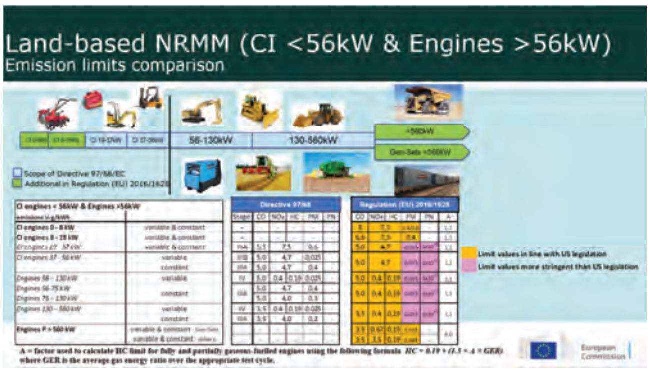

Fig. 6. Outline of the legislative structure for setting emissions control for land-based NRMM, with emissions limits [35]

Prof. Kohei Nakashima (Meijo University, Japan) reported on a concrete aspect of efforts to reduce fuel consumption. Work to reduce fuel consumption has focused on many areas on the powertrain system, as well as the wider vehicle. So-called "mileage competitions", in which teams compete to obtain the best fuel economy results, are examples of situations in which both vehicle and engine parameters are optimised to produce very low fuel consumption (and thus high mileage). However, certain physical boundaries represent challenges which are hard to overcome. One such limitation is the inherent internal friction in a reciprocating engine. Indeed, the piston assembly is the greatest single contributor to internal engine friction. Since the points of contact between the piston assembly and the cylinder liner (i.e. the piston rings) are the sources of this friction, friction reduction studies often replace three-ring piston assemblies with two-ring (or even one-ring) versions, yet data is lacking on the exact frictional impact of such a substitution. Experimental apparatus developed to measure the resistive forces in the piston assembly was used to investigate various piston ring assemblies (with one, two or three rings) at engine speeds ranging from 800 to 1600 rpm and three different oil temperatures – the results of one such measurement are shown in Fig. 7. Significantly, measured piston assembly friction was angle-resolved for full rotation of the crank. Overall, the results indicated that the single-ring assembly caused the lowest friction at all oil temperatures where engine speed was ≤ 1200 rpm; whereas at higher temperature (80°C) and engine speeds ≥ 1400 rpm, friction was lowest with a two-ring assembly (with the top and oil ring installed). Thus, there was no configuration which gave the lowest friction at all engine speeds and all temperatures, highlighting the complexity of the task of reducing fuel consumption via reductions in engine friction [38].

As well as changes to vehicle and engine parameters, a promising direction for emissions reduction (including reduced CO_2) is the use of natural gas as a fuel, as highlighted by Dr. Stefano Golini (CNH Industrial, Italy) in his presentation. FPT Industrial has a long history of offering CNG versions of its heavy-duty powertrains designed for

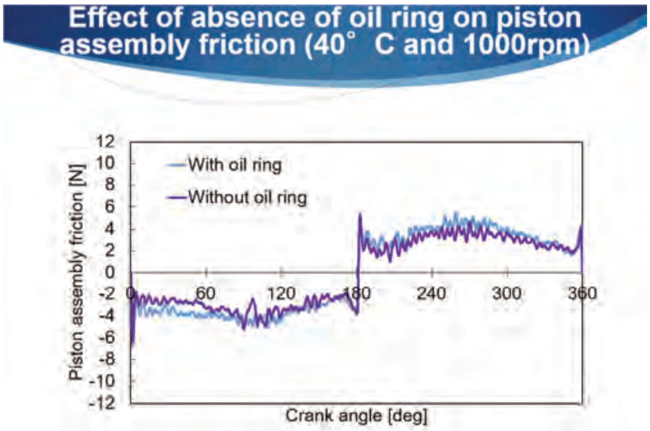

Fig. 7. Crank-angle resolved piston assembly friction for two different piston configurations under low-speed steady state operating conditions [38]

on-road use. CNG is an attractive fuel for a range of reasons, including its low carbon content and soot-free combustion. Furthermore, natural gas (or biomethane) can be obtained from a range of sources, including renewable sources and as such, the potential for GHG emissions reductions can be very high. Heavy-duty vehicles running on CNG have been in use for around 20 years and generally speaking modern CNG-powered engines have comparable performance and durability to their Diesel-powered counterparts. The low energy density of CNG is an inherent disadvantage, but the CNG distribution network is more extensive than often thought and continues to expand. Vehicle size and weight are the main determinants of the most appropriate energy source (fuel type), as shown in Fig. 8.

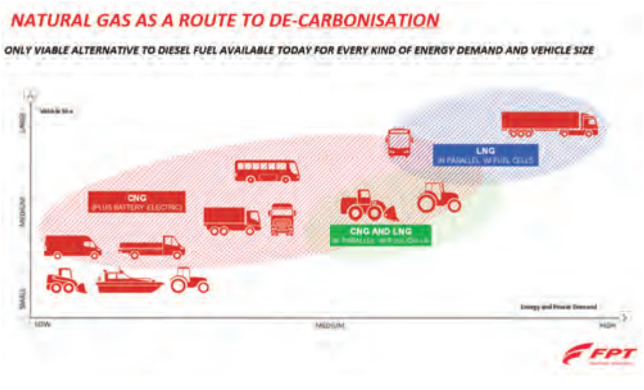

Fig. 8. Schematic of the relationship between vehicle size, energy demand and broad categories of most appropriate fuel type [39]

For large and heavy applications with high energy demand, it is normally more appropriate to store natural gas onboard in the liquid form (LNG). Both CNG and LNG can be used in concert with other technologies for emissions reduction such as fuel cells and externally chargeable hybrid powertrains. Modern HD NG engines offered by FPT achieve Diesel-like performance and high efficiency thanks to several innovative features, including direct injection of natural gas, a specially designed piston and intake system and variable valve timing. Efficiency with these innovations was found to increase by 4% compared to the previous generation – and at some operating points, thermal efficiency exceeded 40%. In light of these encouraging results, CNG appears to be a viable tool to facilitate ongoing efforts to reduce harmful emissions and GHG emissions from the HD sector. Restrictions or outright bans on Diesel-powered vehicles in some areas (for example: in city centres, port areas or national parks) may make NG-powered vehicles an especially attractive option in some contexts [39].

NRMM As mentioned previously, many industry segments share certain challenges in terms of emissions control; nevertheless, there are sector-specific challenges and limitations. This was explained during the presentation focussing on the sector delivered by Dr. Toni Kinnunen (Proventia, Finland). NRMM is (or will soon be) subject to stricter emissions limits – for example, Stage 5 limits in the EU. There is now also a focus on achieving low real-world emissions from NRMM; the EU is introducing in-service monitoring (ISM) making use of PEMS measurements. An essential tool in efforts to reduce emissions (in general – and especially to comply with the aforementioned legislation) from such applications is appropriate aftertreatment. NRMM applications are dominated by compression ignition engines (although spark ignition engines are sometimes used) and as such have certain traits in common with on-road heavy-duty applications. However, there are a number of constraints, difficulties and challenges which are specific to NRMM. These constraints are, for the most part, relate to fundamental design parameters of such applications (length, engine location) and the needs for machinery to move and operate in highly demanding environments (aftertreatment cannot be exposed in vulnerable locations, for example: underneath the chassis). Such constraints, difficulties and specific challenges are summarised in Fig. 9.

Fig. 9. Key technical factors determining design of exhaust aftertreatment systems in the NRMM sector [40]

In order to achieve truly low emissions under real-world operating conditions, compression ignition engines fitted to NRMM require an integrated DOC + SCR system (sometimes with a DPF), with all relevant mechanical and thermal conditions considered in the design process. As is well known, SCR requires space for the UWS to mix and react and this is very challenging where the layout precludes the installation of extended sections of straight tubing. UWS wall wetting and urea deposit formation are challenges that result from this constraint. The relatively low exhaust gas temperatures and extended periods of idling experienced by NRMM mean that thermal management is an important issue. Testing has revealed that NRMM aftertreatment systems are ideal candidates for thermal coatings, which can reduce heat losses by up to 67% compared to an uncoated system, thereby increasing the efficiency of the SCR and reducing the need for fuel-consuming warm-up strategies. The high amplitude vibrations encountered in off-road environments (up to 100 times higher than for road vehicles) must also be considered in the design process – this fundamental difference is one of the many reasons why bespoke solutions are required [40].

For low fuel/energy consumption and low exhaust emissions under real-world conditions, a huge number of factors must be considered, including – but also extending well beyond – the performance of the internal combustion engine itself. Dr. Joachim Deppe of LaVision (Germany) explained the nature of these challenges and how they can be approached in his wide-ranging presentation. The ability of systems to work in tandem with the powertrain from the chemical and physical points of view is an aspect which must be given careful consideration. More holistically, a number of components which are not part of the engine system must be carefully considered in the context of ongoing efforts to reduce vehicle mass, rolling resistance, aerodynamic resistance, etc. – potentially including myriad components, from bearings to tyres to window glass. These materials' optimisation challenges must be informed by quantitative data, with a range of tools used to quantify parameters such as deformation under load, thermal resistance, chemical durability, onset of deformation, etc. Many such measurements have something in common with optical analysis of the combustion process: namely, that the measurement/image gathering process is often relatively simple – powerful, accurate and insightful post-processing of the measurement and images gathered is the key to maximising the utility of such measurements. Indeed, as shown in Fig. 10, using what might appear to be rather trivial "photographs" of an element under testing (or a combustion cycle within a cylinder), a number of parameters can be derived via digital post-processing software, such as calculation of temperature, heat flow, strain propagation, flame speed, etc – and even the derivation of the concentration of pollutants (e.g. soot, via two-colour pyrometry) [41].

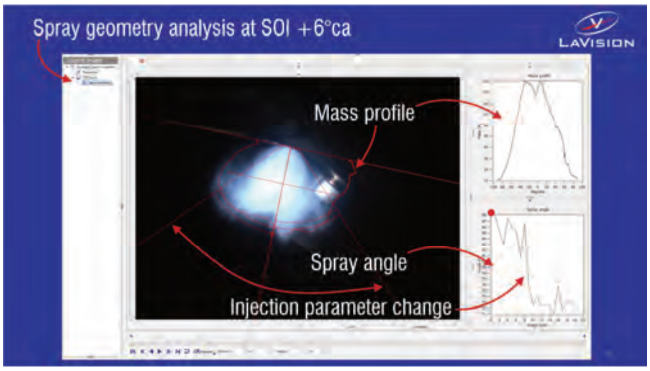

Fig. 10. Computer processing of an image to extract quantitative data on the physicochemical processes captured in the photograph [41]

3.4. 4th session – Fuel development and its impact on engine technology

Dr. Christopher Kolodziej (Argonne National Laboratory, USA) gave a presentation on the well-known (but not always widely understood) subject of knock resistance characteristics of liquid fuels. One of the main parameters determining whether a fuel is suitable for use in SI engines is its octane number, necessarily determined according to a standardised method. This parameter is used to define and compare fuels – and to control the quality of fuels sold for public use. The actual knock resistance of a given fuel depends on many factors, not least of which is the test method used – hence the well-known RON-MON difference, with this difference commonly termed *sensitivity*. A significant consideration is the fact that the knock resistance varies with λ and – significantly – fuels are not RON tested at lambda 1 (i.e. stoichiometric conditions), at least not according to standard procedures. Furthermore, there are significant differences between RON method and modern SI engines. A range of experimental work was undertaken to characterize the difference between two knock intensity measurement methods and to identify the effect of λ on a fuel's octane rating behaviour. A range of fuels were investigated, which showed variable, λ-specific behaviour, as shown in Fig. 11; for example, ethanol strongly reduced the maximum amplitude of pressure oscillations under rich conditions. There are certain contradictors trends and trade-offs. Because of this complex behaviour, use of alternative procedure more reflective of the characteristics and typical operation conditions of modern engines provide a more useful and complete picture of the real knocking tendency (and knock resistance) of a given fuel or fuel blend [42].

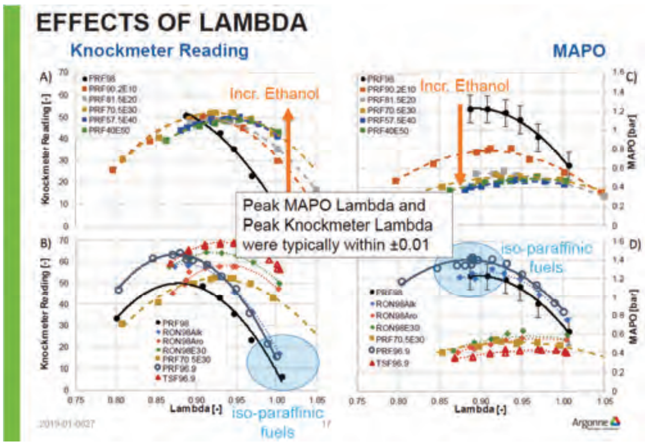

Fig. 11. Knock characterisation of a range of fuels for a range of lambda values [42]

Dr. Tadeu Cordeiro de Melo (Petrobras, Brazil) gave a presentation on the subject of renewable fuels for diesel engines. Motivated by sustainability concerns, increasing attention has been paid to renewable fuels. Biocomponents for use in compression ignition engines are known as biodiesel, which are in widespread use in many markets. The proportion of biodiesel in blends approved for sale in brazil is high compared to other markets – but there are plans to possibly move to even higher levels (15% biodiesel). In light of this, quantifying the impact of such levels of biocomponents on exhaust emissions is a priority. Testing was carried out to quantify the emissions impact of using such blends on several engines, with the test blends containing soy- and tallow-based biocomponents. The overall literature consensus was confirmed by this work – generally speaking, there were modest reductions in particulate emissions (although levels were sometimes unchanged); NO_x generally increased somewhat (although levels were unchanged in one case). These findings have obvious implications for the exhaust aftertreatment of such engines running on such blends, and therefore further work on that subject is recommended [43].

Dr. Cecile Pera (at the time an employee of Convergent Science, Austria) spoke about computational fluid dynamics (CFD) and the role it plays in research on combustion engines and closely related topics. Combustion systems in general, and especially modern vehicular powertrains, are characterised by a large number of variables and parameters. Continuing development towards higher efficiency, reduced pollutant formation, extended durability, etc requires quantitative investigation of the impact of varying these parameters. In the case of vehicular powertrains, fuel, lubricant and aftertreatment systems must be included in the overall system-level optimization effort. The sheer number of parameters to be investigated, as well as the fact that much of the low-hanging fruit has already been plucked, has vastly increased the scale and overall complexity of such optimization tasks and computational fluid dynamics (CFD) is an essential tool in this area. CFD is of high utility in tackling essentially all of the challenges currently faced by ICE, and can do so in an interconnected and holistic fashion. Modelling of relevant phenomena often involves consideration of the interactions between matter in three different states, requiring complex physical models of appropriate resolution. Recent advances mean that pollutant formation can be modelled with high accuracy; aftertreatment system functionality may also be modelled, for which parametrised chemical models must obviously be included in order to accurate predict system-level behaviour. High-fidelity simulations are not restricted to modelling the transfer of matter (i.e. mass) – the flow of heat and other quantities such as the frictional forces resulting from reciprocal motion can also be computed. CFD lends itself to investigation of disruptive technologies for use in multiple sectors and to work on new (or revisited) concepts for engine hardware, as well as modified fuels and engine-fuel combinations [44].

Dr. Hu Li (University of Leeds, UK) gave a presentation on biofuel options for Diesel engines and their impact on emissions. The desire to improve the life-cycle performance of fuels used in road transport, as well as general sustainability concerns and an overall drive to reduce pollutant emissions, has led to demand for drop-in biofuels which can be blended into fossil diesel in varying proportions. Fatty acid methyl esters (FAME) have been very well-studied in this context; a newer research direction concerns the use of GTL (Gas to Liquid) and HVO (Hydrotreated Vegetable Oil). Both those fuel types show promise as fuels with good performance in terms of overall carbon intensity and pollutant formation during combustion. Differences in the physiochemical properties of GTL and HVO cause significant differences for various phenomena in terms of the combustion process (e.g. ignition delay, in-cylinder pressure) and thereby cause differences in pollutant formation – it is especially important to identify optimal blend levels, since trends are not always linear with respect to increasing blend content and so-called "bounce-back" effects have been identified. Furthermore, for engines used in applications characterised by transient operation, such as road transport, it is vital to investigate performance over a wide range of operating conditions. Such investigations have revealed GTL and HVO to be advantageous from many points of view, including the reduced formation of NO_x and PN observed with those fuel types [45].

Yuri Kroyan (Aalto University, Finland) gave a presentation covering recent efforts to model the effect of fuel properties on end-use engine performance. As was also noted by other presenters, the implementation of renewable fuels for transportation is becoming a very important step in the reduction of the sector's carbon footprint. The effective solution for GHGs reduction is the substitution of fossil fuels used in the current fleet by fuels produced from renewable sources such as biofuels. Work has been conducted to investigate how alternative fuel properties affect engine performance and greenhouse gases (GHG) emissions of the current fleet of light-duty vehicles. Based on the experimental results, data-driven black-box modelling has been applied to develop two models, one for spark-ignition (SI) and the second for compression-ignition (CI) unmodified engines. The multiple independent variables of the models (inputs) are represented by fuel properties, whereas single dependent variable (output) stands for fuel consumption (FC) over driving cycles such as Worldwide harmonized Light-duty Test Cycle (WLTC) or New European Driving Cycle (NEDC). Both input and outputs are described by percentage changes relative to the standard fossil-based fuel, gasoline for SI and diesel for CI engines. The chosen modelling methodology is based on multilinear regression. Additionally, quantitative analysis was performed in order to achieve the final state of inputs, significance level below 5%. In both cases, coefficients of determination (R-squared) turned out to be relatively high for the SI case: 0.99; and 0.97 for the CI case. The model for SI engines represents how fuel consumption is affected by the research octane number (RON), density, net calorific value volume based (NCV vol.) and oxygen content based (O_2). Whereas the model for the CI part reveals density, cetane number (CN) and net calorific value mass based (NCV mass) impact on FC. Developed models represent the end-use performance of alternative fuels and are dedicated to supporting decision-makers and accelerating the commercialization of transport biofuels [46].

3.5. 5th session – Testing requirements/methodologies – impact on powertrain development

David Miller (3DATX, USA) gave a wide-ranging presentation on how portable emissions measurement systems can meet the industry's needs regarding development of powertrains for various applications. The key engine development trend at the time of writing and in recent years is the simultaneous reduction of both fuel consumption and regulated emissions. Both those aspects (FC/emissions) have been subject to revelations and concerns that much of the progress has been only on paper, rather than delivering real benefits under actual conditions of use. While fuel consumption automatically measured by all modern vehicles and instantaneous and accrued information available to the driver, emissions of regulated pollutants under in the real world under normal operating conditions were not known until the advent of PEMS. As such, based on the fact that a PEMS is much smaller, cheaper and easier to obtain than a full emissions laboratory with chassis dynamometer, PEMS represents an opening up of the field, as it allows parties who otherwise would not have been able to perform emissions testing to perform tests under real-world conditions (normal or non-normal). PEMS is required for legislative purposes (HD ISC in the EU, HD ISC in the EU, LD type approval and market surveillance in the EU), but may also be used by a range of parties for a wide range of purposes and test types. The very wide range of applications equipped with ICEs is starting to cause the PEMS market to deliver specialised devices – in many situations, a full legislation-compliant PEMS is simply not necessary. In the same way that computers have reduced their size and weight by orders of magnitude while increasing computing power, PEMS designs are evolving – the term 'portable' can be subject to many interpretations, but some systems can be safely lifted by one person and even transported in an aircraft as hand-baggage. Making use of such downsized, simplified systems has obvious financial benefits, but can also increase the availability of required data and thereby reduce the so-called "PEMS bottleneck" (which particularly affects the LD sector, but is also present in other sectors). Four categories of PEMS equipment can be defined, ranging from fully legislative to high downsized nano-PEMS, each with specific advantages in certain contexts, as shown in Fig. 12. A key difference between the USA and EU is that the former has no defined specification for LD PEMS. Unsurprisingly, simplified systems of lower cost have to trade-off some accuracy, but if the correlation to official measurements is well-known and closely constrained, then the post-processed data generated by such devices can be acceptable for most purposes [47].

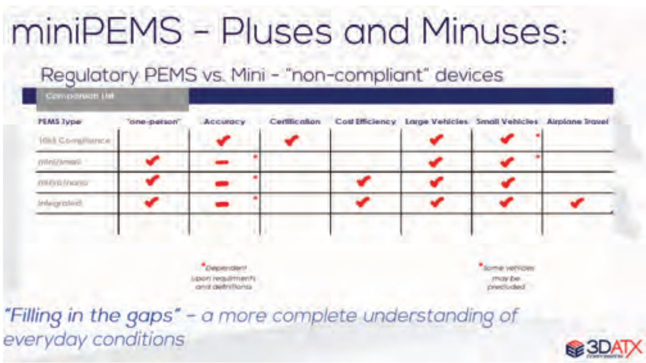

Fig. 12. Matrix of suitability and applicability of different types of PEMS for testing emissions from combustion engines under real operating conditions [47]

Dr. Xin Wang (Beijing Institute of Technology, China) gave a presentation on RDE requirements in China. While RDE is the term used in the EU, PEMS testing traces its origins to the USA. Recently, a number of Asian countries have announced their intention to introduce RDE-like testing. One such country is China, a highly populous and rapidly developing country facing well-known air quality challenges. Chinese RDE is inspired by – and largely based on – the EU RDE procedure, but features some important differences. Firstly, the conformity factors are numerically higher than the values currently mandated in in the EU, taking values of 2.1 for NO_x and PN (for the time being). As a related point, it should be noted that the base emissions limits for China 6 are fuel-neutral, with no Diesel NO_x "allowance". Secondly, the moving average window method is used for the final calculation of emissions results (while EU legislation has dropped this requirement). Finally, Chinese topography mean that large numbers of vehicles are operated at high altitudes – and so China has an additional category of boundary condition called "Further extended altitude condition" for altitudes between 1300 and 2400 m above sea level. This last point represents a significantly more demanding aspect of Chinese RDE legislation compared to EU RDE legislation. The emissions excess allowed in this category is relatively large (the correction factor by which results are divided is 1.8). The fact that more than 25% of Chinese territory (and thus a large number of major roads) lie at altitudes > 1000 m and that, in contrast, there are few major roads in Europe at altitudes > 1300 m explains this divergence from the EU RDE legislation. Emissions control at elevated altitudes is sometimes (but not necessarily always) challenging; however, at present limited data are available as the vast majority of powertrain research is conducted at low altitudes. A variety of effects can complicate engine operation and worsen emissions at high altitude, but these may not always translate into increased exhaust emissions if the efficiency of the aftertreatment system remains high, as shown in Fig. 13. The requirement to meet emissions limits over such a wide altitude range (relatively wide in the case of the EU; very wide in the case of China) complicates development and pre-certification testing [48].

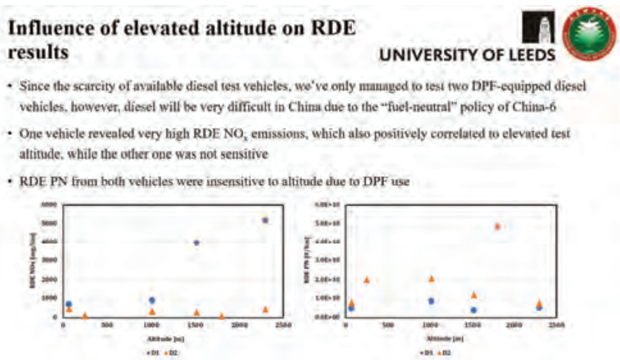

Fig. 13. Exhaust emissions of NO_x and PN obtained under Chinese RDE conditions (included extended altitude) [48]

Daisy Thomas (University of Leeds, UK) reported on her work on particulate emissions from modern powertrains (in the form of RDE testing of a hybrid passenger car). Hybrid powertrains continue to attract significant interest and represent a growing market share of new vehicles, not only in the context of reducing fuel consumption and CO_2 emissions, but also due to their potential to reduce exhaust emissions of regulated (and unregulated) harmful compounds. The vast majority of hybrid powertrains feature a spark ignition engine as their combustion engine component. In such a configuration, the spark ignition may start frequently and run for short periods of time, with impacts on exhaust emissions. Particulate from SI engine with indirect injection have traditionally been judged to be low and virtually ignored (current EU legislation does not require PM or PN measurements for such engines, whether part of a hybrid powertrain or not). SI engines with indirect injection produce particulate of relatively low number and very small size, making gravimetric emissions extremely low. However, the particle number emissions are measurable and in the special case of hybrid powertrains, the question arises as to what the impact of repeated starts and interrupted engine warmup has on PN emissions from vehicles fitted with such powertrains under real driving conditions. Similar vehicles featuring SI engines with direct injection are subject to PM and PN limits in the EU, with PN assessed during real driving conditions via RDE tests. A series of tests was carried out under normal driving conditions (RDE-compliant) using PEMS to measure PN and gaseous emissions. Both vehicles showed significant peaks resulting from the engine on events which occurred during the cycle; despite the fact that the combustion engine was off for a significant portion of the test, the final PN results were judged to be higher than for similar vehicles with conventional powertrains under the same driving conditions. Every engine start, even for a warm/hot engine, caused a spike in PN emissions, although the size of the particles (and therefore the hazard they pose to human health) changed significantly once the engine had warmed up, as shown in Fig. 14. The ambient temperature, hybrid battery state of charge and powertrain control strategy all have a significant impact on the PN results [49].

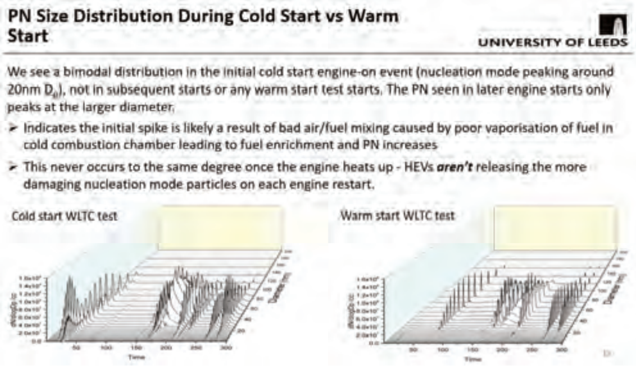

Fig. 14. Time-resolved PN size distribution profile for a hybrid vehicle running over the WLTP from cold and warm start conditions [49]

Maciej Jaskiernik (FEV, Poland/Germany) gave a presentation covering simulation of oil flow. The trend for reducing emissions and increasing fuel efficiency is not exclusive to the on road sector (LD/HD) – marine engines, inter alia, are also under pressure to achieve reductions. Changes made to engine hardware to achieve the required effects have increased parameters such as peak, pressure, BMEP, thermal load and mechanical load on bearings. In order to maintain reliability and durability, changes to engine hardware must be carefully considered and investigated. The vast number of parameters and very wide range of potential operating conditions means that the research effort involved in such investigations is immense. For that reason, simulation can be an attractive option, reducing the development cost and helping to meet tight deadlines. One area where such an approach has been adopted is in modelling the oil flow through the connecting rod to the piston cooling channels in medium speed engines. Self-evidently, such simulation is a complex CFD task. By making some simplifications and deriving equations to describe the motion in terms of translation, angular acceleration and rotation and adding CFD models to describe oil flow and sloshing, it is possible to examine the oil flow through the crank mechanism. Differences from preliminary calculations can be identified and attributed to various physical effects (including oil sloshing) [50].

The final presentation was unfortunately not delivered, due to the speaker's unforeseen inability to attend the Congress [51].

4. Summary and overall conclusions

Despite ongoing changes (for example, powertrain electrification and historically low fuel consumption in many new passenger cars) and the relatively low price of oil, there is continuing pressure to make a partial – or even perhaps full – switch to alternative fuels and low carbon or even carbon-free fuels [52]. The process of substituting mineral fuels with biofuels continues to make slow, uneven progress – recently, the USA allowed the sale of E15 (i.e. 15% ethanol content by volume) during the summer throughout the USA. In the EU, all Diesel sold contains biocomponents (83% of all Diesel sold containing FAME at concentrations $\leq$ 7%), 85% of all gasoline sold in the EU contained ethanol, but the vast majority of ethanol-bearing gasoline contained $\leq$ 5% ethanol and some 15% of all gasoline sold contained no ethanol at all. This means that the overwhelming majority of the fuel (and energy) used for propulsion of road vehicles is derived from crude oil. Currently, interest in HVO is very high, yet sales volumes remain vanishingly small compared to standard B7 diesel.

As the sine qua non of a combustion engine's operation is the combustion event itself, it is important to focus on combustion phenomena and their fundamental causes and practical implications when considering any aspect of the use of conventional vehicles. Even plug-in hybrids and range extended EVs are equipped with a combustion engine which is used for a non-negligible portion of the vehicle's lifetime [53, 54]; only battery electric vehicles (BEV) with no range extender are completely combustion-free during use [55–57]. Thus, research on combustion itself remains an essential and indispensable part of efforts to improve the environmental performance of vehicles, even (and arguably especially) in the age of powertrain electrification. While hybrid powertrains are normally mentioned first and foremost in the context of reduced fuel consumption/CO_2 emissions, they can also offer significant benefits in terms of reductions of pollutant emissions [49, 53]. Consideration of the above, together with general consumer demands, creates a highly demanding environment for engineering work of this type. The increase in the number of degrees of freedom resulting from powertrain hybridisation and adequate consideration of the long-term energy balance under realistic real-world conditions [53] significantly complicates development and optimisation processes. The market currently contains a wider variety of solutions and overall powertrain characteristics than is sometimes assumed (see [54] for a detailed review). This diversity of options, plus the vast scale of a modern electronic powertrain control strategy (calibration), mean that methods and strategies employed in the past are simply no longer viable in some cases. Even purely electric vehicles must also undergo a highly complex process during their development – here again, there is diversity in terms of powertrain characteristics and the market-available solutions of this type (see [57] for a detailed review and [3] for general information and [55] for information on the EU market). Regardless of powertrain type/configuration, in the era of big data, harvesting and processing relevant data, available at high resolution and on a massive scale, are key elements in the powertrain (and indeed vehicle) design and development process [4]. As the range of engine designs, sizes, operating conditions and even fuel types is large, numerical approaches taking advantage of the capabilities of modern computers have evident advantages in terms of the depth and resolution of data they can provide. However, a balanced approach has to be maintained: real-world scenarios (rather than idealised laboratory conditions) must be used as evaluation conditions to ensure that R&D advances translate into real benefits for society and the environment, while avoiding (or minimising) increased financial costs. For example, continuing efforts to increase the efficiency of conventional combustion engines have made great advances in recent years, yet the operating points at which these highest efficiency level is achieved does not necessary respond to a typical real-world-duty cycle for a passenger car. Indeed, the part load problem continues to be a significant disadvantage and the cause of significant excess fuel consumption, a problem which occurs on a very wide scale. While exhaust emissions at idle are low, pull away and acceleration events, as are inherent in heavy urban traffic continue to account for a very large share of total exhaust emissions. A range of engine redesign options (including, but not limited to, hybridisation) are attractive options to solve this problem [58]. However, the other side of the coin is infrastructure – the road itself and the flow traffic upon it. There appears to be considerable scope to make use of the abundance of electronics in modern vehicles, the ubiquity of the internet [4] and adaptive systems to optimise traffic flow and attempt to increase the mean travel speed, thus reducing journey time and thereby reducing emissions. For full hybrids – especially plug-in hybrids – there may be future requirements for geofencing, whereby the vehicle realises that it is in a designated low emissions zone and limits the use of the combustion engine accordingly. Such discussions extend well beyond powertrain engineering, yet could prove to be deciding factors in the near future regarding the design of automotive propulsion systems, for both light- and heavy-duty [59, 60].

A very wide range of objects, activities and areas of human endeavour are united by a shared factor: their reliance on combustion engines. In terms of debates on the environmental performance of such units, road transport usually comes to the fore, with a particular focus on passenger cars. While segments and applications can indeed be examined individually, there can be a surprising amount of cross-over and transferability between segments. The use of CNG as fuel has perhaps expanded more slowly (and less widely) than was predicted, but it has made advances in both the light and heavy-duty branches of road transport, among others, presenting many opportunities for mutually beneficial lessons to be learned. The rapid and expansive rollout of SCR in the on-road heavy-duty sector paved the way for implementation in light-duty applications, but heavy-duty SCR was itself built upon the successes of that technology in the power generation sector. Information-sharing between segments, branches and industries is key to progress and can significantly speed up market-ready implementation, while reducing costs. SCR is widely regarded as the best available technology for NO_x control from lean-burning engines of all types; SCR using ammonia as the reducing agent was patented in 1957, yet it took over 60 years for the majority of new passenger cars in the EU running on Diesel to feature SCR aftertreatment. While there are certain important differences between DPFs and GPFs, the rollout of the latter was aided by experience gained from the rollout and gradual optimisation of the former [61, 62].

Legislative requirements are moving away from a vague minimum performance-type structure (i.e. the setting of maximum emissions limits, tested under very well-defined, inflexible test conditions) towards a more comprehensive, multipronged approach in which limits not only have to be met under a wide range of conditions (i.e. during RDE/ISC testing), but certain technical decisions must also be revealed and justified (auditing of emissions control strategies). The number of pollutants for which legal limits are set is also set to expand somewhat, although some pollutants can be controlled indirectly, i.e. by limiting compounds with which they share a strong correlation in terms of exhaust emissions levels.

Planned emission standards for LDV and HDV for the future (Euro 7/VII regulations) are as follows:

- Pollutant emissions to be considered along with GHG emissions (perhaps via CO_2-equivalent values being applied to CH_4 and N_2O, both of which are powerful GHG),
- Low ambient temperature cold start test using the WLTP methodology,
- Currently unregulated emissions may also be considered (GHG: N_2O, CH_4; harmful species NH_3, NO_2, broader measurement of particulates: PN 10 nm),
- Fuel- and technology-neutral regulations and emissions; possible setting of equivalent (not identical) emissions limits for LD and HD,
- A move from onboard diagnostics of emissions malfunctions to continuous on-board monitoring of emissions (i.e. OBD→OBM).

While the majority of the most recent legislative developments have been applicable to light-duty vehicles, further changes are underway (or will be soon confirmed) in other sectors, even those far removed from roads (like the marine sector). The setting of precedents in one sector or geographic area is highly significant, as this can then serve as a justification for the setting of equivalent (or even identical) limits in other jurisdictions and other sectors. While the main focus of powertrain development is currently on emissions reduction (achieved by means emphatically not limited to aftertreatment and hybridisation), such efforts are underpinned by core research on "traditional" engine fundamentals such as combustion, thermodynamic considerations, gas kinetics, tribology/lubrication, etc. By bringing together progress and advances in many areas, powertrain concepts may be devised which provide genuine benefit for users, society and indeed the environment. Future congresses to be organised by PTNSS (and its various partners) will aim to continue to facilitate the exchange of information and ideas that is required for the efforts discussed in this paper.

Bibliography

[1] BP Energy Outlook, 2020 edition. https://www.bp.com/

[2] NEUGEBAUER, S. Technological scenarios for the decarbonization of road transport. In "Connectivity–Key to future emission and consumption reduction? *Proceedings of the Vehicle and Powertrain" 30th International AVL Conference "Engine & Environment"*, Graz, Austria, 7-8 June 2018.

[3] CUI, H., HALL, D., LUTSEY, N. Update on the Global Transition to Electric Vehicles Through 2019. *ICCT*. Washington, DC, USA, 2020.

[4] ABE, S. The future direction of the electrified vehicle – utilizing of big data. Proceedings "Connectivity – The key to future emission and consumption reduction? In: *Vehicle and Powertrain" 30th International AVL Conference "Engine & Environment"*, Graz, Austria, 7-8 June 2018.

[5] SUAREZ-BERTOA, R. Preparing new European emission standards post-Euro 6, *3rd China-EU Workshop on Emissions Standards and Regulations*. Xi'an, China, October 9-11, 2019.

[6] EUROPEAN COURT OF AUDITORS. Air pollution: Our health still insufficiently protected. Special Report EN No 23/2018. *EU Publications Office*. Luxembourg 2018.

[7] WINKLER, S.L., ANDERSON, J.E., GARZA, L. et al. Vehicle criteria pollutant (PM, NO_x, CO, HCs) emissions: how low should we go? *Climate and Atmospheric Science*. 2018, **1**, 26. https://doi.org/10.1038/s41612-018-0037-5

[8] VEHICLE EMISSIONS CONTROL CENTRE (CHINA). Real Driving Emissions (RDE) Technical Specification & Test Study of Light-duty Vehicle in China. *3rd China-EU Workshop on Emissions Standards and Regulations*. Xi'an, China, October 9-11, 2019.

[9] RODRIGUEZ, F. Post-Euro 6/VI standards: An opportunity for international harmonization. *3rd China-EU Workshop on Emissions Standards and Regulations*. Xi'an, China, October 9-11, 2019.

[10] MERKISZ, J., PIELECHA, J., BIELACZYC, P. et al. Analysis of emission factors in RDE tests as well as in NEDC and WLTC chassis dynamometer tests. *SAE Technical Paper* 2016-01-0980, 2016. https://doi.org/10.4271/2016-01-0980

[11] GIECHASKIEL, B., LAHDE, T., SUAREZ-BERTOA, R. et al. Particle number measurements in the European legislation and future JRC activities. *Combustion Engines*. 2018, **174**(3), 3-16. https://doi.org/10.19206/CE-2018-301

[12] BIELACZYC, P. Particulate number (PN) & gaseous emissions in the EU automotive emissions context. Expert Panel Discussion EU/China Emissions Regulations. *SAE 2019 WCX World Congress*. Detroit, MI, USA.

[13] GIECHASKIEL, B., LAHDE, T., CLAIROTTE, M. et al. Post Euro 6/VI activities focusing on particle number. *SAE 2019 WCX World Congress*. Detroit, MI, USA. https://doi.org/10.13140/RG.2.2.26039.37286

[14] GIECHASKIEL, B., MAMAKOS, A., WOODBURN, J. et al. Evaluation of a 10 nm Particle Number Portable Emissions Measurement System (PEMS). *Sensors*. 2019, **19**, 5531. https://doi.org/10.3390/s19245531

[15] BIELACZYC, P. Global development of emissions reduction strategies from light-duty vehicles. *IOP Conf. Series: Earth and Environmental Science*. 2019, **214**, 012139, IOP Publishing. https://doi.org/10.1088/1755-1315/214/1/0121

[16] BIELACZYC, P., WOODBURN, J., Current directions in LD powertrain technology in response to stringent exhaust emissions and fuel efficiency requirements. *Combustion Engines*. 2016, **166**(3), 62-75. https://doi.org/10.19206/CE-2016-341.

[17] MCKINSEY & COMPANY. The future of mobility is at our doorstep. *Compendium.* 2019/2020.

[18] BIELACZYC, P., WOODBURN, J. Powertrain development for low-to-zero emissions and efficient energy usage – the Industry Session held during 5th PTNSS Congress on Combustion Engines. *Combustion Engines.* 2013, **155**(4), 75-79.

[19] BIELACZYC, P., WOODBURN, J., GANDYK, M. Trends in automotive emissions, fuels, lubricants, legislation and test methods – a global view, with a focus on the EU & US – Summary of the 5th International Exhaust Emissions Symposium (IEES). *Combustion Engines*. 2016, **166**(3), 76-82. https://doi.org/10.19206/CE-2016-342

[20] BIELACZYC, P., WOODBURN, J. Trends in automotive emission legislation: impact on LD engine development, fuels, lubricants and test methods: a global view, with a focus on WLTP and RDE regulations. *Emissions Control Science Technology*. 2019, **5**(1), 86-98. https://doi.org/10.1007/s40825-019-0112-3

[21] HILL, L. Global trends in emissions legislation. *The VIII PTNSS International Congress on Combustion Engines*. 17-19 June 2019, Krakow, Poland.

[22] BIELACZYC, P., KLIMKIEWICZ, D., WOODBURN, J. et al. Exhaust emission testing methods – BOSMAL's legislative and development emission testing laboratories. *Combustion Engines*. 2019, **178**(3), 88-98. https://doi.org/10.19206/CE-2019-316

[23] PAJDOWSKI, P., WOODBURN, J., BIELACZYC, P. et al. Development of RDE test methodology in light of Euro 6d emissions limits. *Combustion Engines*. 2019, **178**(3), 274-282. https://doi.org/10.19206/CE-2019-348

[24] BIELACZYC, P. Global trends in vehicular emissions regulations, current "hot topics" and their impact on powertrain technology – introduction to the subject. *VIII International PTNSS Congress on Combustion Engines*. 17-19 June 2019, Krakow, Poland.

[25] VALVERDE-MORALES, V. Overview of the light-duty vehicles tailpipe emissions regulations in the European Un-

ion: status and upcoming type-approval and market surveillance schema. *Combustion Engines*. 2020, **180**(1), 3-7. https://doi.org/10.19206/CE-2020-101

[26] JOSHI, A. Review of vehicle engine efficiency and emissions. *SAE International Journal of Advances and Current Practices in Mobility*. 2019, **1**(2), 734-761. https://doi.org/10.4271/2019-01-0314

[27] JOSHI, A. Overview of technologies for near-zero tailpipe emissions from light- and heavy-duty vehicles. *The VIII PTNSS International Congress on Combustion Engines*. 17-19 June 2019, Krakow, Poland.

[28] MERKISZ, J. Development trends in road transport powertrains. *The VIII PTNSS International Congress on Combustion Engines*. 17-19 June 2019, Krakow, Poland.

[29] FRIEDL, H., FRAIDL, G., KAPUS, P. Highest efficiency and ultra-low emission – internal combustion engine 4.0. *Combustion Engines*. 2020, **180**(1), 8-16. https://doi.org/10.19206/CE-2020-102

[30] ENGELJEHRINGER, K. LD vehicle emission challenge from legislation to testbed. *The VIII PTNSS International Congress on Combustion Engines*. 17-19 June 2019, Krakow, Poland.

[31] MASON, A., ROBERTS, P., WHELAN, S. et al. RDE plus – a road to rig development methodology for complete RDE compliance: road to chassis perspective. *SAE International Journal of Advances and Current Practices in Mobility*. 2020, **2**(3), 1361-1381. https://doi.org/10.4271/2020-01-0378.

[32] WHELAN, S., ROBERTS, P. Meeting the demands of future powertrain test & development with an integrated RDE+ road-to-rig approach. *The VIII PTNSS International Congress on Combustion Engines*. 17-19 June 2019, Krakow, Poland.

[33] ALONSO BAEZ, M. Investigation of the mechanism of the soot in oil contamination: overtaking the limits of the combustion. *The VIII PTNSS International Congress on Combustion Engines*. 17-19 June 2019, Krakow, Poland.

[34] ROLANDO, L., ZANELLI, A., MILLO, F. Potential of electric supercharging for performance and fuel economy enhancement of passenger car gasoline engines. *The VIII PTNSS International Congress on Combustion Engines*. 17-19 June 2019, Krakow, Poland.

[35] PERUJO, A., BONNEL, P., GIORIA, R. et al. Large and small engines: overview of the heavy-duty vehicles and non-road mobile machinery tailpipe emissions regulations in the EU. *The VIII PTNSS International Congress on Combustion Engines*. 17-19 June 2019, Krakow, Poland.

[36] AOYAGI, Y. Measurement of flame temperature and soot amount for effective NO_x and PM reduction in a heavy-duty diesel engine. *Combustion Engines*. 2019, **179**(4), 32-39. https://doi.org/10.19206/CE-2019-405

[37] AOYAGI, Y. Effective NO_x and PM reduction by means of flame temperature measurement in a single cylinder diesel engine. *The VIII PTNSS International Congress on Combustion Engines*. 17-19 June 2019, Krakow, Poland.

[38] NAKASHIMA, K., UCHIYAMA, Y. Experimental development of apparatus to measure piston assembly friction in an eco-mileage vehicle engine. *Combustion Engines*. 2019, **177**(2), 55-59. https://doi.org/10.19206/CE-2019-210

[39] GOLINI, S. NG engines as a means for an increasingly sustainable powertrain. *The VIII PTNSS International Congress on Combustion Engines*. 17-19 June 2019, Krakow, Poland.

[40] KINNUNEN, T. Engine-integrated off-road stage-V after-treatment system. *The VIII PTNSS International Congress on Combustion Engines*. 17-19 June 2019, Krakow, Poland.

[41] DEPPE, J. Turn-key „Inspex" systems for industries to quantify optically spray & combustion phenomena and to analyze material characteristics by DIC. *The VIII PTNSS International Congress on Combustion Engines*. 17-19 June 2019, Krakow, Poland.

[42] KOLODZIEJ, C., ROCKSTROH, T., HOTH, A. et al. Gasoline composition effects on knocking characteristics between the CFR RON test engine and a modern GDI engine. *The VIII PTNSS International Congress on Combustion Engines*. 17-19 June 2019, Krakow, Poland.

[43] CORDEIRO DE MELO, T., GOMES, H.O., MOREIRA, M.F. et al. Influence of biodiesel blends on the emissions of different engine technologies. *The VIII PTNSS International Congress on Combustion Engines*. 17-19 June 2019, Krakow, Poland.

[44] PERA, C. How engine technology and fuel proprieties can be optimised thanks to CFD. *The VIII PTNSS International Congress on Combustion Engines*. 17-19 June 2019, Krakow, Poland.

[45] LI, H., WU, Y., ANDREWS, G. Combustion and emissions of alternative fuels in a diesel engine. *The VIII PTNSS International Congress on Combustion Engines*. 17-19 June 2019, Krakow, Poland.

[46] KROYAN, Y., WOJCIESZYK, M., LARMI, M. et al. Modeling the effect of fuel properties on end-use engine performance. *The VIII PTNSS International Congress on Combustion Engines*. 17-19 June 2019, Krakow, Poland.

[47] BERRY, M., MILLER, D. The democratization of vehicle emissions testing. *The VIII PTNSS International Congress on Combustion Engines*. 17-19 June 2019, Krakow, Poland.

[48] WANG, X. RDE regulation and practice in China. *The VIII PTNSS International Congress on Combustion Engines*. 17-19 June 2019, Krakow, Poland.

[49] THOMAS, D., LI, H., WANG, X. et al. Tailpipe exhaust particle size distribution from a hybrid car. *The VIII PTNSS International Congress on Combustion Engines*. 17-19 June 2019, Krakow, Poland.

[50] JASKIERNIK, M., BUCZEK, K., WALKOWIAK, J. Simulation of the oil supply through the connecting rod to the piston cooling channels in medium speed engines. *Combustion Engines*. 2020, **180**(1), 25-30. https://doi.org/10.19206/CE-2020-104

[51] BUSTIN, L. Variable partial flow dilution and conditioning system for TSI engine exhaust particle sizer. *The VIII PTNSS International Congress on Combustion Engines*. 17-19 June 2019, Krakow, Poland.

[52] PALENCIA, J.C.G., NGUYEN, V.T., ARAKI, M. et al. The role of powertrain electrification in achieving deep decarbonization in road freight transport. *Energies*. 2020, **13**, 2459. https://doi.org/10.3390/en13102459

[53] PIELECHA, J., MERKISZ, J., BIELACZYC, P. et al. Gaseous emissions from a hybrid vehicle and a non-hybrid vehicle measured under real driving conditions via PEMS. *FISITA Technical Paper* F2018/F2018-PTE-266.

[54] ZHUANG, W., LI (EBEN), S., ZHANG, X. et al. A survey of powertrain configuration studies on hybrid electric vehicles. *Applied Energy*. 2020, **262**, 114553. https://doi.org/10.1016/j.apenergy.2020.114553

[55] HALL, D., WAPPELHORST, S., MOCK, P. et al. European Electric Vehicle Fact Book 2019/2020. *ICCT*. Washington, USA 2020.

[56] BIELACZYC, P. Global trends in electrified powertrains - challenges. in testing methods. *Polish Conference on Hydrogen Energy and Technology (PCHET 2020)*. 22-23.09.2020, Cluster of Hydrogen Technologies, Gdansk, Poland.

[57] LI, Z., KHAJEPOUR, A., SONG, J. A comprehensive review of the key technologies for pure electric vehicles. *Energy*. 2019, **182**, 824-839. https://doi.org/10.1016/j.energy.2019.06.077.

[58] GÓMEZ VILCHEZ, J.J., JOCHEM, P. Powertrain technologies and their impact on greenhouse gas emissions in key car markets. *Transportation Research Part D: Transport and Environment*. 2020, **80**, 102214, https://doi.org/10.1016/j.trd.2019.102214

[59] SMALLBONE, A., JIA, B., ATKINS, P. et al. The impact of disruptive powertrain technologies on energy consumption and carbon dioxide emissions from heavy-duty vehicles. *Energy Conversion and Management.* 2020, **6**, 100030. https://doi.org/10.1016/j.ecmx.2020.100030

[60] KOERFER, T. Hybridized diesel powertrains for LCV applications to meet the Stringent 2025 standards for pollutant- and CO_2-emissions. *SAE Technical Paper* 2020-01-2252. 2020. https://doi.org/10.4271/2020-01-2252

[61] DZIDA, J., BIELACZYC, P., BRZEŻAŃSKI, M. The variation of functional characteristics of a Euro VI selective catalytic reduction reactor after ageing. *SAE Technical Paper* 2020-01-2205. 2020. https://doi.org/10.4271/2020-01-2205

[62] JOSHI, A. Review of vehicle engine efficiency and emissions. *SAE International Journal of Advances and Current Practices in Mobility*. 2020, **2**(5), 2479-2507. https://doi.org/10.4271/2020-01-0352.

Piotr Bielaczyc, DEng., FSAE – Scientific Secretary, BOSMAL Automotive Research and Development Institute Ltd in Bielsko-Biala, Poland

e-mail: *piotr.bielaczyc@bosmal.com.pl*

Joseph Woodburn, MSci – Exhaust Emission Laboratory, BOSMAL Automotive Research and Development Institute Ltd in Bielsko-Biała, Poland

e-mail: *joseph.woodburn@bosmal.com.pl*

Ameya Joshi, DEng. – Director of Emerging Technologies, Corning Incorporated, USA

e-mail: *joshia@corning.com*

Article citation info:
HUNICZ, J., KRZACZEK, P., GĘCA, M. et al. Comparative study of combustions and emission of diesel engine fuelled with FAME and HVO. *Combustion Engines*. 2021, **184**(1), 72-78. https://doi.org/ 10.19206/CE-135066

Jacek HUNICZ
Paweł KRZACZEK
Michał GĘCA
Arkadiusz RYBAK
Maciej MIKULSKI

Comparative study of combustion and emissions of diesel engine fuelled with FAME and HVO

This study investigates combustion and emission characteristics of a contemporary single-cylinder compression ignition engine fuelled with diesel, fatty acid methyl esters (FAME) and hydrotreated vegetable oil (HVO). These two drop-in fuels have an increasing share in automotive supply chains, yet have substantially different physical and auto-ignition properties. HVO has a lower viscosity and higher cetane number, and FAME has contrary characteristics. These parameters heavily affect mixture formation and the following combustion process, causing that the engine pre-optimized to one fuel option can provide deteriorated performance and excess emissions if another sustainable option is applied. To investigate the scale of this problem, injection pressure sweeps were performed around the stock, low NO_x and low PM engine calibration utilizing split fuel injection. The results showed that FAME and HVO prefer lower injection pressures than diesel fuel, with the benefits of simultaneous reduction of all emission indicators compared to DF. Additionally, reduction of injection pressure from 80 MPa to 60 MPa for biodiesels at low engine load resulted in improved brake thermal efficiency by 1 percentage point, due to reduced parasitic losses in the common rail system.

Key words: *diesel engine, renewable fuels, HVO, emissions*

1. Introduction

The limits for toxic emissions and CO_2 produced by the internal combustion engines are the main challenges in the light of transport sustainability. The earlier issue is especially valid for diesel engines, which are more prone to higher emissions of particulate matters (PM) and nitrogen oxides (NO_x), than they spark ignition competitors. However, the pros of diesel engines are their higher thermal efficiency and scalability. Due to these advantages, diesel engines are estimated to power about 42% of todays' passenger cars in the European Union [24]. Moreover, heavy-duty transport, including waterborne, is almost completely dominated by diesel engines. The wide use of internal combustion engines as transport power plants results in the fact that they release approximately 10% of the global gaseous emissions nowadays [21].

Assuming the typical fleet renewal intervals in the heavy-duty sector from 10 (trucks) to 25 (ship propulsion) years, the short route towards decarbonisation is the use of non-fossil fuels (obtained from biomass or waste) with minimal consumption of energy from the current mix [18]. According to the European Biodiesel Board the use of biodiesel reduces CO_2 emissions by 65%–90% [23]. Nowadays there are two leading technologies for the production of non-fossil diesel substitutes from biomass, because of their infrastructural maturity and availability of the feedstock. Transesterification of oils using methanol, or other alcohols, is one of the methods of biofuel production. As a result of this process, fatty acid methyl esters (FAMEs) are obtained. One should note that on the worldwide biofuel market FAME has a 32% share [25]. The hydrotreated vegetable oil (HVO) is an alternative biofuel with a rapidly growing market share, currently approximately at the level of 6%. HVO like FAME can be produced from waste biomass such as animal fats and the used cooking oils. In such case, these fuels can be classified as second-generation biofuels, not competing with food production [11]. During the production of HVO and FAME natural gas is utilized, however, a comparison of carbon footprints of HVO and FAME indicates HVO as more greenhouse friendly [7].

It should be noted that the quality of FAME strongly depends on the feedstock [8], while the quality of HVO is more neutral. Therefore, HVO can be produced using various oils, e.g. rapeseed, sunflower, soy. Importantly, HVO can be produced from non-edible oils like algae, jatropha, camelina, etc. as well as from waste fats. Therefore HVO outperforms FAME in terms of the food-or-fuel dilemma [3].

Side by side to CO_2 footprint, fuel effect on toxic exhaust components should be taken into consideration. Emission-wise, ideal diesel fuel should not have any C-C bonds. Such fuel hardly produces particulates. On the other side, double and triple carbon bonds are determinants for soot formation. Therefore the production of soot is chemically increased by the presence of alkynes and polycyclic aromatic hydrocarbons (PAH) in fuel Furthermore, fuel sulphur increases particulate emissions [2]. HVO is formed by solely paraffinic hydrocarbons and does not contain any sulphur. Therefore, chemically HVO is superior to mineral diesel fuel (DF) and also FAME, which has double carbon bonds.

Physically, FAME has higher viscosity than DF and higher end of distillation temperature, which poses some low-temperature issues [17]. Greater density results from high oxygen content [15], which further translate to lower calorific value and lower stoichiometric air requirement. Auto-ignition properties of FAME are similar to DF. HVO is characterized by lower viscosity and density as compared to conventional diesel fuel that shortens the evaporation time and simplifies obtaining a more homogeneous air-fuel mixture. Higher cetane number of HVO, as well as the paraffinic structure, lead to shorter ignition delay and, consequently, to prolongation of soot oxidation time.

Numerous studies shown that the use of HVO can help reduce PM emissions by 50–70%, when compared to DF.

Received 24 March 2021; Received in revised form 25 March 2021; Accepted 26 March 2021
Available online 28 March 2021

Emissions of CO and unburnt hydrocarbons (UHC) are also lower by the same amount. At the same time NO_x emissions are almost unaffected [1, 12, 22]. Average emission impact of FAME was reported by Demirbas [4]; NO_x emissions were increased by 10%, PM and CO emissions were decreased by 45% and UHC emissions were decreased by 65%. In contrast Koszałka et al. [14] showed that comparison of DF and FAME over whole engine operating area revealed virtually no difference. There is the abundant amount of research into the effects of HVO and FAME on emissions, however much less effort is put into the isolation of the mixture formation strategies on combustion and emissions.

Liu et al. [16] compared combustion and emissions of combustion of DF and high (60%) fractions of FAME and HVO at variable exhaust gas recirculation (EGR) rates. Combustion analysis at split injection revealed that pilot fuel of HVO ignited earlier, than in the case of DF and FAME. Main fuel combustion ran with the same rate for all three fuels. In terms of emissions, both biofuels produced approximately 30% less UHC than DF, independently of EGR rate. In case of smoke emission, DF and FAME produced similar numbers, while HVO halved the emission. Omari et al. [20] optimised EGR control strategies for pure HVO combustion and pointed out that due to higher cetane number (CN), HVO preferred cooled EGR. Recently Dimitriadis et al. [5] pointed out that due to different combustion characteristics of HVO it is possible to improve PM-NO_x trade-off by injection timing adjustment. Retard of the main injection dose enabled 20% reduction of NO_x emissions, while maintaining low PM emissions, 30% below DF baseline.

The premise of the current study is based on the different physical properties of the DF and their renewable substitutes. The differences in volatilities and chemical ignition delays between fuels can require different fuel injection pressures. Therefore in this research DF, FAME and HVO sensitivities to injection pressure were compared using state of the art diesel engine.

2. Methods

2.1. Fuels

The Tested DF is a standard ultra-low sulphur diesel, according to EN590. FAME was obtained from cold-pressed rapeseed oil, trans-esterified at laboratory conditions. The process conditions were adjusted to meet the European norm for biofuels (EN 14214). HVO comes from the fuel company Neste Oil, and as meeting the EN590 standard is commercially available for on-road transport, as Neste Renewable Diesel [6]. Note that HVO tested here is lubricity improved. Neither DF nor HVO contained any FAME.

Significant physicochemical parameters of the tested fuels are summarized in Table 1. Data for HVO are courtesy of VEBIC fuel laboratory (University of Vaasa) Finland, while FAME and DF were characterized in the fuel laboratory of Lublin University of Life Sciences. All fuels are analysed according to EN 590, EN 14214 and other related standards.

Table 1. Fuel properties

Parameter	Unit	DF	FAME	HVO
Density @ 15°C	g/ml	0.837	0.882	0.764
Viscosity @ 40°C	mm^2/s	2.94	4.43	2.88
Lower heating value	MJ/kg	42.8	38.3	43.7
Stoichiometric air demand	kg/kg	14.73	13.7	15.14
Cetane number (CN)	–	54.1	55.2	74.5
Cold filter plugging point	°C	–22	–11	–44
Flash point	°C	70.5	165	66.3
Lubricity @ 60°C	μm	406	190	344
C/H ratio	kg/kg	6.4	7.7	5.5
Sulphur content	mg/kg	6.1	1	< 1
Ash content	%wt.	0.014	0.01	0.002

The differences between the tested fuels highlighted in the introduction are confirmed in Table 1. HVO has a significantly higher CN value, which affects the auto-ignition properties. Thanks to slightly lower viscosity, HVO also boasts better spraying properties. Note that FAME has over 50% higher viscosity compared to HVO or DF. It should be emphasized that the significantly better low-temperature properties of HVO in relation to DF result in a lower flash-point.

When analysing the properties of fuels, resulting from the composition of the mixture, it can be noticed that the LHV values for DF and HVO are similar and amount to about 43 MJ/kg. FAME, on the other hand, has much lower LHV, which is however compensated by lower air demand. The mass ratio of carbon to hydrogen (C/H) is in favour of HVO. It determines cleaner combustion in terms of tank-to-wheel CO_2 emissions. The undoubted advantage of HVO and FAME is the total content of pollutants an order of magnitude lower than in the case of DF, thus potentially reducing SO_x and PM emissions.

2.2. Engine test stand

The engine test stand at Lublin University of Technology is particularly suitable for end-use validation of alternative fuels. The single-cylinder research engine (AVL 5402 CR DI) is the heart of the research platform. The engine's displacement is 510 cm^3, at a 17:1 compression ratio. The combustion chamber is toroidal in shape, while the valves, including the dedicated swirl port (AVL-LEADER concept), are angled at 3.5°. The fuel is supplied via a Bosch CP4.1 high-pressure common rail system equipped with a seven-hole electromagnetic injector. Etas INCA software is used to supervise a fully open Bosch engine control unit. Figure 1 shows the instrumented test stand, while Table 2 summarizes the basic engine parameters.

All measurements in this research are performed in steady-state conditions. To ensure that the system is thermally stable and to minimize the influences of external disturbances on measurement results, various conditioning measures are applied. The fuel consumption is measured gravimetrically, with the AVL 733S dynamic fuel meter and the fuel is thermally conditioned via the corresponding AVL 753C fuel temperature conditioner. Thermal conditioning is also applied to the coolant and lubricant circuits. The in-house system maintains the desired temperature of both media with 0.5°C accuracy, regardless of the operating point.

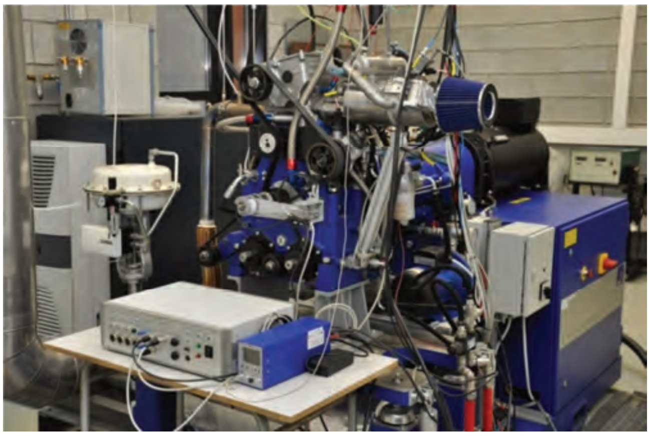

Fig. 1. Engine research test stand at Lublin University of Technology

Table 2. Parameters of the research engine

Type	AVL 5402
Configuration	Four-stroke, single-cylinder
Bore	85 mm
Stroke	90 mm
Displacement	510.5 cm^3
Compression ratio	17:1
No. of valves	4
Combustion type	Direct injection
Max. fuel pressure	180 MPa
Injection system	Common rail CP4.1
Engine management	AVL-RPEMS, ETK7-Bosch

On the intake side, the research stand is equipped with an electrically-driven Roots compressor (up to 2 bar boost pressure) with a controllable charge air cooler. On the exhaust, side the backpressure control, realised by a proportional butterfly valve, mimics turbocharger operation. The engine has both high- and low-pressure EGR systems, where the latter is equipped within the Roots blower. Note that neither boost nor EGR is used in the current experiment. The intake air flow rate is measured with a mass flow meter. Using the Bosch LSU 4.2 lambda probe and the ETAS LA4 lambda sensor, the excess air coefficient (λ) is calculated with pressure compensation [13].

Low-frequency transducers mounted on the intake manifold, exhaust manifold, EGR path, cooling and lubrication systems, provide information on the thermal state of the entire system. All the above-described measurement and control functionalities are governed by an in-house test bench management/data acquisition system.

The present research further utilizes the benefits of detail combustion and emission analysis. The first functionality is based on instantaneous in-cylinder pressure measurement, provided by the AVL GU22C piezo-electric transducer installed in the cylinder head. The transducer is connected to the indication system via the compatible charge amplifier and an optical encoder is used to trigger pressure measurement every 0.1° crank angle (CA).

AVL SESAM multi-component gas analyzer is used to determine the concentration of individual exhaust gas components. The measurement incorporates Fourier Transform Infrared (FTIR) technique and enables over 20 legislated and unlegislated exhaust gas components to be characterized simultaneously. The concentration of particulates is measured separately using the Maha MPM-4 analyser.

2.3. Experimental conditions and procedures

The tests are carried out for a single mid-load operating point with net IMEP 0.5 MPa. The fuel value is adjusted to keep the load constant, across all the parameter sweeps, irrespectively to the fuel used. In this campaign, the engine is operated naturally aspirated and without external EGR. At these conditions excess air ratio λ is close to 2.2, however, varying slightly to satisfy the constant load condition.

The engine speed was kept fixed at 1500 rpm. The engine coolant and lubricating oil temperatures were independently conditioned to 85°C. The temperature in the fuel entering the high-pressure pump is also fixed at 30°C.

The rail pressure is set according to a predefined engine control map to 80 MPa. For each fuel, this parameter was swept ±20 MPa, pertaining to the goal of the present study. Note that the fuel is injected using a multi-pulse injection scheme, where approximately 12% of the total fuel value accounts for an early pilot with the start of injection (SOI) at 20°CA before the top dead centre (bTDC). The remaining (main) pulse is commenced at SOI = 8°CA bTDC.

The recorded in-cylinder pressure data is pegged, filtered and averaged over 100 cycles. The pressure signal is further subjected to a standard first-law heat release analysis, with correction for convective heat loss through cylinder walls (Hohenberg heat transfer model). The calculations are supported by AVL Boost software, to accommodate for detail cylinder mass flow rate estimation.

Slow-changing quantities, such as fuel consumption and emissions, are averaged in individual measurement points of the campaign, over a standard 60-second window, to satisfy the steady-state measurement principle. Since the current study investigated single operating point with roughly constant in-cylinder air value, emission factors are analysed as concentrations on a mole basis – pertaining to the direct output of respective emission analysers.

3. Results and discussion

3.1. Effects of fuels on combustion

We open up the discussion of the results with a benchmark of tested fuels at baseline conditions i.e. at 80 MPa rail pressure. In this respect, it is critical to consider differences in combustion as a driving force to emission formation. Without any detailed analysis, it can be noted that the combustion of the three fuels runs similarly, however only if the main, diffusion-controlled combustion phase is considered. This phase corresponds to the third, dominant peak on the heat release rate (HRR) presented in Fig. 2. The insensitivity is driven by the phenomenology of the multi-pulse combustion concept realised. Namely, the primarily premixed pilot combustion, visible as the first two characteristics peaks, HRRs (respectively, cool flames and negative temperature coefficient reactions followed by the high-temperature premixed phase), acts as a primer towards the main injection. The main injection pulse ignites instantly after reaching the hot burnt zone of the pilot, located near the combustion chamber walls. Therefore, the similarity results from the fact that fuel-to-fuel viscosity differences reported in Table 1, are too small to cause significant differences in spray penetration lengths.

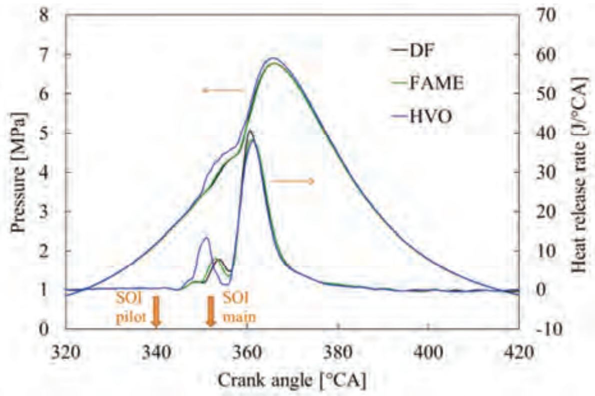

Fig. 2. In-cylinder pressures and HRRs for investigated fuels at 80 MPa rail pressure

The higher CN of HVO manifests in ignition characteristics of the pilot, which is notably different compared to both DF and FAME. Namely, the high-temperature combustion of the pilot fuel starts approximately 2°CA earlier for HVO. Moreover, the HRR drop to a constant, near-zero value, between 354.5°CA and 356°CA, indicates that the HVO pilot is completely burnt before the main fuel starts to burn. The more complete oxidation of the pilot translates into an increase of the in-cylinder pressure before TDC, as evident for HVO in Fig. 2. It should be noted that the combustion characteristics of FAME and DF are very similar. However, slightly advanced pilot fuel combustion of FAME is visible.

A superposition of the combustion characteristics derived from Fig. 2 in this section, with physical properties of individual fuels, discussed in Table 1, allows concluding that even large-scale differences in viscosity (roughly 70% between FAME and DF) have an indirect effect on combustion in the considered multi-pulse injection strategy. The fuels CN shapes the premixed pilot combustion, which forms a direct trigger for the main phase.

3.2. Effects of fuel pressure on combustion

The combustion analysis from section 3.1 forms the background for understanding the response of the fuels to changes in injection pressure. These responses concerning HRR are shown in Fig. 3, for DF, FAME and HVO respectively.

Increasing the injection pressure in principle manifests in (i) reducing the pilot HRR and (ii) increasing the main HRR. Let's discuss these effects one by one based on the DF reference, following with fuel-to-fuel differences.

Concerning the first effect, the pilot heat release diminishes cumulatively – less fuel is burnt during the pilot stage while elevating the injection pressure from 80 to 100 MPa. This indicates a potential wall-wetting effect while injecting and early pilot with higher spray penetration velocities (direct effect of elevated injection pressure). Interesting is the fact that reducing the rail pressure from 80 to 60 MPa does not cause a further increase in the pilot HRR but, what is evident in the case of HVO, can even slightly decrease the amount of pilot fuel burnt. This non-monotonic response of pilot combustion to injection pressure indicates that there is another mechanism involved. Mapping the HRR results from Fig. 3 with physicochemical properties of subsequent fuels does not reveal any particular relationship, however.

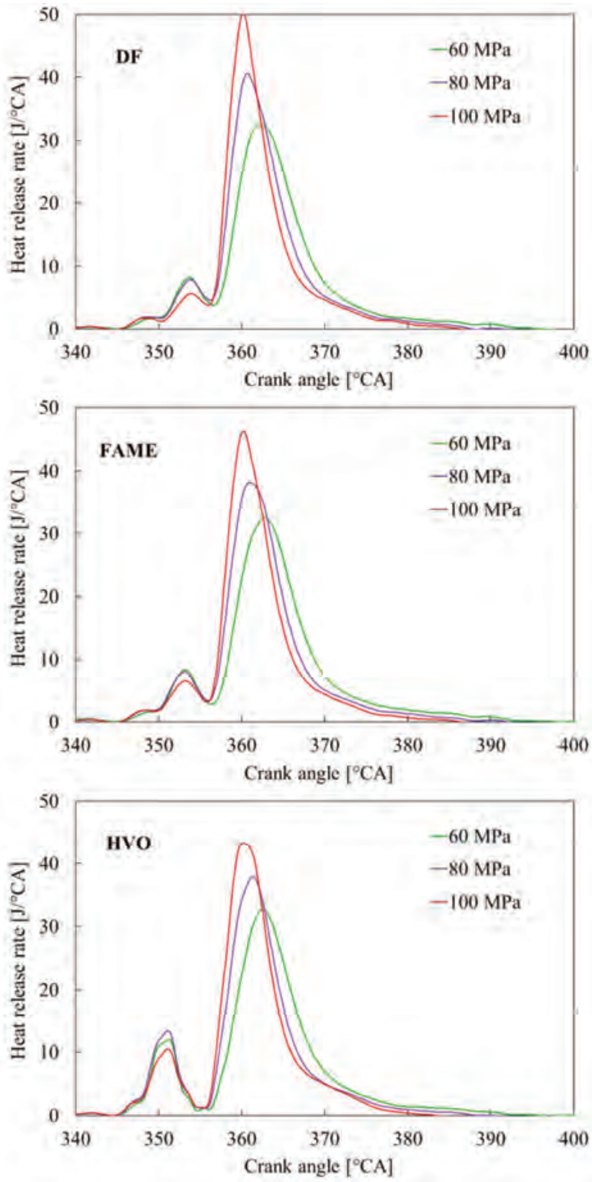

Fig. 3. HRRs for investigated rail pressures and for DF, FAME and HVO

As far as there is some ambiguity in the injection pressure effect on the pilot combustion, the influence of this calibration parameter on the main combustion phase is transparent from Fig. 3. Elevating injection pressure makes the main HRR more rapid and this combustion phase tends to start earlier. The more rapid combustion is invoked by the fact that with elevated injection pressure the main spray reaches the pilot burn zone faster when the premixed combustion is still in progress. The main combustion hence has more favourable conditions to progress within a hotter, more reactive, and oxygen richer environment of the developing premixed flame. Note that the higher main peak HRRs at elevated injection pressure are additionally reinforced by better fuel atomization within the main spray. Finally, there are evident couplings between the amount of heat released in the pilot phase, and how the main combustion proceeds. For cases in which elevated injection pressure causes the wall-wetting affected reduction of pilot HRR, the accumulated hydrocarbons are partially picked-up by the main combustion adding to the cumulative heat released in this phase. The cases with reduced pilot HRR also partially balance-out the combustion-accelerating effect of faster main spray propagation. As a result, the main HRRs for 80 MPa and 100MPa start roughly at the same CA.

These effects related to the main combustion are evident for all tested fuels, as visible in Fig. 3. The magnitude of those effects depends however on how the pilot combustion develops – not particularly on fuel properties directly. Hence, for instance, DF exhibits by far the highest sensitivity to injection pressure – attributed to the fact that elevated rail pressure deteriorates the pilot combustion the most and that the two combustion phases are closely coupled (minimum dwell between the pilot and main HRR). According to the same logic in the case of HVO, where the combustion phases are clearly separated, the relative changes in pilot HRR affect the main combustion to the least extent.

3.3. Effects of fuel pressure on emissions

Assessing the fuel's emission performance in Fig. 4 shows that, independently of fuel pressure, HVO and FAME have a better PM/NO_x trade-off. Namely, both biofuels roughly halved PM emissions when compared to DF. At the same time, biofuels produce only 2–3% higher NO_x emissions. The propensity of the fuel to create PM seems to correlate to the sulphur and ash content (refer to Table 1). Fuel-bound sulphur is known to form a good nesting for particulates formation [19]. Its oxidation products (SO_3 particularly) bind with water to sulfuric acid which condenses to soot when exhaust gasses cool down. Hence, HVO with the lowest level of contaminants produces the least PM.

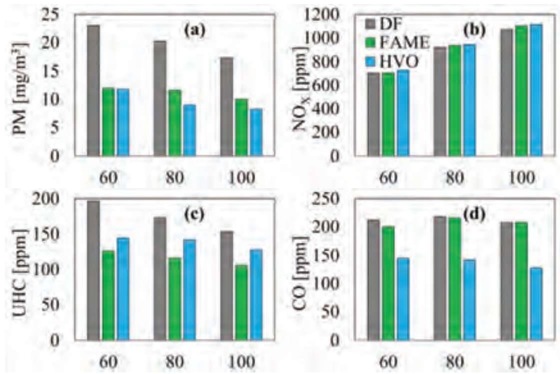

Fig. 4. Concentrations of major legislative emission components for DF, FAME and HVO; rail pressure sweep

FAME, due to fuel-bound oxygen is known to produce more NO_x compared to its unoxygenated counterparts [9, 10]. Interestingly, however, this has not been confirmed in this study, suggesting that local oxygen availability is not limiting the NO_x formation and the mechanism is predominantly thermal-driven.

Biofuels ultimately burn more completely than DF. Cumulative CO and UHC emissions are around 25–30% in favour of both fuels, while HVO exerts lower CO emissions than FAME. The trend in UHC is the opposite.

In the light of largely similar combustion behaviour of DF, HVO and FAME (Fig. 2), the above-discussed fuel to fuel differences in emissions are resulting directly from physicochemical properties. According to Fig. 4 these fuel-specific emissions are maintained thought the injection pressure sweep. The effects here are rather straightforward. Elevated injection pressure reduces PM and UHC emissions due to better fuel atomization and increased in-cylinder turbulence. Both mechanisms support more complete oxidation. The fuel wetting during pilot combustion, at elevated rail pressure is not evident through emissions results, suggesting that main combustion successfully after-burns potential residues from the pilot.

NO_x emission increases with injection pressure and this effect can be attributed directly to changes in the HRR rate observed in Fig. 3. Namely, more rapid main combustion yields higher peak temperatures, intensifying Zeldovich reactions responsible for NO_x formation.

3.4. Discussion

Comparison of the three tested fuels in Fig. 4 shows that all toxic exhaust gas components, except NO_x increase when fuel pressure is reduced. However, the baseline levels of PM and UHC for biofuels are much lower than for DF. Assuming the PM limit as given by DF reference, it is reasonable to reduce injection pressure if biofuels are considered. Reducing injection pressure from baseline 80 MPa to 60 MPa cuts down NO_x by 20% while for HVO and FAME PM is still over 30% lower compared to DF baseline. Assuming the slightly retarded combustion onset, resulting from this measure (Fig. 3), thermal efficiency can be further optimized with the main injection timing. Therefore, reduction of injection pressure, enabled by wider emission tolerances of FAME and HVO, can be essential for maximizing overall engine efficiency.

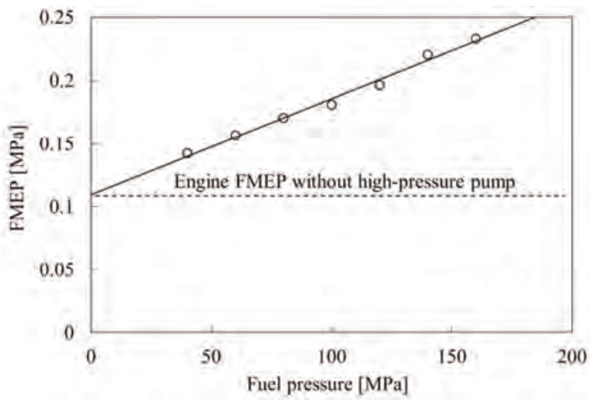

Fig. 5. Effect of fuel pressure on friction mean effective pressure of the engine at constant IMEP of 0.5 MPa; DF reference

Discussion of Fig. 5 explains this issue on the basis of engine friction losses, expressed here in the units of friction mean effective pressure (FMEP). FMEP is obtained by subtracting the brake mean effective pressure (BMEP), measured on the engine dyno, from IMEP, calculated from in-cylinder pressure.

You can note that, at the given operating point, the pressure-dependent parasitic losses of the common-rail fuel pump can form up to 50% of the overall engine friction losses. To this end, reducing fuel pressure from 80 MPa to 60 MPa cuts down mechanical losses by 11%, which translates to roughly 1% of the total fuel consumption.

Finally, note that the particularly low heating value of FAME (Table 1) translates to additional injection pump expenditure – hence larger parasitic losses. The effect is however order of magnitude smaller and remains practically unnoticeable on the scale of Fig. 5.

4. Conclusion

Within the boundaries of the discussed combustion regime, the fuel cetane number has a dominant effect on fuels combustion performance, affecting pilot fuel combustion. Due to the strong coupling of the main combustion with the early pilot, the main combustion remains largely insensitive to changes in fuel, hence all react to injection pressure similarly.

Despite large-scale differences in viscosity and flashpoint between tested fuels, the effect of all other fuel parameters on combustion is an order of magnitude lower than that of cetane number. The present scope of experiments ultimately fails to decouple those secondary effects. Such decoupling is however desired and for that, future research should involve tailor-made fuels with large-scale differences only in individual physicochemical parameters.

The oxygenated nature of FAME and its large viscosity ultimately do not deteriorate emissions in the realized combustion concept. The fuel-to-fuel differences result directly from sulphur and ash content in the fuel, rather than from different combustion characteristics. Hence, HVO and FAME exhibit a more favourable PM/NO_x trade-off than DF. These more favourable biofuel characteristics allow reduction of injection pressure from baseline 80 to 60 MPa while being superior in all emission factors and brake efficiency. Injection pressure-optimized, emissions from FAME and HVO were similar, and respectively 20% and 40% lower in terms of NO_x and PM, compared to diesel-optimized conditions.

Acknowledgements

The authors wish to thank AVL List GmbH for making the simulation software available within a framework of the AVL University Partnership Program.

The authors wish to thank researchers form VEBIC Fuel Laboratory for HVO fuel delivery and analyses.

Nomenclature

BMEP	brake mean effective pressure
bTDC	before the top dead centre
C/H	mass ratio of carbon to hydrogen
CA	crank angle
CN	cetane number
CO	carbon monoxide
CO_2	carbon dioxide
DF	diesel fuel
EGR	exhaust gas recirculation
FAME	fatty acid methyl esters
FMEP	friction mean effective pressure
FTIR	Fourier Transform Infrared
HRR	heat release rate
HVO	hydrotreated vegetable oil
IMEP	indicated mean effective pressure
LHV	lower heating value
NO_X	nitrogen oxides
PM	particulate matters
SOI	start of injection
SO_X	sulfur oxides
UHC	unburnt hydrocarbons

Bibliography

[1] AATOLA, H., LARMI, M., SARJOVAARA, T. et al. Hydrotreated Vegetable Oil (HVO) as a renewable diesel fuel: trade-off between NO_x, particulate emission, and fuel consumption of a heavy duty engine. *SAE International Journal of Engines*. 2008, **1**, 1251-1262. https://doi.org/10.4271/2008-01-2500

[2] BAE, C., KIM, J. Alternative fuels for internal combustion engines. *Proceedings of the Combustion Institute*. 2017, **36**(3), 3389-3413. https://doi.org/10.1016/j.proci.2016.09.009

[3] BEZERGIANNI, S., DIMITRIADIS, A. Comparison between different types of renewable diesel. *Renewable and Sustainable Energy Reviews*. 2013, **21**, 110-116. https://doi.org/10.1016/j.rser.2012.12.042

[4] DEMIRBAS, A. Progress and recent trends in biodiesel fuels. *Energy Conversion and Management*. 2009, **50**, 14-34. https://doi.org/10.1016/j.enconman.2008.09.001

[5] DIMITRIADIS, A., SELJAK, T., VIHAR, R. et al. Improving PM-NO_x trade-off with paraffinic fuels: A study towards diesel engine optimization with HVO. *Fuel*. 2020, **265**, 116921. https://doi.org/10.1016/j.fuel.2019.116921

[6] Engine Technology International. March 2021, 60-61.

[7] GARRAÍN, D., HERRERA, I., LAGO, C. et al. Renewable diesel fuel from processing of vegetable oil in hydrotreatment units: theoretical compliance with European Directive 2009/28/EC and ongoing projects in Spain. 2010, **4**. https://doi.org/10.4236/sgre.2010.12011

[8] GOLIMOWSKI, W., BERGER, W.A., PASYNIUK, P. et al. Biofuel parameter dependence on waste fats' fatty acids profile. *Fuel*. 2017, **197**, 482-487. https://doi.org/10.1016/j.fuel.2017.02.067

[9] GOLIMOWSKI, W., KRZACZEK, P., MARCINKOWSKI, D. et al. Impact of biogas and waste fats methyl esters on NO, NO_2, CO, and PM emission by dual fuel diesel engine. *Sustainability*. 2019, **11**(6), 1799. https://doi.org/10.3390/su11061799

[10] GRACZ, W., CZECHLOWSKI, M., MARCINKOWSKI, D. et al. The impact of the temperature of rapeseed oil methyl esters on nitrogen oxides emissions. *E3S Web of Conferences*. 2020, **171**, 01002. https://doi.org/10.1051/e3sconf/202017101002

[11] GRZELAK, P., ŻÓŁTOWSKI, A. Environmental assessment of the exploitation of diesel engines powered by biofuels. *Combustion Engines*. 2020, **180**(1), 31-35. https://doi.org/10.19206/CE-2020-105

[12] HUNICZ, J., MATIJOŠIUS, J., RIMKUS, A. et al. Efficient hydrotreated vegetable oil combustion under partially premixed conditions with heavy exhaust gas recirculation. *Fuel*. 2020, **268**, 117350. https://doi.org/10.1016/j.fuel.2020.117350

[13] KASPRZYK, P., HUNICZ, J., RYBAK, A. et al. Excess air ratio management in a diesel engine with exhaust backpressure compensation. *Sensors*. 2020, **20**(22), 6701. https://doi.org/10.3390/s20226701

[14] KOSZAŁKA, G., HUNICZ, J., NIEWCZAS, A. A comparison of performance and emissions of an engine fuelled with diesel and biodiesel. *SAE International Journal of Fuels and Lubricants*. 2010, **3**, 77-84. https://doi.org/10.4271/2010-01-1474

[15] KRZACZEK, P., RYBAK, A., BOCHNIAK, A. The impact of selected biofuels on the performance parameters of the common rail power system in the utility engine. *MATEC Web of Conferences*. 2018, **234**, 03004. https://doi.org/10.1051/matecconf/201823403004

[16] LIU, D., GHAFOURIAN, A., XU, H. Phenomenology of EGR in a light duty diesel engine fuelled with hydrogenated vegetable oil (HVO), used vegetable oil methyl ester (UVOME) and their blends. *SAE Technical Paper* 2013-01-1688. 2013. https://doi.org/10.4271/2013-01-1688

[17] MARCINKOWSKI, D., RUKOWICZ, B., GOLIMOWSKI, W. et al. Effect of selected depressants on cold filter plugging point for methyl esters obtained from transesterification of waste vegetable and animal fats. *Przemysł Chemiczny*. 2017, **96**(9), 1927-1930. https://doi.org/10.15199/62.2017.9.22

[18] MIKULSKI, M., AMBROSEWICZ-WALACIK, M., HUNICZ, J. et al. Combustion engine applications of waste tyre pyrolytic oil. *Progress in Energy and Combustion Science*. 2021, **85**, 100915. https://doi.org/10.1016/j.pecs.2021.100915

[19] NEEFT, J.P.A., MAKKEE, M., MOULIJN, J.A. Diesel particulate emission control. *Fuel Processing Technology*. 1995, **47**(1), 1-69. https://doi.org/10.1016/0378-3820(96)01002-8

[20] OMARI, A., PISCHINGER, S., BHARDWAJ, O.P. et al. Improving engine efficiency and emission reduction potential of HVO by fuel-specific engine calibration in modern passenger car diesel applications. *SAE International Journal of Fuels and Lubricants.* 2017, **10**(3), 756-767. https://doi.org/10.4271/2017-01-2295

[21] REITZ, R.D., OGAWA, H., PAYRI, R. et al. IJER editorial: The future of the internal combustion engine. *International Journal of Engine Research*. 2020, **21**(1), 3-10. https://doi.org/10.1177/1468087419877990

[22] SUGIYAMA, K., GOTO, I., KITANO, K. et al. Effects of hydrotreated vegetable oil (HVO) as renewable diesel fuel on combustion and exhaust emissions in diesel engine. *SAE International Journal of Fuels and Lubricants*. 2011, **5**, 205-215. https://doi.org/10.4271/2011-01-1954

[23] www.ebb-eu.org/biodiesel.php. On-line access: 02.2021.

[24] www.eea.europa.eu/data-and-maps/daviz/dieselisation-of-diesel-cars-in-4#tab-chart_1. On-line access: 02.2021.

[25] www.ifpenergiesnouvelles.com/article/biofuels-dashboard-2019. On-line access: 02.2021.

Jacek Hunicz, DSc., DEng. – Faculty of Mechanical Engineering, Lublin University of Technology.
e-mail: *j.hunicz@pollub.pl*

Paweł Krzaczek, DEng. – Faculty of Production Engineering, University of Life Sciences.
e-mail: *pawel.krzaczek@up.lublin.pl*

Michał Gęca, MEng. – Faculty of Mechanical Engineering, Lublin University of Technology.
e-mail: *michal.geca@pollub.pl*

Arkadiusz Rybak, MEng. – Faculty of Mechanical Engineering, Lublin University of Technology.
e-mail: *a.rybak@pollub.pl*

Maciej Mikulski, DEng. – School of Technology and Innovation, Energy Technology, University of Vaasa.
e-mail: *maciej.mikulski@uwasa.fi*

IX INTERNATIONAL CONGRESS
ON COMBUSTION ENGINES

POLISH SCIENTIFIC SOCIETY
OF COMBUSTION ENGINES

27th-28th September 2021

Lublin University of Technology
Faculty of Mechanical Engineering
Nadbystrzycka 36, 20-618 Lublin, Poland

IX INTERNATIONAL CONGRESS ON COMBUSTION ENGINES

POLISH SCIENTIFIC SOCIETY OF COMBUSTION ENGINES

congress.ptnss.pl

27^{th}-28^{th} September 2021

The Polish Scientific Society of Combustion Engines and the Mechanical Engineering Faculty of the Lublin University of Technology cordially invite engineers and researchers to the 9^{th} International Congress on Combustion Engines that will be held on September 27-28, 2021 in Lublin, Poland. This biennial event is a forum for the exchange of experiences between experts from science and industry, promoting and supporting the development of ICE science and engineering. The aim of the event is to present the latest achievements and state of the art in ICEs, also in a holistic and interdisciplinary context. Special attention will be given to new research results creating global trends that are important from the applicability perspective.

The Congress will host presentations and an exhibition, being a source of information and ensuring the dissemination of technical achievements and ideas related to ICEs. More and more frequently we observe that interdisciplinary teams, cooperating in various areas, participate in research works. Therefore, we invite participants not only from the field of ICE but also from related fields to share their experience and knowledge.

We encourage the ICE community to actively participate in thematic, interactive, problem and interdisciplinary sessions, and to attend meetings with experts and exhibitors. Participants will have an excellent opportunity to meet engineers and researchers from around the world and discuss current trends in the engine technology, share innovative ideas and promote collaboration.

CONGRESS TOPICS

- New engines and engine components
- Hybrid and electric powertrains
- Engine combustion
- Engine testing and modelling
- Fuels and lubricants
- Exhaust emissions and aftertreatment
- Sustainability and global trends in powertrain technology

RESEARCH PAPERS

- All papers after positive review will be published in **Combustion Engines** journal (MEiN: 20 pts).
- Top 10 papers will be recommended for publication in a Congress special issue of the **International Journal of Engine Research** (IF: 2.382, MEiN: 100 pts).
- There is also possibility to publish a paper in a special issue Energy Transfer in Alternative Vehicles of the journal **Energies** (MDPI) with 20% discount (IF: 2.702, MEiN: 140 pts).

Deadline for submitting paper proposals (abstracts): ***April 30 2021***

Lublin University of Technology
Faculty of Mechanical Engineering
Nadbystrzycka 36, 20-618 Lublin, Poland

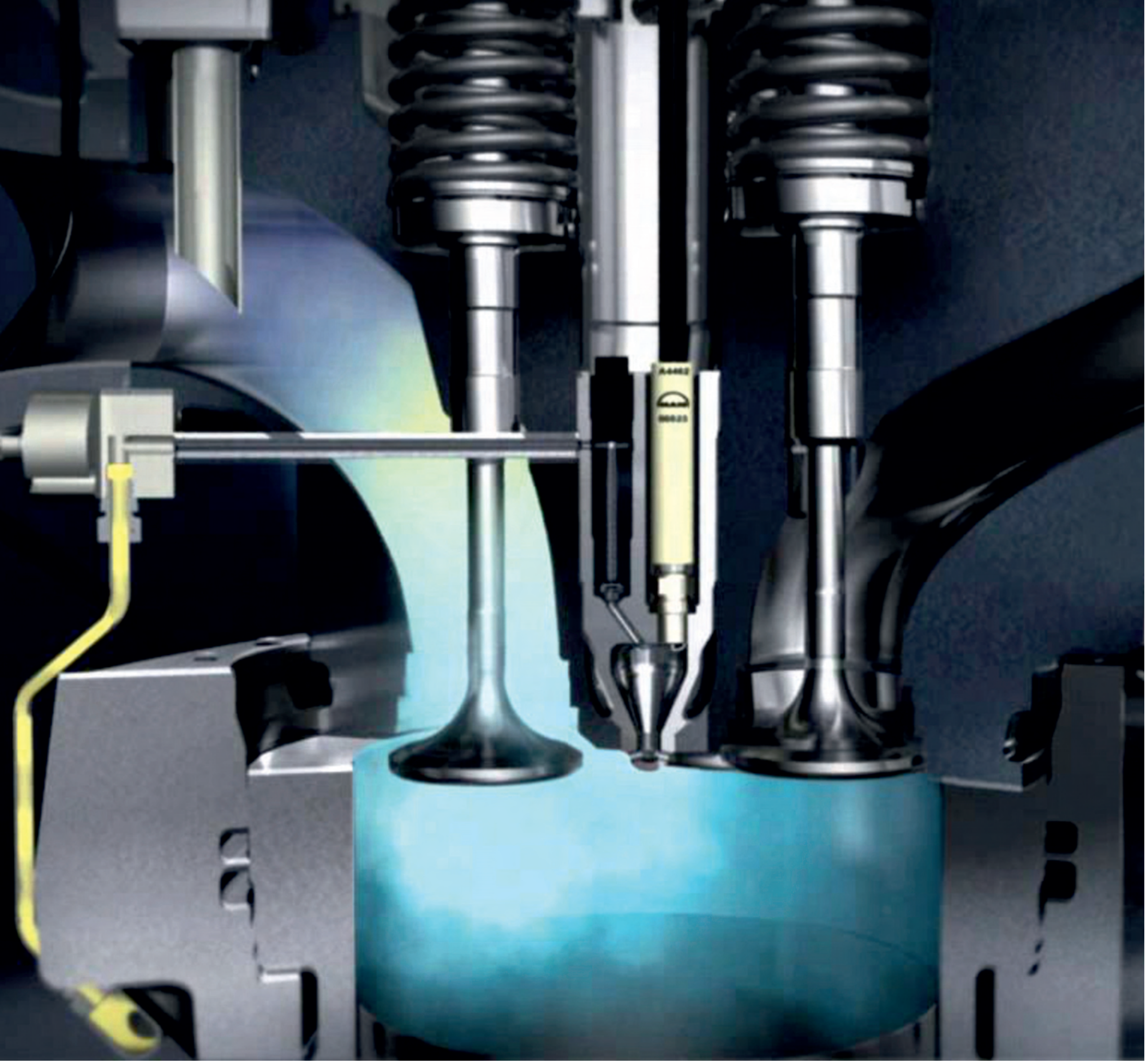

Publisher:

Polish Scientific Society of Combustion Engines

Combustion Engines

Polskie Towarzystwo Naukowe Silników Spalinowych

9 772300 989002

ISSN: 2300-9896
eISSN: 2658-1442